

**Achieving Fine Absolute Positioning Accuracy  
in Large Powerful Manipulators**

by

**Marco Antonio Meggiolaro**

M.Sc. Mechanical Engineering  
Catholic University of Rio de Janeiro, 1996

Submitted to the Department of Mechanical Engineering in Partial Fulfillment of the  
Requirements for the Degree of

**Doctor of Philosophy in Mechanical Engineering**

at the

**Massachusetts Institute of Technology**

September 2000

©2000 Marco Antonio Meggiolaro.  
All rights reserved.

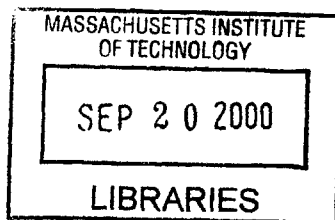
The author hereby grants to MIT permission to reproduce and to distribute publicly paper  
and electronic copies of this thesis document in whole or in part.

Signature of Author: \_\_\_\_\_  
Department of Mechanical Engineering  
August 14, 2000

Certified by: \_\_\_\_\_  
Steven Dubowsky  
Professor of Mechanical Engineering  
Thesis Supervisor

Accepted by: \_\_\_\_\_  
Ain A. Sonin

Professor of Mechanical Engineering  
Chairman, Departmental Graduate Committee



**BARKER**

# **Achieving Fine Absolute Positioning Accuracy in Large Powerful Manipulators**

by

Marco Antonio Meggiolaro

Submitted to the Department of Mechanical Engineering  
on August 14, 2000, in Partial Fulfillment of the Requirements for the Degree of  
Doctor of Philosophy in Mechanical Engineering

## **ABSTRACT**

Large robotic manipulators are needed in such fields as nuclear maintenance, field, undersea and medical applications to perform high accuracy tasks requiring the manipulation of heavy payloads. Achieving such high accuracy is difficult because of the manipulator's size and its need to exert substantial task forces. Therefore, there is a need for model-based error identification and compensation techniques. While classical calibration methods can achieve such compensation for some systems, they cannot correct the errors in large systems with significant elastic deformations. They do not explicitly consider the effects of task forces and structural compliance. To consider these using "brute force" numerical computation methods is not feasible. A method to identify and compensate for system geometric and elastic distortion positioning errors is introduced. The method is applied to a high accuracy medical robot and a Schilling hydraulic manipulator.

Further there is a fundamental problem that has often caused unexpected degradation in classical geometric calibration. That is in the calibration process some of the generalized errors are redundant, namely the effects of these errors are not observable in the manipulator output. These redundant error parameters must be eliminated from the error model prior to the identification process to perform calibration with improved accuracy. In this thesis, the analytical expressions and physical interpretation of the redundant error parameters are presented for a generic serial link manipulator.

After choosing an appropriate identification model, it is still necessary to measure the manipulator pose to perform calibration. However, most manipulator calibration techniques require expensive and/or complicated pose measuring devices, such as theodolites. A calibration method, called Single Endpoint Contact (SEC) calibration, is investigated. In SEC, the manipulator endpoint is constrained to a single contact point while the robot executes self-motions. This method is able to identify elastic structural deformation errors, since arbitrary task forces can be applied to the SEC constraint. It is shown that from the easily measured joint angle readings, and an identification model, the manipulator is calibrated.

Thesis Supervisor: Steven Dubowsky  
Title: Professor of Mechanical Engineering

## Acknowledgements

I would like to thank Professor Steven Dubowsky for his insight, ideas, and guidance during my time with the Field and Space Robotics Laboratory. I would also like to thank the other members of the FSRL who made my experience an enjoyable one.

In particular, I would like to thank my colleagues Constantinos Mavroidis, Philippe Drouet, Peter Jaffe, Guglielmo Sciffignano, Vivek Sujan and Karl Iagnemma as well as Dr. Byung-Hak Cho of the Korean Electric Power Research Institute (KEPRI) for their invaluable help and technical contributions to this work.

I am eternally grateful to my loving parents, whose constant support made this possible. Finally, I would like to thank my soon-to-be wife, Melissa, for her loving encouragement and patience. I definitely could not have done it without you.

This thesis describes research performed at the MIT Field and Space Robotics Laboratory under the sponsorship of the National Institutes of Health, the Korean Electricity and Power Company, Electricité de France, and the Brazilian government (through CAPES). Thanks for providing the financial support for this project.

# Table of Contents

<b>Chapter 1 Introduction .....</b>	<b>11</b>
1.1 Background and Literature Review .....	11
1.2 Objectives of this Thesis and Summary of Results .....	17
1.3 Applications .....	18
1.3.1 Patient Positioning System .....	19
1.3.2 Nozzle Dam Placement .....	21
1.4 Outline of this Thesis .....	24
<b>Chapter 2 Analytical Background .....</b>	<b>26</b>
2.1 Introduction .....	26
2.2 Base Sensor Control (BSC) .....	26
2.3 Classical Manipulator Calibration .....	29
2.4 Summary and Conclusions .....	35
<b>Chapter 3 Elimination of Redundant Error Parameters .....</b>	<b>37</b>
3.1 Introduction .....	37
3.2 Eliminating Redundant Errors .....	37
3.2.1 Linear Combinations of the Identification Jacobian matrix .....	38
3.2.2 Physical Interpretation of the Linear Combinations .....	41
3.2.3 Partial Measurement of End-Effector Pose .....	43
3.2.4 Number of Independent Generalized Errors .....	44
3.2.5 Extension to Four-Parameter Error Representations .....	45
3.3 Simulation Results .....	47



3.4	Summary and Conclusions .....	47
<b>Chapter 4</b>	<b>Geometric and Elastic Error Compensation (GEC) .....</b>	<b>49</b>
4.1	Introduction .....	49
4.2	GEC Theory .....	49
4.3	Application to the Patient Positioning System.....	52
4.4	Application to the Nozzle Dam Task .....	63
4.5	Summary and Conclusions .....	70
<b>Chapter 5</b>	<b>Single Endpoint Contact Calibration (SEC).....</b>	<b>71</b>
5.1	Introduction .....	71
5.2	SEC Theory .....	71
5.2.1	Analytical Development .....	73
5.2.2	Control .....	76
5.2.3	Optimization of the Fixture Location .....	77
5.3	Results .....	79
5.3.1	Simulation Results .....	80
5.3.2	Experimental Results .....	86
5.4	Summary and Conclusions .....	92
<b>Chapter 6</b>	<b>Force-Updated Virtual Viewing System .....</b>	<b>94</b>
6.1	Introduction .....	94
6.2	Contact Force Estimation .....	94
6.3	Virtual Environment Teleoperator Software .....	98
6.4	Experimental Verification .....	101
6.5	Summary and Conclusions .....	103

<b>Chapter 7 Conclusions and Suggestions for Future Work.....</b>	<b>104</b>
7.1 Contributions of This Work.....	104
7.2 Suggestions for Further Work.....	106
<b>References .....</b>	<b>107</b>
<b>Appendix A Linear Dependency Calculations.....</b>	<b>118</b>
<b>Appendix B Patient Positioning System Kinematic Description.....</b>	<b>124</b>
<b>Appendix C Schilling Titan II Kinematic Description.....</b>	<b>130</b>

# List of Figures

Figure 1.1 - The PPS and the Gantry.....	19
Figure 1.2 - The Patient Positioning System .....	20
Figure 1.3 - Nuclear Reactor.....	22
Figure 1.4 - Simulated Robotic Nozzle Dam Task .....	22
Figure 2.1 - External and Dynamic Wrenches .....	28
Figure 2.2 - BSC Control Loop.....	29
Figure 2.3 - Frame Translation and Rotation Due to Errors for $i^{\text{th}}$ Link .....	31
Figure 2.4 - Translational and Rotational Generalized Errors for $i^{\text{th}}$ Link .....	32
Figure 2.5 - Error Compensation Scheme .....	34
Figure 3.1 - Linear Combination of Translational Generalized Errors .....	41
Figure 3.2 - Error Combinations Resulting in Same End-Effector Errors .....	42
Figure 3.3 - Linear Combinations of Generalized Errors in Prismatic Joints.....	42
Figure 4.1 - Flow-chart of the Method to Identify Generalized Errors .....	52
Figure 4.2 - Joint Parameter Definition for the PPS .....	53
Figure 4.3 - Leica 3D Laser Tracking System.....	54
Figure 4.4 - Close-up View of the PPS Couch .....	54
Figure 4.5(a) - Measured and Residual Errors After Compensation.....	56
Figure 4.5(b) - Measured and Residual Errors After Compensation .....	57
Figure 4.6 - Repeatability Distribution.....	58
Figure 4.7 - Measured and GEC Predicted Errors along the X Axis at NTP .....	60
Figure 4.8 - Measured and GEC Predicted Errors along the Y Axis at NTP .....	61

Figure 4.9 - Measured and GEC Predicted Errors along the Z Axis at NTP.....	62
Figure 4.10 - Statistics of the Compensated PPS Errors at NTP .....	63
Figure 4.11 - Schilling Titan II Manipulator .....	64
Figure 4.12 - Base Sensor Control and Error Compensation Scheme .....	65
Figure 4.13 - Nozzle Dam Experimental System.....	66
Figure 4.14 - Repeatability with and without BSC .....	68
Figure 4.15 - Measured and Residual Errors After Compensation .....	69
Figure 5.1 - Real and Ideal Positions of a Manipulator End-Effector.....	74
Figure 5.2 - Calibration of Elastic Errors due to an Arbitrary Force .....	75
Figure 5.3 - Stabilization of the Arm Self-Motions .....	76
Figure 5.4 - ICR Volume as a Function of the Fixture Location .....	80
Figure 5.5 - ICR Volume as a Function of SEC Fixture Location.....	81
Figure 5.6 - Measurement Configurations for an SEC Fixture at (6,0).....	82
Figure 5.7 - Extrapolated and Interpolated Regions for an SEC Fixture at (6,0) .....	82
Figure 5.8 - Extrapolated and Interpolated Regions for an SEC Fixture at (10,0) .....	83
Figure 5.9 - RMS Residual Error as a Function of the Number of Measurements.....	85
Figure 5.10 - Experimental System.....	86
Figure 5.11 - SEC Fixture Using Four Spheres .....	87
Figure 5.12 - SEC Fixture Using Three Rotary Joints .....	88
Figure 5.13 - SEC Fixture Using a Spherical Joint .....	89
Figure 5.14(a) - Measured and Residual Errors After Compensation.....	91
Figure 5.14(b) - Measured and Residual Errors After Compensation.....	92
Figure 6.1 - Contact Force and Wrist Force/Torque Sensor Readings.....	96

Figure 6.2 - Real (a) and Simulated (b) Experimental System.....	99
Figure 6.3 - Base Sensor Control and Contact Force Estimation Scheme .....	101
Figure 6.4 – Typical Placement Steps Using Contact Force Visualization.....	102
Figure B.1 - Parameter Definitions for the PPS.....	124
Figure C.1 - Side view of the Schilling Titan II.....	130
Figure C.2 - Top View showing the Base Force/Torque Sensor Frame.....	131

## List of Tables

Table 3.1 – Number of Independent Generalized Errors.....	44
---	----

### 1.1 Background and Literature Review

Large robotic manipulators are needed in field, service, manufacturing and medical applications to perform high accuracy tasks. Examples are manipulators that perform decontamination tasks in nuclear sites, space manipulators such as the Special Purpose Dexterous Manipulator (SPDM) and manipulators for medical treatment (Vaillancourt et al. 1994; Flanz 1996; Hamel et al. 1997). In these applications, a large robotic system is often needed to have very fine precision while exerting substantial task forces and torques. Its accuracy specifications may be very small fractions of its workspace. Achieving such high accuracy is difficult because of the manipulator's size and its need to carry heavy payloads, as well as high joint friction. Further, many tasks, such as space applications, require systems to be lightweight, and thus structural deformation errors can be large.

A number of approaches exist for improving fine motion manipulator performance through friction compensation. Some of these require modeling of the difficult to characterize joint frictional behavior (Canudas de Wit et al. 1996; Popovic,

Shimoga and Goldenberg, 1994). Some require the use of specially designed manipulators that contain complex internal joint-torque sensors (Pfeffer, Khatib and Hake, 1989). A simple, yet effective control method has been developed that is modelless and does not require internal joint sensors (Morel and Dubowsky, 1996; Iagnemma et al., 1997; Morel et al., 2000). The method, called Base Sensor Control (BSC), estimates manipulator joint torques from a self-contained external six-axis force/torque sensor placed under the manipulator's base. The joint torque estimates allow for accurate joint torque control that has been shown to greatly improve repeatability of both hydraulic and electric manipulators, but not their absolute accuracy. Here repeatability is defined as how well the system returns to its original configuration after being moved to arbitrary configurations.

Even with fine repeatability, high absolute positioning accuracy is still difficult to achieve with a large manipulator. Two principal error sources create significant end-effector errors. The first is kinematic errors due to the non-ideal geometry of the links and joints of manipulators, such as errors due to machining tolerances. These errors are often called geometric errors.

The second error source that can limit the absolute accuracy of a large manipulator is the elastic errors due to the distortion of a manipulator's mechanical components under large task loads or even its own weight.

Task constraints often make it impossible to use direct end-point sensing in a closed-loop control scheme to compensate for these errors. Therefore, there is a need for model-based error identification and compensation techniques, often called robot calibration. However, classical error compensation methods cannot correct the errors in



large systems with significant elastic deformations, because they do not explicitly consider the effects of task forces and structural compliance. Methods have been developed to deal with this problem (Drouet et al. 1998; Drouet 1999), however they depend on analytical models of the manipulator structural properties that are not easy to obtain.

Considerable research has been performed in classical robot calibration without consideration of elastic deformations (Roth et al. 1986; Hollerbach 1988; Hollerbach et al. 1996; Zhuang et al. 1996). In these methods robot position accuracy is improved using compensation methods that identify a functional relationship between the joint transducer readings and the workspace position of the end-effector based on experimental calibration measurements. The process requires the identification of the manipulator generalized errors from calibration measurements. Generalized errors characterize the relative position and orientation of frames defined at the manipulator links. These errors are found from measured data and used to predict, and compensate for, the end-point errors as a function of configuration. A major component of this process is the development of manipulator error models, some of which consider the effects of manipulator joint errors, while others focus on the effects of link dimensional errors (Waldron et al. 1979; Wu 1984; Vaishnav et al. 1987; Mirman et al. 1993). Error models have been developed specifically for use in the calibration of manipulators (Broderick et al. 1988; Zhuang et al. 1992). Some researchers have studied methods to find the optimal configurations during the calibration measurements to reduce the manipulator errors by calibration (Borm et al. 1991; Zhuang et al. 1996). Solution methods for the identification of the manipulator's unknown parameters have been studied for these

model-based calibration processes (Dubowsky et al. 1975; Zhuang et al. 1993). Most calibration methods have been applied to industrial or laboratory robots, achieving good accuracy when geometric errors are dominant and elastic errors can be neglected.

In the past, calibration methods have not explicitly compensated for elastic errors due to the wrench at the end-effector. Recently in our laboratory a method to address this problem has been developed, however it requires explicit structural modeling of the system (Drouet et al. 1998; Drouet 1999). While conceptually very similar to the classical geometric problem, the combined problem is far more complex. Compensating for geometric errors requires building a model that is a function of the  $n$  (usually 6) joint variables. To compensate for a general 6 variable end-point task wrench (three end-point forces and three end-point moments) requires a model that is a function of both the joint variables and the end-point wrench variables, or a function of at least 12 variables. The number of measurements required to characterize this 12 dimensional space is far larger than required for the 6 dimensional space. The time and cost of the physical calibration measurements often dominates the calibration problem. Simple calculations suggest that a brute force identification would require several million calibration measurements.

In addition, when implementing the above methodologies, a fundamental problem inherent in robot calibration is encountered that has not been addressed in previous research. That is, in the calibration process some of the generalized errors are redundant, and thus the effects of these redundant errors are not observable in the manipulator output. These redundant error parameters must be eliminated from the error model prior to the identification process to perform calibration with improved accuracy (Hollerbach and Wampler 1996; Ikits and Hollerbach, 1997).

A number of coordinate system representations have been considered to model the manipulator errors. The four-parameter representations (such as the Denavit-Hartenberg representation) are attractive since they are the minimal parameter set required to locate the reference frames of the joints (Roth, Mooring and Ravani, 1987). Such representation reduces the number of error combinations to be found, however the redundant parameters are not necessarily eliminated. In addition, the Denavit-Hartenberg (D.H.) error representation does not model some of the generalized errors in the presence of parallel joints. The entire calibration can be compromised if such errors are significant. Also, the D.H. representation is ill-conditioned when neighboring joint axes are nearly parallel. Incorporating Hayati's proposed modification to the D.H. parameterization (Hayati, 1983) eliminates the ill-conditioning problem, however it has a singularity when axes are nearly perpendicular (Hollerbach, 1988). Some authors have proposed a five-parameter representation (Hsu, Everett, 1985), however this parameterization has a sensitivity problem when neighboring coordinate origins are close together (Ziegert and Datseris, 1988).

Many papers have abandoned the D.H. representation of the errors, treating the general case of two coordinate systems related by six parameters. The six-parameter representation of the errors, called generalized error model, does not have the sensitivity problems of the D.H. representation. However, it has the disadvantage of increased redundancy (Hollerbach, 1988). Numerical methods have been proposed to eliminate redundant errors (Schröer, 1983; Everett and Suryohadiprojo, 1988; Zhuang, Roth and Hamano, 1992), however they must be formulated in a case-by-case basis (Hollerbach and Wampler, 1996). An analytical algorithm has been proposed to eliminate the

redundant errors in the D.H. error representation (Khalil, Gautier and Enguehard, 1991), however it cannot be applied to the generalized error formulation.

After choosing an appropriate identification model and eliminating the redundant error parameters it is still necessary to measure the manipulator pose as a function of the joint angles and task loads. However, most manipulator calibration techniques require expensive and/or complicated pose measuring devices, such as theodolites. Obtaining pose measurements is generally very costly and time consuming, and must be performed regularly for very high precision systems (Everett and Lin, 1988). Many pose measurement devices have been proposed. The theodolite triangulation method consists of two or more theodolites aimed at a common target on the robot wrist (Johnson, 1980). Vira and Lau used laser interferometers with steerable reflectors to measure position and orientation of a target in space (Vira and Lau, 1986). Telescoping ball bars have been used to measure contouring accuracy along a circular contour (Lau et al., 1984).

Bennett and Hollerbach defined a general class of calibration methods, called closed-loop calibration, in which constraints are imposed on the end-effector of the robot (Bennett and Hollerbach, 1991). In this method the easily-measured joint angles are adequate to calibrate the manipulator, without requiring any external metrology system. Past closed-loop methods have required the robot to move along an unsensed sliding joint at the endpoint, or constraining the end-effector to lie on a set of planes (Scheffer, 1976; Warnecke et al., 1980; Ikits and Hollerbach, 1997; Zhuang et al., 1999).

## 1.2 Objectives of this Thesis and Summary of Results

The goal of this thesis is to develop methods to substantially improve the absolute accuracy in strong powerful manipulators lacking good repeatability and having significant geometric and elastic errors – in other words, a manipulator with real characteristics. In this work, a method that compensates for the position and orientation errors caused by geometric and elastic errors in such large manipulators is presented. The method, called Geometric and Elastic Error Compensation (GEC), explicitly considers the task load dependency of the errors, modeling both deformation and more classical geometric errors in a unified manner. A set of experimentally measured positions and orientations of the robot end-effector and measurements of the payload wrench are used to calculate the robot generalized errors without using an explicit manipulator elastic model (Meggiolaro, Mavroidis and Dubowsky, 1998). Generalized errors are those parameters that characterize the relative position and orientation of frames defined at the manipulator links. They are determined from measured data as a function of the system configuration and the task wrench. Knowing these generalized errors, the manipulator end-effector errors are compensated at any configuration. In the GEC method each generalized error parameter can be represented as a function of only a few of the system variables. As a result, the number of measurements required to characterize the system is dramatically smaller than might be expected (Meggiolaro, Dubowsky and Mavroidis, 2000). The GEC method is applied in concert with a previously developed concept called Base Sensor Control (BSC), which ensures good repeatability by compensating for joint friction. The combined methods do not require joint velocity or acceleration measurements, a model of the actuators or friction, or the

knowledge of manipulator mass parameters or link stiffnesses, yet they are able to improve substantially its absolute positioning accuracy (Meggiolaro, Jaffe and Dubowsky, 1999).

As discussed before, to improve calibration accuracy, redundant error parameters must be eliminated from the error model prior to the identification process. In this thesis, analytical expressions and physical interpretation of all redundant error parameters are developed for any serial link manipulator. These expressions allow for systematic calibration with improved accuracy of any serial link manipulator (Meggiolaro and Dubowsky, 2000).

After choosing an appropriate identification model and eliminating its redundant error parameters, it is still necessary to measure the manipulator pose at different configurations. However, most manipulator calibration techniques require expensive and/or complicated pose measuring devices, such as theodolites. This thesis presents a calibration method, called Single Endpoint Contact (SEC) calibration, where the manipulator endpoint is constrained to a single contact point while the robot executes self-motions. From the easily-measured joint angle readings and an identification model, the manipulator is calibrated (Meggiolaro, Scriffignano and Dubowsky, 2000).

### **1.3 Applications**

Two real applications are studied in this thesis. They are a patient positioning system for radiation therapy and a maintenance task in the nuclear power industry.

### 1.3.1 Patient Positioning System

The robotic Patient Positioning System (PPS) at the proton therapy research facility constructed at the Massachusetts General Hospital (MGH), the Northeast Proton Therapy Center (NPTC), is an example of a large medical manipulator (Flanz et al. 1995; Flanz et al. 1996). The PPS places a patient in a high energy proton beam delivered from a proton nozzle carried by a rotating gantry structure (see Figure 1.1). The PPS is a six degree-of-freedom manipulator that covers a large workspace of more than 4m radius while carrying patients weighing as much as 300 lbs (see Figure 1.2). Patients are immobilized on a “couch” attached to the PPS end-effector. The PPS, combined with the rotating gantry that carries the proton beam, enables the beam to enter the patient from any direction, while avoiding the gantry structure. Hence programmable flexibility offered by robotic technology is needed.

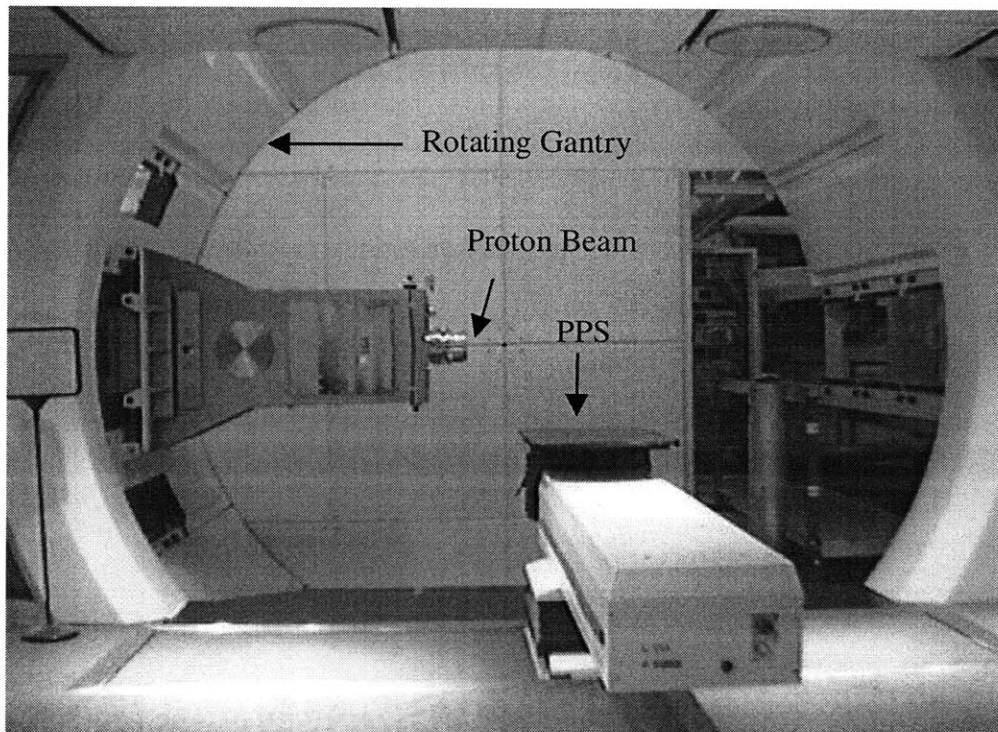


**Figure 1.1 - The PPS and the Gantry [Ref. Flanz, 1996]**

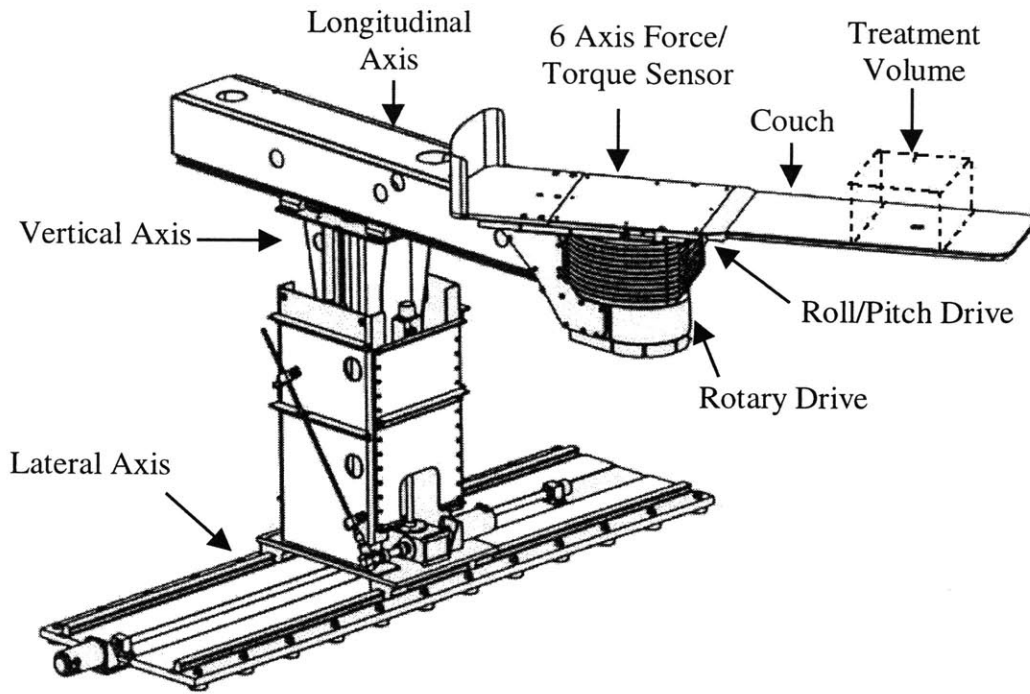


**Figure 1.2 - The Patient Positioning System [Ref. Flanz, 1996]**

The required absolute positioning accuracy of the PPS is  $\pm 0.5$  mm. This accuracy is critical as larger errors may be dangerous to the patient (Rabinowitz 1985). The required accuracy is roughly  $10^{-4}$  of the nominal dimension of the system workspace. This is a greater relative accuracy than most industrial manipulators. In addition, FEM studies and experimental results show that with a changing payload (between 1 and 300 pounds) and changing configuration the end-effector errors due to elastic deformations and geometric errors are of the order of 6-8 mm. Hence the accuracy is 12 to 16 times the system specification (Mavroidis et al. 1997). However, since the repeatability error of the PPS, defined here as how well the system returns to certain arbitrary configurations, is less than 0.15mm, it is a good candidate for a model based error correction method.



The GEC calibration method was applied to the PPS with a force/torque sensor built into the system to measure the wrench applied by the patient's weight. It was found that using only 450 calibration measurements the end-point errors could be reduced to well within the required specification. In fact, experimental results show that the maximum error is reduced by a factor of 18.

### **1.3.2 Nozzle Dam Placement**

Another application of large robotic manipulators is in the nuclear power industry. The dangerous task of steam generator maintenance is currently performed by workers, who are referred to as "jumpers." Once a year, each nuclear reactor is shutdown for a month to swap old fuel rods in the reactor core with new ones (Figure 1.3 shows a graphical overview of the process for a Westinghouse type F steam generator). At the same time the fuel cells are replenished, the U-tubes in the steam generator must be inspected for damage. In order for workers to enter the steam generator, the water in the reactor core must be prevented from entering the steam generator's water chamber. This is achieved by covering the two large portals, one meter in diameter, that connect the hot and cold pipes to the steam generator (Cho, 1997). Each portal has a nozzle ring into which a device referred to as a nozzle dam is inserted with a tolerance of approximately 1mm. The nozzle dam is installed in two phases, the first of which is fitting the nozzle dam side plate in the nozzle ring (Figure 1.4a), and then the nozzle dam center plate is placed within the side plate (Figure 1.4b). This provides the necessary seal to prevent water leakage, thereby allowing workers to enter the steam generator and inspect the U-tubes.

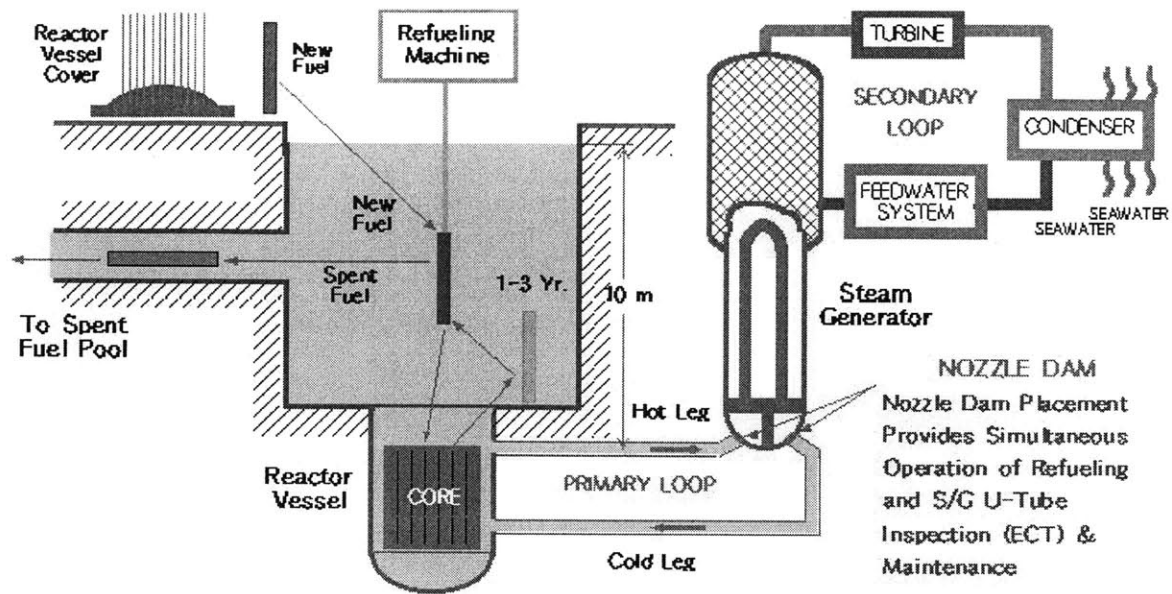


Figure 1.3 - Nuclear Reactor [Ref. Cho, 1997]

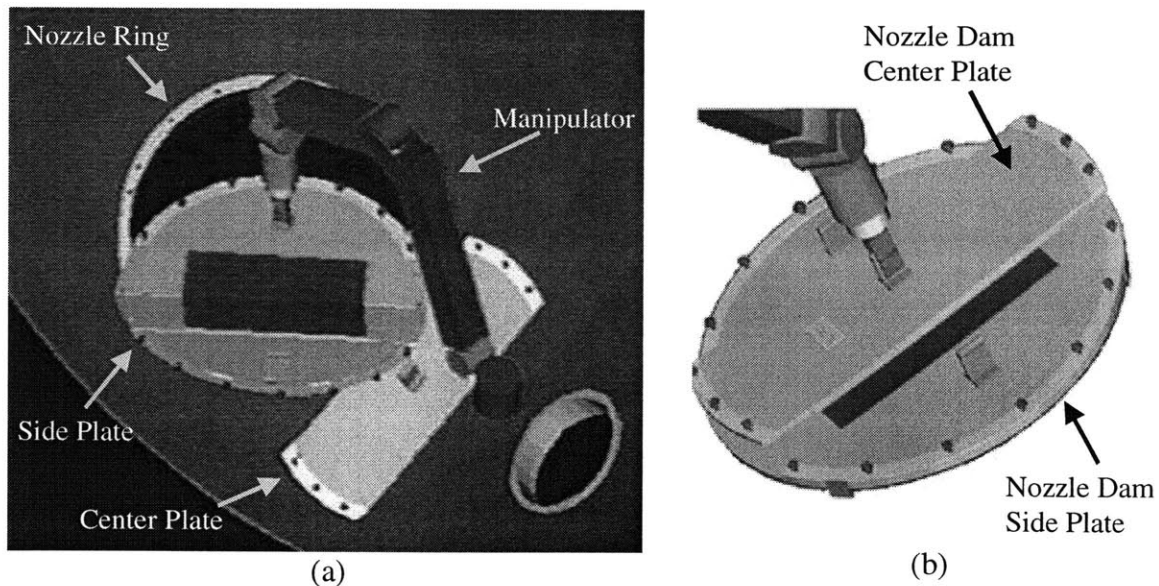


Figure 1.4 - Simulated Robotic Nozzle Dam Task

Installing one nozzle dam requires hours of manual labor during which time the workers are exposed to high doses of residual radiation. Jumpers can only remain in the steam generator chamber for three minutes before receiving their maximum acceptable

yearly radiation dosage. At this point, the worker leaves the chamber through the 0.8 m diameter access portal and another worker enters to resume the task (Zezza, 1985). The manpower and time required to complete this task, as well as the health risks imposed on the workers, make this task well suited to investigations in automating the process. Recent attempts to place the nozzle dam with a manipulator have taken very long because of the combination of poor teleoperator visibility and lack of manipulator accuracy. Successful completion of the task with a manipulator would eliminate radiation exposure as well as save money by reducing the time required to place the nozzle dam. For each hour that the reactor is off line, \$40,000 in potential revenues is lost. The key to achieving this task is improving manipulator accuracy as well as the operator interface. The typical repeatability of manipulators capable of handling the required load, such as the Schilling Titan II manipulator, is in the range of 10 to 20 mm. The absolute accuracy can be several times these amounts. The automation of this task would require absolute accuracy of only a few millimeters.

Also, contact force information between the manipulator end-effector and the environment is fundamental for teleoperated placement tasks with small tolerances. However, a wrist force/torque sensor alone provides limited information to locate the contact point. In the case where there is only one contact point with the environment and where the contact torque is zero, it is possible to calculate the contact information required for control. This can be obtained from wrist force/torque information combined with knowledge of the geometry of the manipulator end-effector. A method is developed to estimate the contact forces between the manipulator end-effector and the environment

from wrist sensor and task geometry, and graphically displays this contact force information to a teleoperator (Meggiolaro, Jaffe, Iagnemma and Dubowsky, 1999).

In addition, a virtual viewing system based on 3-D kinematic models is developed to perform the nozzle dam task. The system contains 3-D kinematic models of the manipulator and the workspace, reflecting the actual system configuration. The interface provides improved operator visibility by allowing *virtual viewing* of physically obscured regions using *virtual cameras*. The virtual cameras also allow for magnifying the mating edges in order to aid in teleoperated insertion tasks. The virtual viewing system is combined with real-time contact force measurements to improve teleoperation. Laboratory experiments show that successful nozzle dam placements could be performed using the combined GEC/BSC techniques and the visualization system with a conventional Schilling hydraulic manipulator.

## **1.4 Outline of this Thesis**

This thesis is divided into seven chapters. This chapter serves as an introduction and overview of the work. Chapter 2 reviews the Base Sensor Control method as applied to the fine-motion positioning problem, and presents the generalized error formulation applied to classical manipulator calibration.

Chapter 3 presents a general analytical method to eliminate the redundant error parameters in robot calibration. Simulation results are presented for a PUMA 560 and for an Adept SCARA manipulator.

Chapter 4 describes the GEC (Geometric and Elastic Error Compensation) theory and shows experimental results for the calibration of the Patient Positioning System and of a Schilling Titan II manipulator used in the nozzle dam placement task.

Chapter 5 investigates the SEC (Single Endpoint Contact) calibration method, where the robot endpoint is constrained to a single contact point. Optimization of the SEC fixture location is discussed. Simulations and experimental results are presented for a Schilling Titan II manipulator.

Chapter 6 explores a method to obtain contact force information between the manipulator end-effector and the environment. This method is applied to a virtual environment teleoperator interface developed for the nozzle dam placement task. This system is then integrated with control hardware to provide a comprehensive teleoperation package.

Chapter 7 summarizes the conclusions regarding the integration of the above methodologies. Finally, suggestions for further work are presented.

The appendices to this thesis give detailed information on specific topics related to the practical implementation of the work presented. Appendix A provides the proof of the linear combination expressions of the columns of the Identification Jacobian matrix. These expressions are used to eliminate the redundant parameters from the error model in robot calibration. Appendix B provides a kinematic description of the Patient Positioning System, including the associated error matrices. Appendix C provides the error matrices for the Schilling Titan II manipulator.

## Analytical Background

---

### 2.1 Introduction

This chapter reviews the analytical background for Base Sensor Control and classical calibration techniques. Section 2.2 reviews the theoretical framework for the BSC method, and discusses important simplifications that can be made for the fine-motion case. Section 2.3 presents the generalized error formulation applied to classical robot calibration.

### 2.2 Base Sensor Control (BSC)

The following is a brief review of the basis for BSC (Base Sensor Control) based on (Morel et al., 2000), where the complete development is presented. A simplified version of the algorithm sufficient and effective for fine-motion control is formulated in (Iagnemma, 1997).

BSC has been developed to compensate for nonlinear joint characteristics in robotic manipulators, such as high joint friction, to improve system repeatability. BSC estimates manipulator joint torques from a self-contained external six-axis force/torque

sensor placed under the manipulator's base. The joint torque estimates allow for accurate joint torque control that has been shown to greatly improve repeatability of both hydraulic and electric manipulators.

As shown in Figure 2.1, the wrench,  $\mathbf{W}_b$ , exerted by the manipulator on its base sensor can be expressed as the sum of three components:

$$\mathbf{W}_b = \mathbf{W}_g + \mathbf{W}_d + \mathbf{W}_e \quad (2.1)$$

where  $\mathbf{W}_g$  is the component due to gravity,  $\mathbf{W}_d$  is caused by manipulator motion, and  $\mathbf{W}_e$  is the wrench exerted by the payload or task on the end-effector. Note that joint friction does not appear in the measured base sensor wrench. In the fine-motion case, it is assumed that the gravity wrench is essentially constant, and this wrench can be approximated by the initial value measured by the base sensor. Hence, the complexity of computing the gravitational wrench, such as identification of link weights and a static manipulator model, is eliminated. Under this assumption, the Newton Euler equations of the first  $i$  links are:

$$\left\{ \begin{array}{l} \mathbf{W}_{0 \rightarrow 1} = -\mathbf{W}_b \\ \mathbf{W}_{1 \rightarrow 2} = \mathbf{W}_{0 \rightarrow 1} - \mathbf{W}_{d_1} \\ \vdots \\ \mathbf{W}_{i \rightarrow i+1} = \mathbf{W}_{i-1 \rightarrow i} - \mathbf{W}_{d_i} \\ \vdots \\ -\mathbf{W}_e = \mathbf{W}_{n-1 \rightarrow n} - \mathbf{W}_{d_n} \end{array} \right. \quad (2.2)$$

where  $\mathbf{W}_{i \rightarrow i+1}$  is the wrench exerted by link  $i$  on link  $i+1$ , and  $\mathbf{W}_{d_i}$  is the dynamic wrench for link  $i$ .

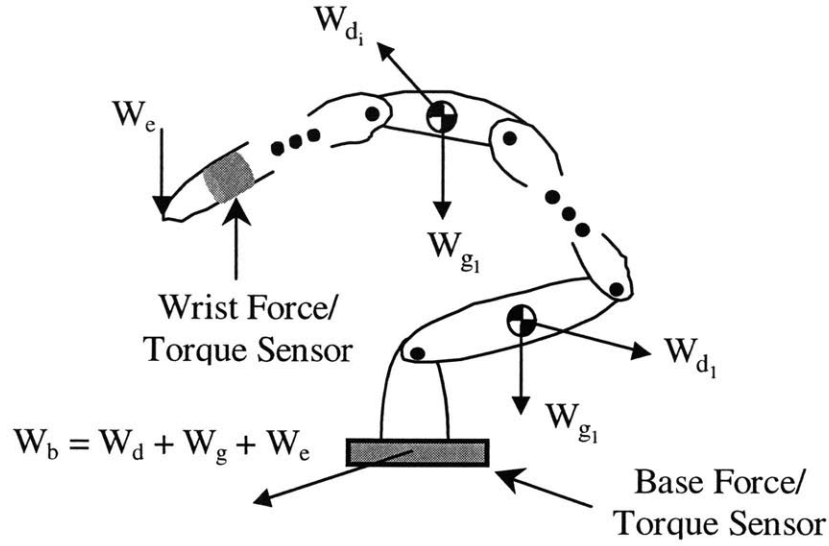


**Figure 2.1 - External and Dynamic Wrenches [Ref. Morel et al., 1996]**

For fine tasks it is assumed that the manipulator moves very slowly so that  $W_d$  can be neglected. Therefore, for slow, fine motions, only the measured wrench at the base is used to estimate the torque in joint  $i+1$ . The estimated torque in joint  $i+1$  is obtained by projecting the moment vector at the origin  $O_i$  of the  $i^{\text{th}}$  reference frame along the joint axis  $z_i$ :

$$\tau_{i+1} = -z_i^T \cdot \mathbf{W}_b^{O_i} \quad (2.3)$$

The value of  $\tau_{i+1}$  depends only on the robot's kinematic parameters, joint angles and base sensor measurements.

With estimates of the joint torque, it is possible to perform high performance torque control that can greatly reduce the effects of joint friction and nonlinearities. This results in greatly improved repeatability. Figure 2.2 shows BSC schematically.



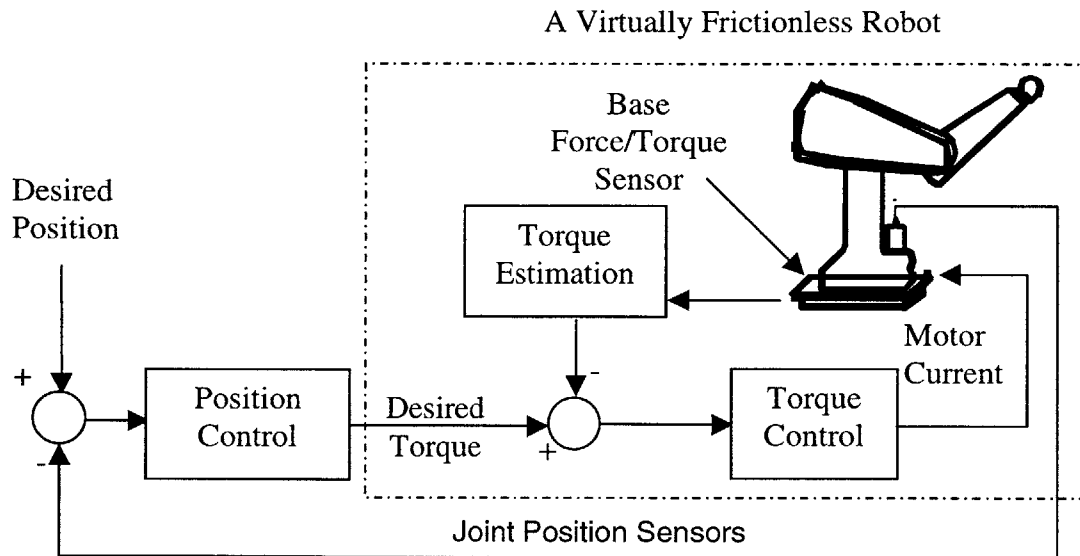


**Figure 2.2 - BSC Control Loop [Ref. Morel et al., 1996]**

However, the BSC method will not compensate for sources of random repeatability errors, such as limited encoder resolution. In addition, a manipulator with good repeatability may not have fine absolute position accuracy. After improving the system repeatability using BSC, a model-based error correction method can be applied to reduce the absolute accuracy errors. The next section presents a classical formulation for manipulator calibration.

## 2.3 Classical Manipulator Calibration

There are many possible sources of errors in a manipulator. These errors are referred to as "physical errors," to distinguish them from the generalized errors defined in Chapter 1. In most cases, while the actual physical errors are relatively small, their effect at the end-effector is large. The main sources of physical errors in a manipulator are:

- **Mechanical system errors:** These errors result from machining and assembly tolerances of the manipulator's mechanical components.

- **Deflections:** Elastic deformation of the manipulator's members under task loads and gravity can result in large end-effector errors, especially in long reach manipulator systems.
- **Measurement and Control:** Measurement, actuator, and control errors that occur in the control systems will create end-effector positioning errors. The resolution of encoders and stepper motors are examples of this type of error.
- **Joint errors:** These errors include bearing run-out in rotating joints, rail curvature in linear joints, and backlash in manipulator joints and actuator transmissions.

Further, errors can be distinguished into “repeatable” and “random” errors (Slocum, 1992). Repeatable errors are those whose numerical value and sign are constant for a given manipulator configuration and task load. An example of a repeatable error is an assembly error. Random errors are errors whose numerical value or sign changes unpredictably. An example of a random error is the error that occurs due to backlash of an actuator gear train. Classical kinematic calibration and correction can only deal with repeatable errors. It will be shown experimentally in Chapter 4 that repeatable errors dominate in the performance of the PPS and of the Schilling manipulator.

To describe the kinematics of a manipulator, Denavit-Hartenberg reference frames are defined at the manipulator base, end-effector, and at each manipulator joint (Craig, 1989). The position and orientation of a reference frame  $F_i$  with respect to the previous reference frame  $F_{i-1}$  is defined with a 4x4 matrix  $A_i$  that has the general form:

$$A_i = \begin{bmatrix} \mathbf{R}_i & \mathbf{T}_i \\ 0 & 1 \end{bmatrix} \quad (2.4)$$

The  $\mathbf{R}_i$  term is a 3x3 orientation matrix composed of the direction cosines of frame  $F_i$  with respect to frame  $F_{i-1}$ , and  $\mathbf{T}_i$  is a 3x1 vector of the coordinates of center  $O_i$  of frame  $F_i$  in  $F_{i-1}$ , see Figure 2.3. The elements of matrices  $\mathbf{A}_i$  depend on the geometric parameters of the manipulator and the manipulator joint variables  $\mathbf{q}$ .

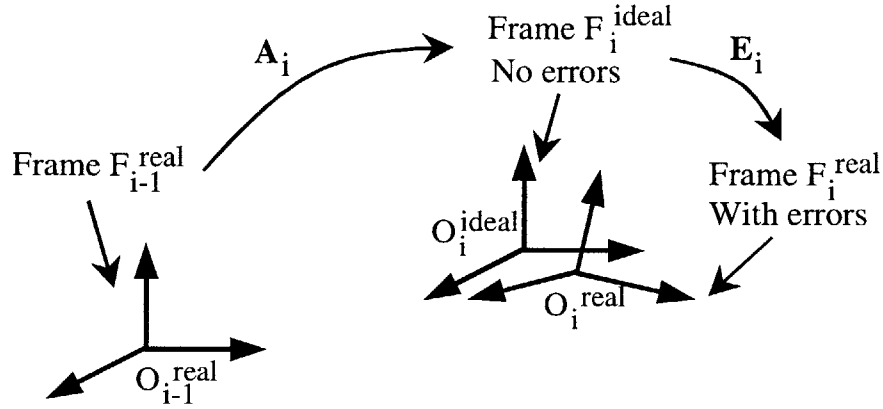


**Figure 2.3 - Frame Translation and Rotation Due to Errors for  $i^{\text{th}}$  Link**

Physical errors cause the geometric parameters of a manipulator to be different from their ideal values. As a result, the frames defined at the manipulator joints are slightly displaced from their expected, ideal locations, creating significant end-effector errors. The position and orientation of a frame  $F_i^{\text{real}}$  with respect to its ideal location  $F_i^{\text{ideal}}$  is represented by a 4x4 homogeneous matrix  $\mathbf{E}_i$ , see Figure 2.3. The translational part of matrix  $\mathbf{E}_i$  is composed of the 3 coordinates  $\epsilon_{x,i}$ ,  $\epsilon_{y,i}$  and  $\epsilon_{z,i}$  of point  $O_i^{\text{real}}$  in  $F_i^{\text{ideal}}$  (along the X, Y and Z axes respectively, defined using the Denavit-Hartenberg representation), see Figure 2.4. The rotational part of matrix  $\mathbf{E}_i$  is the result of the product of three consecutive rotations  $\epsilon_{s,i}$ ,  $\epsilon_{r,i}$ ,  $\epsilon_{p,i}$  around the Y, Z and X axes respectively (also shown in Figure 2.4). These are the Euler angles of  $F_i^{\text{real}}$  with respect to  $F_i^{\text{ideal}}$ . The subscripts s, r, and p represent spin (yaw), roll, and pitch, respectively. The 6 parameters  $\epsilon_{x,i}$ ,  $\epsilon_{y,i}$ ,  $\epsilon_{z,i}$ ,  $\epsilon_{s,i}$ ,  $\epsilon_{r,i}$  and  $\epsilon_{p,i}$  are called generalized error parameters, which can be a

function of the system geometry and joint variables. For an  $n$  degree of freedom manipulator, there are  $6(n+1)$  generalized errors which can be written in the form of a  $6(n+1) \times 1$  vector  $\varepsilon = [\varepsilon_{x,0}, \dots, \varepsilon_{x,i}, \varepsilon_{y,i}, \varepsilon_{z,i}, \varepsilon_{s,i}, \varepsilon_{r,i}, \varepsilon_{p,i}, \dots, \varepsilon_{p,n}]^T$ , with  $i$  ranging from 0 to  $n$ , assuming that both the manipulator and the location of its base are being calibrated. If the manipulator is being calibrated with respect to its own base, then the error matrix  $\mathbf{E}_0$  (which models the errors of the base location) is eliminated, reducing the number of generalized errors to  $6n$ . The generalized errors that depend on the system geometry, the system task loads and the system joint variables can be calculated from the physical errors link by link. Note that system weight effects can be included in the model as a simple function of joint variables.

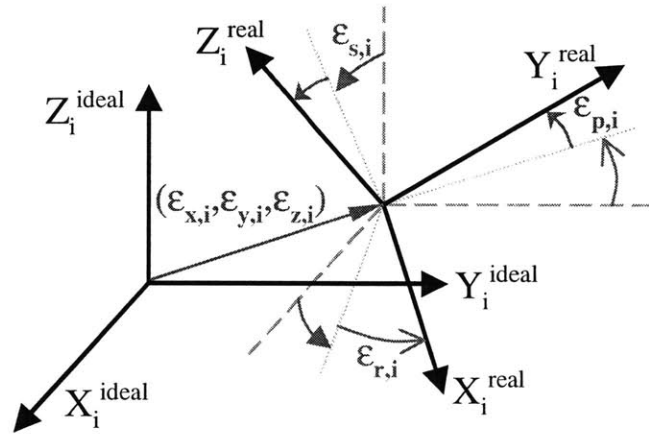


**Figure 2.4 - Translational and Rotational Generalized Errors for  $i^{\text{th}}$  Link**

With generalized errors the manipulator loop closure equation takes the form:

$$\mathbf{A}_{LC}(\mathbf{q}, \varepsilon, \mathbf{s}) = \mathbf{E}_0 \mathbf{A}_1 \mathbf{E}_1 \mathbf{A}_2 \mathbf{E}_2 \dots \mathbf{A}_n \mathbf{E}_n \quad (2.5)$$

where  $\mathbf{A}_{LC}$  is a  $4 \times 4$  homogeneous matrix of the form of Equation (2.4) that describes the position and orientation of the end-effector frame with respect to the inertial reference frame as a function of the configuration parameters  $\mathbf{q}$ , the vector of the generalized errors

$\epsilon$ , and the vector of the structural parameters  $\mathbf{s}$ . The translational components of the matrix  $\mathbf{A}_{LC}$  and the three angles of its rotational components are the six coordinates of the end-effector position and orientation vector  $\mathbf{X}^{\text{real}}$ .

The end-effector position and orientation error  $\Delta\mathbf{X}$  is defined as the 6x1 vector that represents the difference between the real position and orientation of the end-effector and the ideal one:

$$\Delta\mathbf{X} = \mathbf{X}^{\text{real}} - \mathbf{X}^{\text{ideal}} \quad (2.6)$$

where  $\mathbf{X}^{\text{real}}$  and  $\mathbf{X}^{\text{ideal}}$  are the 6x1 vectors composed of the three positions and three orientations of the end-effector reference frame in the inertial reference system for the real and ideal cases, respectively.

Since the generalized errors are small,  $\Delta\mathbf{X}$  can be calculated by the following linear equation in  $\epsilon$ :

$$\Delta\mathbf{X} = \mathbf{J}_e \epsilon \quad (2.7)$$

where  $\mathbf{J}_e$  is the 6x6(n+1) Jacobian matrix of the end-effector error  $\Delta\mathbf{X}$  with respect to the elements of the generalized error vector  $\epsilon$ , also known as Identification Jacobian matrix (Zhuang et al. 1999). As with the generalized errors,  $\mathbf{J}_e$  depends on the system configuration, geometry and task loads.

If the generalized errors,  $\epsilon$ , can be found from calibration measurements, then the correct end-effector position and orientation error can be calculated using Equation (2.7) and be compensated. Figure 2.5 shows schematically an error compensation algorithm based on Equation (2.7). The method to obtain  $\epsilon$  from experimental measurements is explained below.

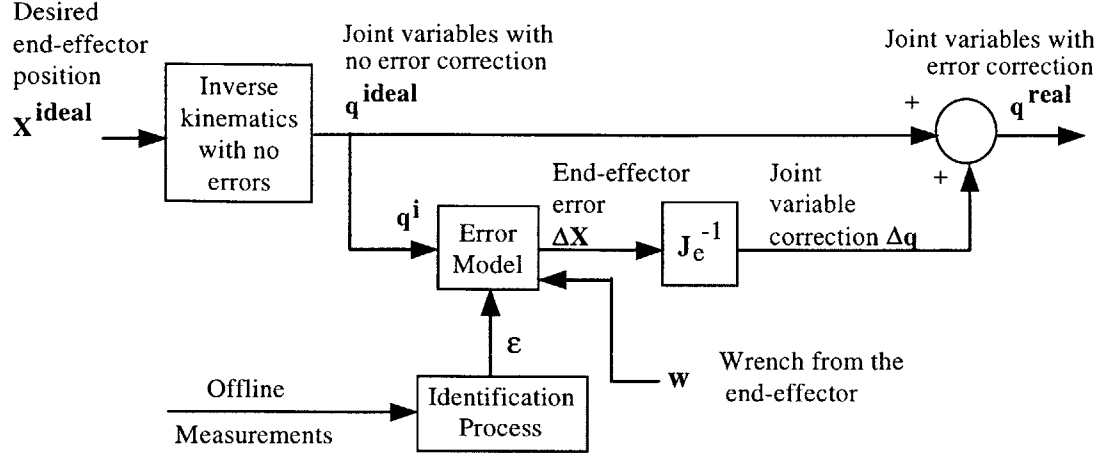


**Figure 2.5 - Error Compensation Scheme**

To calculate the generalized errors  $\epsilon$  it is assumed that some components of vector  $\Delta\mathbf{X}$  can be measured at a finite number of different manipulator configurations. However, since position coordinates are much easier to measure in practice than orientations, in many cases only the three position coordinates of  $\Delta\mathbf{X}$  are measured.

Assuming that all 6 components of  $\Delta\mathbf{X}$  can be measured, for an  $n$  degree of freedom manipulator,  $6(n+1)$  generalized errors  $\epsilon$  can be calculated by measuring  $\Delta\mathbf{X}$  at  $m$  different configurations, defined as  $\mathbf{q}_1, \mathbf{q}_2, \dots, \mathbf{q}_m$ , then writing Equation (2.7)  $m$  times:

$$\Delta\mathbf{X}_t = \begin{bmatrix} \Delta\mathbf{X}_1 \\ \Delta\mathbf{X}_2 \\ \dots \\ \Delta\mathbf{X}_m \end{bmatrix} = \begin{bmatrix} \mathbf{J}_e(\mathbf{q}_1) \\ \mathbf{J}_e(\mathbf{q}_2) \\ \dots \\ \mathbf{J}_e(\mathbf{q}_m) \end{bmatrix} \cdot \epsilon = \mathbf{J}_t \cdot \epsilon \quad (2.8)$$

where  $\Delta\mathbf{X}_t$  is the  $m \times 1$  vector formed by all measured vectors  $\Delta\mathbf{X}$  at  $m$  different configurations and  $\mathbf{J}_t$  is the  $6m \times 6(n+1)$  matrix formed by the  $m$  Identification Jacobian matrices  $\mathbf{J}_e$  at  $m$  configurations, called here Total Identification Jacobian. To reduce the effects of measurement noise, the number of measurements  $m$  is, in general, much larger than  $n$ .

If the generalized errors  $\epsilon$  are constant, then a unique least-squares estimate  $\hat{\epsilon}$  can be calculated by:

$$\hat{\epsilon} = (\mathbf{J}_t^T \mathbf{J}_t)^{-1} \mathbf{J}_t^T \cdot \Delta \mathbf{X}_t \quad (2.9)$$

However, if the Identification Jacobian matrix  $\mathbf{J}_e(\mathbf{q}_i)$  contains linearly dependent columns, Equation (2.9) will produce estimates with poor accuracy due to poor matrix conditioning (Hollerbach et al. 1996). This occurs when there is redundancy in the error model, in which case it is not possible to distinguish the error contributed by each generalized error component. Conventional calibration methods also cannot be successfully applied when some of the generalized errors depend on the manipulator configuration  $\mathbf{q}$  or the end-effector wrench  $\mathbf{w}$ , namely  $\epsilon(\mathbf{q}, \mathbf{w})$ , such as when elastic deflections that depend on the configuration and applied forces at the end-effector are significant. Chapters 3 and 4 present respectively methods for finding the generalized errors ( $\epsilon$ ) for the case where there is a singular Identification Jacobian matrix and where there are significant elastic deformations combined with conventional geometric errors.

## 2.4 Summary and Conclusions

This chapter presented the theoretical framework for the BSC method, and a simplified form of the algorithm was formulated for the fine-motion case. A generalized error formulation was presented for classical manipulator calibration, which can be used to identify the system geometric errors. However, classical calibration methods do not explicitly compensate for elastic errors due to the wrench at the end-effector. In addition, redundant error parameters must be eliminated from the error model prior to the identification process to perform calibration with improved accuracy. Chapters 3 and 4

present an analytical method to eliminate the redundant parameters, and introduce a calibration method that identifies both geometric and elastic deformation errors.



## Elimination of Redundant Error Parameters

---

### 3.1 Introduction

This chapter presents a general analytical method to eliminate redundant error parameters in robot calibration. Section 3.2 presents analytical expressions and physical interpretation of the linear combinations of generalized errors. Section 3.3 contains simulation results for a PUMA 560 and an Adept SCARA manipulator, showing the number of identifiable error parameters in each case and comparing the analytical formulation to ad-hoc methods.

### 3.2 Eliminating Redundant Errors

In robot calibration, redundant errors must be eliminated from the error model prior to the identification process. This is usually done in an ad-hoc or numerical manner by reducing the columns of the Identification Jacobian matrix  $\mathbf{J}_e$  to a linearly independent set (Hollerbach, 1988). Here, an analytical method is presented to eliminate the redundant parameters. Section 3.2.1 presents the linear combinations of the columns of the Identification Jacobian matrix and the method to eliminate the redundant errors to obtain the non-singular Identification Jacobian matrix. Section 3.2.2 discusses physical

interpretations of the linear combinations. Section 3.2.3 presents additional linear combinations introduced when only the end-effector position is measured. Section 3.2.4 shows the number of independent error parameters for a general serial link manipulator. Section 3.2.5 extends the results obtained using the six-parameter representation to the Denavit-Hartenberg error parameterization. It also shows that the D.H. representation of errors does not model some of the generalized errors in the presence of parallel joints, which can adversely affect the identification process.

### 3.2.1 Linear Combinations of the Identification Jacobian matrix

In this section, the linear combinations of the columns of the Identification Jacobian matrix  $\mathbf{J}_e$  are presented. The six-parameter representation is used to define the errors, and the linear combination coefficients are expressed through the robot's D.H. parameters. Defining  $\mathbf{J}_{x,i}$ ,  $\mathbf{J}_{y,i}$ ,  $\mathbf{J}_{z,i}$ ,  $\mathbf{J}_{s,i}$ ,  $\mathbf{J}_{r,i}$  and  $\mathbf{J}_{p,i}$  as the columns of  $\mathbf{J}_e$  associated with the generalized error components  $\epsilon_{x,i}$ ,  $\epsilon_{y,i}$ ,  $\epsilon_{z,i}$ ,  $\epsilon_{s,i}$ ,  $\epsilon_{r,i}$  and  $\epsilon_{p,i}$  respectively ( $i$  between 0 and  $n$ ), Equation (2.7) can be rewritten as

$$\Delta \mathbf{X} = [\mathbf{J}_{x,0}, \dots, \mathbf{J}_{x,i}, \mathbf{J}_{y,i}, \mathbf{J}_{z,i}, \mathbf{J}_{s,i}, \mathbf{J}_{r,i}, \mathbf{J}_{p,i}, \dots, \mathbf{J}_{p,n}] \cdot [\epsilon_{x,0}, \dots, \epsilon_{x,i}, \epsilon_{y,i}, \epsilon_{z,i}, \epsilon_{s,i}, \epsilon_{r,i}, \epsilon_{p,i}, \dots, \epsilon_{p,n}]^T \quad (3.1)$$

For each link  $i$ , between 1 and  $n$ , the following linear combinations are always valid (see Appendix A for proof):

$$\mathbf{J}_{z,(i-1)} \equiv \sin \alpha_i \mathbf{J}_{y,i} + \cos \alpha_i \mathbf{J}_{z,i} \quad (3.2)$$

$$\mathbf{J}_{r,(i-1)} \equiv a_i \cos \alpha_i \mathbf{J}_{y,i} - a_i \sin \alpha_i \mathbf{J}_{z,i} + \sin \alpha_i \mathbf{J}_{s,i} + \cos \alpha_i \mathbf{J}_{r,i} \quad (3.3)$$

where the manipulator parameters are defined using the D.H. representation: link lengths  $a_i$ , joint offsets  $d_i$ , joint angles  $\theta_i$ , and skew angles  $\alpha_i$ . If joint  $i$  is prismatic, then additional combinations of the columns of  $\mathbf{J}_e$  are found:

$$\mathbf{J}_{x,(i-1)} \equiv \mathbf{J}_{x,i} \quad (3.4)$$

$$\mathbf{J}_{y,(i-1)} \equiv \cos \alpha_i \mathbf{J}_{y,i} - \sin \alpha_i \mathbf{J}_{z,i} \quad (3.5)$$

The linear combinations shown above are always present, independently of the values of  $a_i$  and  $\alpha_i$ , even for degenerate cases (such as  $a_i=0$ ). As shown in Appendix A, if the full pose of the end-effector (both position and orientation) is measured, then Equations (3.2-3.5) are the only linear combinations for link  $i$ .

To obtain the non-singular Identification Jacobian matrix, called here  $\mathbf{G}_e$ , columns  $\mathbf{J}_{z,(i-1)}$  and  $\mathbf{J}_{r,(i-1)}$  must be eliminated from the matrix  $\mathbf{J}_e$  for all values of  $i$  between 1 and  $n$ . If joint  $i$  is prismatic, then columns  $\mathbf{J}_{x,(i-1)}$  and  $\mathbf{J}_{y,(i-1)}$  must also be eliminated. For an  $n$  DOF manipulator with  $r$  rotary joints and  $p$  ( $p$  equal to  $n-r$ ) prismatic joints, a total of  $2r+4p$  columns are eliminated from the Identification Jacobian  $\mathbf{J}_e$  to form its submatrix  $\mathbf{G}_e$ . This means that  $2r+4p$  generalized errors cannot be obtained by measuring the end-effector pose.

By definition, the dependent error parameters eliminated from  $\boldsymbol{\varepsilon}$  do not affect the end-effector error, resulting in the identity

$$\Delta \mathbf{X} = \mathbf{J}_e \boldsymbol{\varepsilon} \equiv \mathbf{G}_e \boldsymbol{\varepsilon}^* \quad (3.6)$$

Using the above identity and the linear combinations of the columns of  $\mathbf{J}_e$  from Equations (3.2-3.5), it is possible to obtain all relationships between the generalized error set  $\boldsymbol{\varepsilon}$  and

its independent subset,  $\epsilon^*$  (see Appendix A). If joint  $i$  is revolute ( $i$  between 1 and  $n$ ), then the generalized errors  $\epsilon_{z,(i-1)}$  and  $\epsilon_{r,(i-1)}$  are eliminated, and its values are incorporated into the independent error parameters  $\epsilon_{y,i}^*$ ,  $\epsilon_{z,i}^*$ ,  $\epsilon_{s,i}^*$  and  $\epsilon_{r,i}^*$ :

$$\begin{cases} \epsilon_{y,i}^* \equiv \epsilon_{y,i} + \epsilon_{z,(i-1)} \sin \alpha_i + \epsilon_{r,(i-1)} \cdot a_i \cos \alpha_i \\ \epsilon_{z,i}^* \equiv \epsilon_{z,i} + \epsilon_{z,(i-1)} \cos \alpha_i - \epsilon_{r,(i-1)} \cdot a_i \sin \alpha_i \\ \epsilon_{s,i}^* \equiv \epsilon_{s,i} + \epsilon_{r,(i-1)} \sin \alpha_i \\ \epsilon_{r,i}^* \equiv \epsilon_{r,i} + \epsilon_{r,(i-1)} \cos \alpha_i \end{cases} \quad (3.7)$$

If joint  $i$  is prismatic, then the translational errors  $\epsilon_{x,(i-1)}$  and  $\epsilon_{y,(i-1)}$  are eliminated, and its values are incorporated into the independent error parameters  $\epsilon_{x,i}^*$ ,  $\epsilon_{y,i}^*$  and  $\epsilon_{z,i}^*$ . In this case, Equation (3.7) becomes:

$$\begin{cases} \epsilon_{x,i}^* \equiv \epsilon_{x,i} + \epsilon_{x,(i-1)} \\ \epsilon_{y,i}^* \equiv \epsilon_{y,i} + \epsilon_{y,(i-1)} \cos \alpha_i + \epsilon_{z,(i-1)} \sin \alpha_i + \epsilon_{r,(i-1)} \cdot a_i \cos \alpha_i \\ \epsilon_{z,i}^* \equiv \epsilon_{z,i} - \epsilon_{y,(i-1)} \sin \alpha_i + \epsilon_{z,(i-1)} \cos \alpha_i - \epsilon_{r,(i-1)} \cdot a_i \sin \alpha_i \\ \epsilon_{s,i}^* \equiv \epsilon_{s,i} + \epsilon_{r,(i-1)} \sin \alpha_i \\ \epsilon_{r,i}^* \equiv \epsilon_{r,i} + \epsilon_{r,(i-1)} \cos \alpha_i \end{cases} \quad (3.8)$$

If the vector  $\epsilon^*$  containing the independent errors is constant, then the matrix  $\mathbf{G}_e$  can be used to replace  $\mathbf{J}_e$  in Equation (2.7), and Equation (2.9) is applied to calculate the estimate of the independent generalized errors  $\epsilon^*$ , completing the identification process. However, if non-geometric factors are considered (e.g. link compliance, gear eccentricity), then it is necessary to further model the parameters of  $\epsilon^*$  as a function of the system configuration prior to the identification process. This situation will be discussed in Chapter 4.

### 3.2.2 Physical Interpretation of the Linear Combinations

In this section the physical interpretation of Equations (3.2-3.5) is presented. Each equation associates a generalized error from link  $i-1$  with a combination of errors from link  $i$  that result in end-effector errors of the same magnitude and direction. Since it is not possible to distinguish the amount of error contributed by each generalized error, the errors associated with link  $i-1$  are indistinguishable.

Equation (3.2) reflects the fact that the translational error along the Z-axis of frame  $i-1$  has the same effect as a combination of the translational errors along the Y and Z axes of frame  $i$  (see Figure 3.1). This relation is easily explained by the fact that the skew angle  $\alpha_i$  between the axes of joints  $i-1$  and  $i$  is constant.

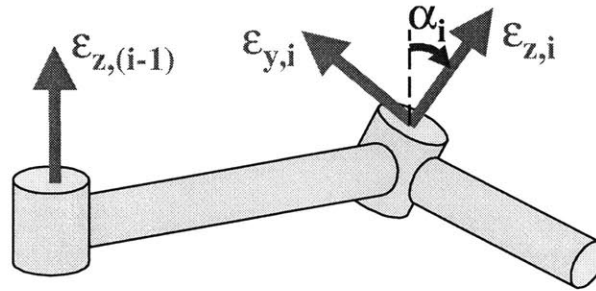


**Figure 3.1 - Linear Combination of Translational Generalized Errors**

Equation (3.3) states that the rotational error along the Z-axis of frame  $i-1$  has the same effect as a combination of the rotational and translational errors along the Y and Z axes of frame  $i$ . For simplicity, a planar manipulator is used to explain this combination (see Figure 3.2). The top figure shows the end-effector translational and rotational errors  $\Delta \mathbf{X}_t$  and  $\Delta \mathbf{X}_r$  caused by the rotational generalized error  $\epsilon_{r,(i-1)}$  of frame  $i-1$ . The bottom figure shows that the same end-effector errors can be reproduced by a specific combination of the translational error  $\epsilon_{y,i}$  and the rotational error  $\epsilon_{r,i}$  of frame  $i$ . To obtain

the same end-effector errors in this case, it is required that  $\epsilon_{y,i} = \epsilon_{r,(i-1)} \cdot a_i$  and  $\epsilon_{r,i} = \epsilon_{r,(i-1)}$  (see the relationship between  $\epsilon^*$  and  $\epsilon$  in Appendix A).

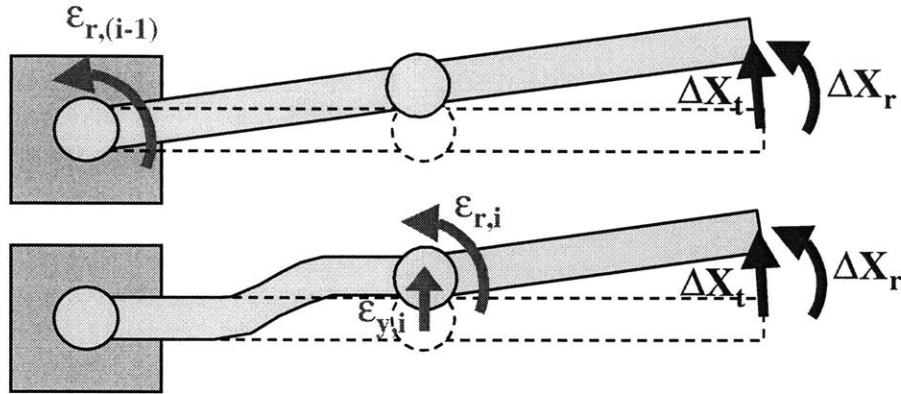


**Figure 3.2 - Error Combinations Resulting in Same End-Effector Errors**

If joint  $i$  is prismatic, then Equations (3.4) and (3.5) are also valid. These combinations simply state that the effects of the generalized errors along the X and Y axes of frame  $i-1$  can always be reproduced by a combination of the three translational generalized errors of frame  $i$  (see Figure 3.3). This is always true for prismatic joints, since such joints only move along the Z-axis of frame  $i-1$  (using the D.H. frame definition).

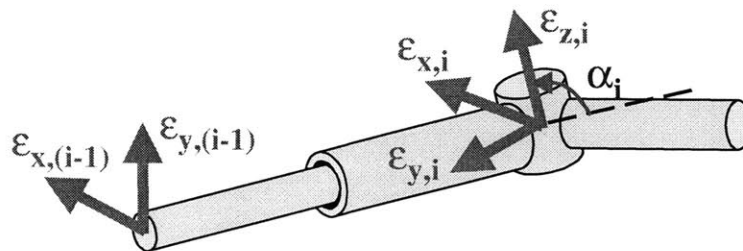


**Figure 3.3 - Linear Combinations of Generalized Errors in Prismatic Joints**

### 3.2.3 Partial Measurement of End-Effector Pose

The linear combinations of the columns of the Identification Jacobian matrix  $\mathbf{J}_e$  shown in Equations (3.2-3.5) are obtained when both position and orientation of the end-effector are considered. In the case where only the end-effector position is measured, its orientation can take any value, resulting in additional linear combinations. In this case, the three last columns of  $\mathbf{J}_e$  are zero vectors (see Appendix A):

$$\mathbf{J}_{s,n} \equiv \mathbf{J}_{r,n} \equiv \mathbf{J}_{p,n} \equiv \mathbf{0} \quad (3.9)$$

Equation (3.9) means, as expected, that the three rotational errors of the end-effector frame  $\epsilon_{s,n}$ ,  $\epsilon_{r,n}$  and  $\epsilon_{p,n}$  do not influence the end-effector position (they only affect the orientation, which is not being measured). As a result, these generalized errors are not obtainable.

If the last joint is prismatic, then no further linear combinations are found. However, if the last joint is revolute and its link length  $a_n$  is zero, then three more linear combinations are present (see Appendix A):

$$\mathbf{J}_{s,(n-1)} \equiv d_n \mathbf{J}_{x,(n-1)} \quad (3.10)$$

$$\mathbf{J}_{p,(n-1)} \equiv -d_n \mathbf{J}_{y,(n-1)} \quad (3.11)$$

$$\mathbf{J}_{r,(n-1)} \equiv \mathbf{0} \quad (3.12)$$

meaning that the effects of  $\epsilon_{s,(n-1)}$  and  $\epsilon_{p,(n-1)}$  cannot be distinguished from the ones caused by  $\epsilon_{x,(n-1)}$  and  $\epsilon_{y,(n-1)}$ , and also the generalized error  $\epsilon_{r,(n-1)}$  is not obtainable. If both link length  $a_n$  and joint offset  $d_n$  are zero, then the origin of frames  $n-1$  and  $n$  coincide at the end-effector position. In this case, Equations (3.9-3.12) can be recursively applied to frames  $n-1$ ,  $n-2$ , and so on, as long as the origin of these frames all lie at the end-effector position. See Appendix A for more details.

### 3.2.4 Number of Independent Generalized Errors

As a corollary of Equations (3.2-3.12), the number of independent generalized errors for a generic serial link manipulator can be calculated. Upper bounds of this number have been presented in the literature (Roth, Mooring and Ravani, 1987; Zhuang, Roth and Hamano, 1992), but not its exact value. Table 3.1 shows the number of generalized errors, the number of linear dependencies, and the number of independent generalized errors for both robot calibration (without modeling its base frame errors) and robot plus base location calibration.

**Table 3.1 – Number of Independent Generalized Errors**

	Robot+Base Calibration	Robot Calibration
# generalized errors	$6(n+1)$	$6n$
# linear dependencies	$2r + 4p + k$	$2r' + 4p' + k$
# independent errors	$6(n+1) - (2r + 4p + k)$	$6n - (2r' + 4p' + k)$

where

$n$  : # of joints in the manipulator

$r ; r'$  : # of revolute joints including/excluding joint 1

$p ; p'$  : # of prismatic joints including/excluding joint 1

$$k : \begin{cases} 0 & \text{if measuring end-effector position and orientation} \\ 3 & \text{if only measuring end-effector position and either the last joint is prismatic or } a_n \neq 0 \\ 3 + 2q & \text{if only measuring end-effector position, the last } q \text{ joints are revolute, and} \\ & a_{n-q+1} \equiv a_{n-q+2} \equiv a_{n-q+3} \equiv \dots \equiv a_n \equiv 0 \text{ and } d_{n-q+2} \equiv d_{n-q+3} \equiv \dots \equiv d_n \equiv 0 \end{cases}$$



### 3.2.5 Extension to Four-Parameter Error Representations

The six-parameter representation of the errors is used above to obtain all linear combinations of the generalized errors. If a four-parameter representation is chosen for the identification process, the previous results can still be applied to eliminate the redundant parameters, through an adaptation of Equations (3.2-3.5). The extension of the results to four-parameter error representations is easily accomplished because such parameterizations are a subset of the generalized error representation.

The four Denavit-Hartenberg error parameters of link  $i$  are exactly the rotational and translational errors along the Z-axis of frame  $i-1$  and the X-axis of frame  $i$  of the six-parameter representation. Namely, the errors along the link lengths  $a_i$ , skew angles  $\alpha_i$ , joint offsets  $d_i$ , and joint angle offsets  $\theta_i$  of link  $i$  are respectively mapped to the generalized errors  $\epsilon_{x,i}$ ,  $\epsilon_{p,i}$ ,  $\epsilon_{z,(i-1)}$ , and  $\epsilon_{r,(i-1)}$ . This implies that the translational and rotational errors along the Y-axis of every frame,  $\epsilon_{y,i}$  and  $\epsilon_{s,i}$ , are not modeled when the D.H. error representation is used. If the manipulator does not have parallel joints then  $\epsilon_{y,i}$  and  $\epsilon_{s,i}$  can be replaced by a combination of the errors along  $d_i$  and  $\theta_i$ , see Equation (3.7). However, if joints  $i-1$  and  $i$  are parallel, then the rotation error  $\epsilon_{s,i}$  cannot be obtained from the D.H. representation. In addition, if the link length  $a_i$  is zero, then the translation error  $\epsilon_{y,i}$  is also non-obtainable. This means that the entire calibration can be compromised if the manipulator has significant errors in those directions. Hayati's modification of the D.H. representation (Hayati, 1983) only partially solves this problem, because it introduces an angular alignment parameter that models the Y-axis rotation error  $\epsilon_{s,i}$ , but not the translation error  $\epsilon_{y,i}$ .

Since the generalized errors  $\epsilon_{y,i}$  and  $\epsilon_{s,i}$  are not modeled when using the D.H. error representation, the column vectors  $\mathbf{J}_{y,i}$  and  $\mathbf{J}_{s,i}$  are not present in the Identification Jacobian. Thus, Equations (3.2-3.5) can only be applied to the D.H. representation if both  $\mathbf{J}_{y,i}$  and  $\mathbf{J}_{s,i}$  are not present in the linear combination. This is never true for Equations (3.3) and (3.5), but Equation (3.2) can be applied if  $\sin(\alpha_i)$  is null, due to parallel joints. In this case, the following linear combinations of the D.H. error parameters are valid:

$$\begin{cases} \epsilon_{z,i}^* = \epsilon_{z,i} + \epsilon_{z,(i-1)} \\ \epsilon_{r,i}^* = \epsilon_{r,i} + \epsilon_{r,(i-1)} \end{cases} \Rightarrow \begin{cases} \delta d_{i+1}^* = \delta d_{i+1} + \delta d_i \\ \delta \theta_{i+1}^* = \delta \theta_{i+1} + \delta \theta_i \end{cases} \quad (3.13)$$

Finally, if joint  $i$  is prismatic, then Equation (3.4) results in one additional linear combination

$$\epsilon_{x,i}^* = \epsilon_{x,i} + \epsilon_{x,(i-1)} \Rightarrow \delta a_i^* = \delta a_i + \delta a_{i-1} \quad (3.14)$$

As seen in Equations (3.13) and (3.14), even though the D.H. representation results in fewer linear combinations, redundant parameters may still be present.

In summary, the D.H. error representation does not model some of the physical errors if parallel joints are present and still presents linear combinations that need to be eliminated. Since the redundancy of the six-parameter error representation can be eliminated with the method described in this chapter, the use of such parameterization in robot calibration is recommended.

### 3.3 Simulation Results

Simulations were performed on a PUMA 560 and an Adept SCARA manipulator. The six-parameter error representation was used and its redundant parameters were eliminated using Equations (3.2-3.5). Simulated measurements were obtained and the introduced error parameters were identified using Equation (2.9).

For the calibration of a PUMA 560 robot and its base by measuring the end-effector position only, 27 error parameters were identified. This result is in agreement with (Ikits and Hollerbach, 1997) and also with Table 3.1 (using  $n=6$ ,  $r=6$ ,  $p=0$  and  $k=3$ ).

For an Adept SCARA robot, 20 error parameters were identified by measuring both end-effector position and orientation, which agrees with Table 3.1 (using  $n=4$ ,  $r=3$ ,  $p=1$  and  $k=0$ ). Although the D.H. error representation also models 20 parameters in this case, only 15 of these parameters are independent and identifiable. The error parameters  $\epsilon_{s,1}$ ,  $\epsilon_{s,2}$ ,  $\epsilon_{s,3}$ ,  $\epsilon_{y,4}$  and  $\epsilon_{s,4}$  cannot be identified using the D.H. error representation due to parallel joints in the system. Even if Hayati's modification (Hayati, 1983) is introduced, the translation error  $\epsilon_{y,4}$  still remains unmodeled, showing that only the six-parameter representation can identify all 20 parameters in this case.

### 3.4 Summary and Conclusions

This chapter presented a general analytical method to eliminate the redundant error parameters in robot calibration. These errors, often non-intuitive, must be eliminated from the error model prior to the identification process, otherwise the robustness of the calibration can be compromised (Hollerbach, 1988). The analytical expressions and physical interpretation of the linear combinations present in the

generalized error parameterization were developed. The non-redundant form of the Identification Jacobian matrix was obtained using these expressions, allowing for the systematic calibration with improved accuracy of any serial link manipulator.

## **Geometric and Elastic Error Compensation (GEC)**

### **4.1 Introduction**

This chapter describes the GEC (Geometric and Elastic Error Compensation) method theory and experimental studies. Section 4.2 presents the theoretical framework for the GEC method. Section 4.3 contains experimental results for the Patient Positioning System. Section 4.4 presents the application of GEC to the nozzle dam placement task and shows experimental results for a Schilling Titan II manipulator.

### **4.2 GEC Theory**

In the GEC method (Geometric and Elastic Error Compensation), elastic deformation and classical geometric errors are considered in a unified manner. The method can identify and compensate for both types of error, without an explicit elastic model of the system. Two steps are necessary to successfully apply the GEC method. In the first step, presented in Chapter 3, the redundant error parameters must be eliminated from the identification model (as with any calibration method). In the second step, the

error model must be extended to consider the task loading wrench and configuration dependency of the errors. In this case, the independent generalized errors  $\epsilon^*$  are modeled as a function of the manipulator configuration  $\mathbf{q}$  and the end-effector wrench  $\mathbf{w}$ , or  $\epsilon^*(\mathbf{q}, \mathbf{w})$ . To predict the endpoint position of the manipulator for a given configuration and task wrench, it is necessary to calculate the generalized errors from a set of offline measurements. The complexity of these calculations can be substantially reduced if the generalized errors are parameterized using polynomial functions. The  $i^{th}$  element of vector  $\epsilon^*$  is approximated by a polynomial series expansion of the form:

$$\epsilon_i^* = \sum_{j=1}^{n_i} c_{i,j} \cdot f_{i,j}(\mathbf{q}, \mathbf{w}), \quad f_{i,j}(\mathbf{q}, \mathbf{w}) \equiv (w_{m_j})^{a_{0,j}} \cdot (q_1^{a_{1,j}} \cdot q_2^{a_{2,j}} \cdot \dots \cdot q_n^{a_{n,j}}) \quad (4.1)$$

where  $n_i$  is the number of terms used in each expansion,  $c_{i,j}$  are the constant polynomial coefficients,  $w_{m_j}$  is an element of the task wrench  $\mathbf{w}$ , and  $q_1, q_2, \dots, q_n$  are the manipulator joint parameters. It has been found that good accuracy can be obtained using only a few terms  $n_i$  in the above expansion (Meggiolaro et al. 1998). If elastic deflections of link  $i$  are considered, then the generalized errors created by these deflections would depend on the task wrench applied at the  $i^{th}$  link. For a serial manipulator, this deflection is due to the wrench at the end-effector and to the configuration of the links after the  $i^{th}$ . Hence, the wrench applied at the  $i^{th}$  link depends only on the joint parameters  $q_{i+1}, \dots, q_n$ . Thus, the number of terms in the products of Equation (4.1) is substantially reduced. Each generalized error parameter is then represented as a function of only a few of the system variables, greatly reducing the number of measurements required to characterize the system using the GEC method. Note that the effects of manipulator deformation due to its own weight are already included in the terms that are solely a function of  $\mathbf{q}$ .

The coefficients  $c_{i,j}$  are grouped into one vector  $\mathbf{c}$ , becoming the unknowns of the problem. The total number of unknown coefficients, called  $n_c$ , is the sum of the number of terms used in Equation (4.1) to approximate each generalized error, i.e.  $n_c = \sum n_i$ . The  $n_c$  functions  $f_{i,j}(\mathbf{q}, \mathbf{w})$  are then incorporated into the non-singular Identification Jacobian matrix  $\mathbf{G}_e$  by substituting Equation (4.1) into (3.6). Equation (3.6) becomes:

$$\Delta \mathbf{X} = \mathbf{G}_e(\mathbf{q}) \cdot \boldsymbol{\varepsilon}^*(\mathbf{q}, \mathbf{w}) \equiv \mathbf{H}_e(\mathbf{q}, \mathbf{w}) \cdot \mathbf{c} \quad (4.2)$$

where  $\mathbf{H}_e$  is the  $(6 \times n_c)$  Jacobian matrix of the end-effector error  $\Delta \mathbf{X}$  with respect to the polynomial coefficients  $c_{i,j}$ . The matrix  $\mathbf{H}_e$ , called here Extended Identification Jacobian matrix, can be obtained from Equations (4.1) and (4.2):

$$\mathbf{H}_e(\mathbf{q}, \mathbf{w}) \equiv [\mathbf{G}_1 \cdot f_{1,1}, \dots, \mathbf{G}_1 \cdot f_{1,n_1}, \dots, \mathbf{G}_i \cdot f_{i,1}, \mathbf{G}_i \cdot f_{i,2}, \dots, \mathbf{G}_i \cdot f_{i,n_i}, \dots] \quad (4.3)$$

where  $\mathbf{G}_i$  is the column of matrix  $\mathbf{G}_e$  associated to the generalized error component  $\varepsilon_i^*$ .

An estimate of the coefficient vector  $\mathbf{c}$  is then calculated by replacing  $\mathbf{J}_e$  with the matrix  $\mathbf{H}_e$  in Equation (2.8) and applying Equation (2.9), completing the identification process. Once the polynomial coefficients,  $\mathbf{c}$ , are identified, the end-effector position and orientation error  $\Delta \mathbf{X}$  can be calculated and compensated using Equation (4.2). The method of identifying the generalized errors as a function of the manipulator configuration and the end-effector wrench is summarized in Figure 4.1.

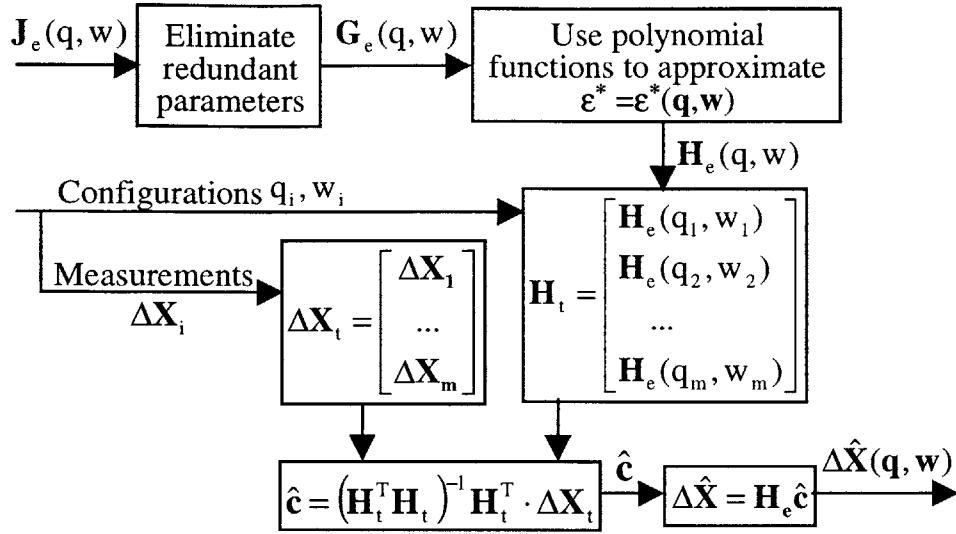


**Figure 4.1 - Flow-chart of the Method to Identify Generalized Errors**

### 4.3 Application to the Patient Positioning System

The PPS is a six degree of freedom robot manipulator (see Figure 1.2) built by General Atomics (Flanz et al. 1996). The first three joints are prismatic, with maximum travel of 225cm, 56cm and 147cm for the lateral (X), vertical (Y) and longitudinal (Z) axes, respectively. The last three joints are revolute joints. The first joint rotates parallel to the vertical (Y) axis and can rotate  $\pm 90^\circ$ . The last two joints are used for small corrections around an axis of rotation parallel to the Z (roll) and X (pitch) axes, and have a maximum rotation angle of  $\pm 3^\circ$ . The manipulator "end-effector" is a couch which supports the patient in a supine position, accommodating patients up to 188 cm in height and 300 lbs in weight in normal operation.

The intersection point of the proton beam with the gantry axis of rotation is called the system isocenter. The couch treatment volume is defined by a treatment area on the couch of 50cm x 50cm and a height of 40cm (see Figure 1.2). This area covers all



possible locations of treatment points (i.e. tumor locations in a patient). The objective is for the PPS to make any point in this volume be coincident with the isocenter at any orientation.

The joint parameters of the PPS are the displacements  $d_1$ ,  $d_2$ ,  $d_3$  of the three prismatic joints and the rotations  $\theta$ ,  $\alpha$ ,  $\beta$  of the three rotational joints, see Figure 4.2. A 6 axis force/torque sensor is placed between the couch and the last joint. By measuring the forces and moment at this point, it is possible to calculate the patient weight and the coordinates of the patient center of gravity. The system motions are very slow and smooth due to safety requirements. Hence, the system is quasi-static, and its dynamics do not influence the system accuracy and are neglected.

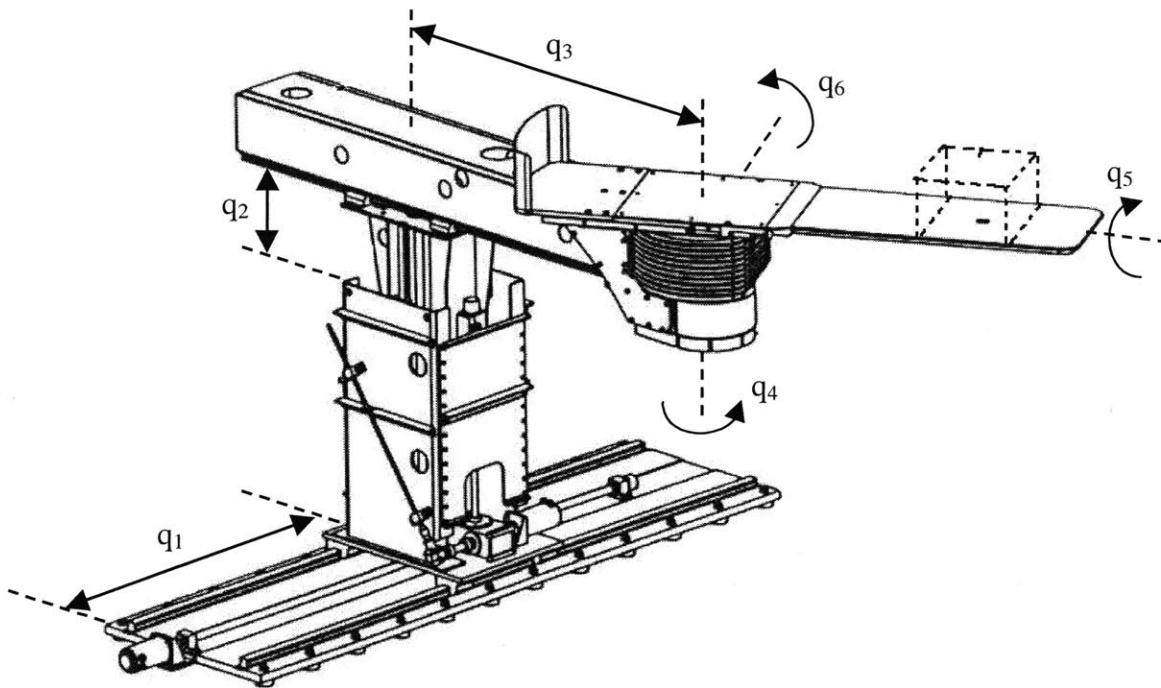


**Figure 4.2 - Joint Parameter Definition for the PPS [Ref. Flanz, 1996]**

The accuracy of the PPS was measured using a Leica 3D Laser Tracking System (see Figure 4.3). These measurements were to evaluate the PPS repeatability, the

nonlinearity of its weight dependent deflections, the inherent uncompensated PPS accuracy, and the method developed above.

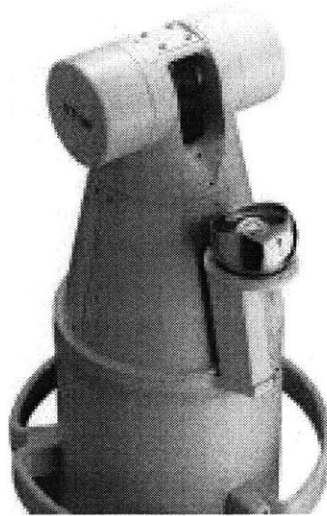


**Figure 4.3 - Leica 3D Laser Tracking System**

Three targets were placed on the couch at the positions  $P_1$ ,  $P_2$  and  $P_3$ , shown in Figure 4.4. The targets are located about 10 mm above the couch. The position accuracy of the measurements is approximately 0.04 mm.

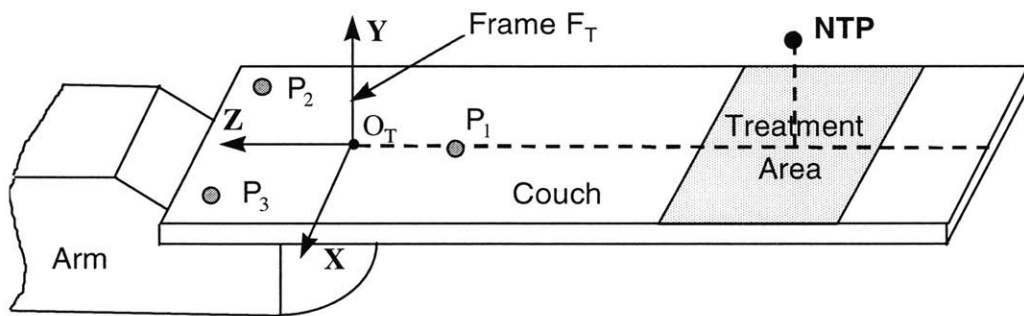


**Figure 4.4 - Close-up View of the PPS Couch**

A reference frame  $F_T$  is fixed to the couch (see Figure 4.4). The intersection point of the plane ( $P_1 P_2 P_3$ ) with the Y axis of the fixed reference frame is called  $O_T$ . A fixed reference frame,  $F_o$ , is used to express the coordinates of all points. When the PPS is at

its home configuration (all joint variables set equal to zero) the reference frames  $F_T$  and  $F_0$  are coincident. The location of a tumor on a patient, defined as the Nominal Treatment Point (NTP), is specified in the frame coordinate  $F_T$ . For the results presented below, the NTP coordinates in  $F_T$  are taken as (0, 90, -840) mm.

For more than 700 different configurations of the PPS and different weights the location of points  $P_1$ ,  $P_2$  and  $P_3$  in frame  $F_0$  were measured and the NTP coordinates in frame  $F_0$  calculated. From the ideal system kinematic model, the ideal coordinates of the NTP were calculated and subtracted from the experimentally measured values to yield the vector  $\Delta\mathbf{X}(\mathbf{q}, \mathbf{w})$ . 450 measurements were used to evaluate the basic uncompensated accuracy of the PPS and the accuracy of the compensation method described above. Two different payload configurations were used: one with no payload and another with a 154 lbs weight at the center of the treatment area. The PPS configurations used were grouped into two sets:

Set a) *Treatment Volume*. The 8 vertices of the treatment volume (see Figure 1.2) are reached with the NTP with angle  $\theta$  taking values from  $-90^\circ$  to  $90^\circ$  with a step of  $30^\circ$ , for a total of 112 configurations.

Set b) *Independent Motion of Each Axis*. Each axis is moved independently while all other axes are held at the home (zero) values. The step of motion for  $d_1$  is 50 mm, for  $d_2$  20 mm, for  $d_3$  25mm and for  $\theta$   $5^\circ$ , resulting in 338 configurations.

The PPS uncompensated accuracy combining the two sets is shown in Figures 4.5(a-b). The data points represent the positioning errors of NTP. In spite of the high quality of the PPS physical system, its uncompensated accuracy is on the order of 10mm. This is approximately 20 times higher than the specification of  $\pm 0.50$ mm.

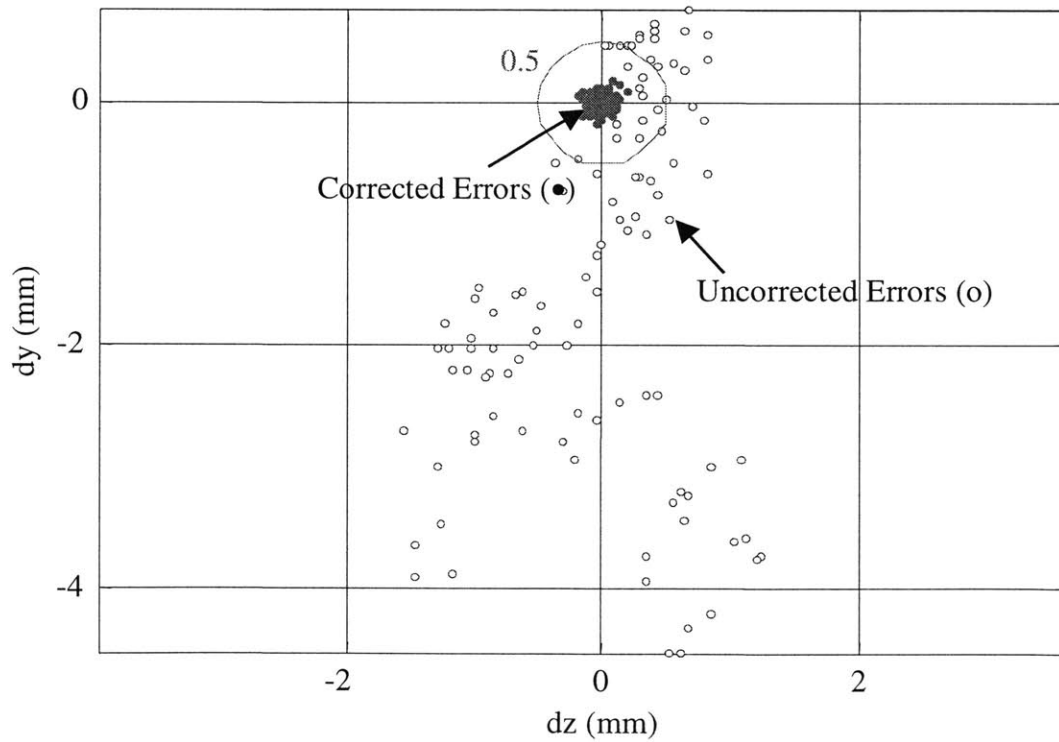
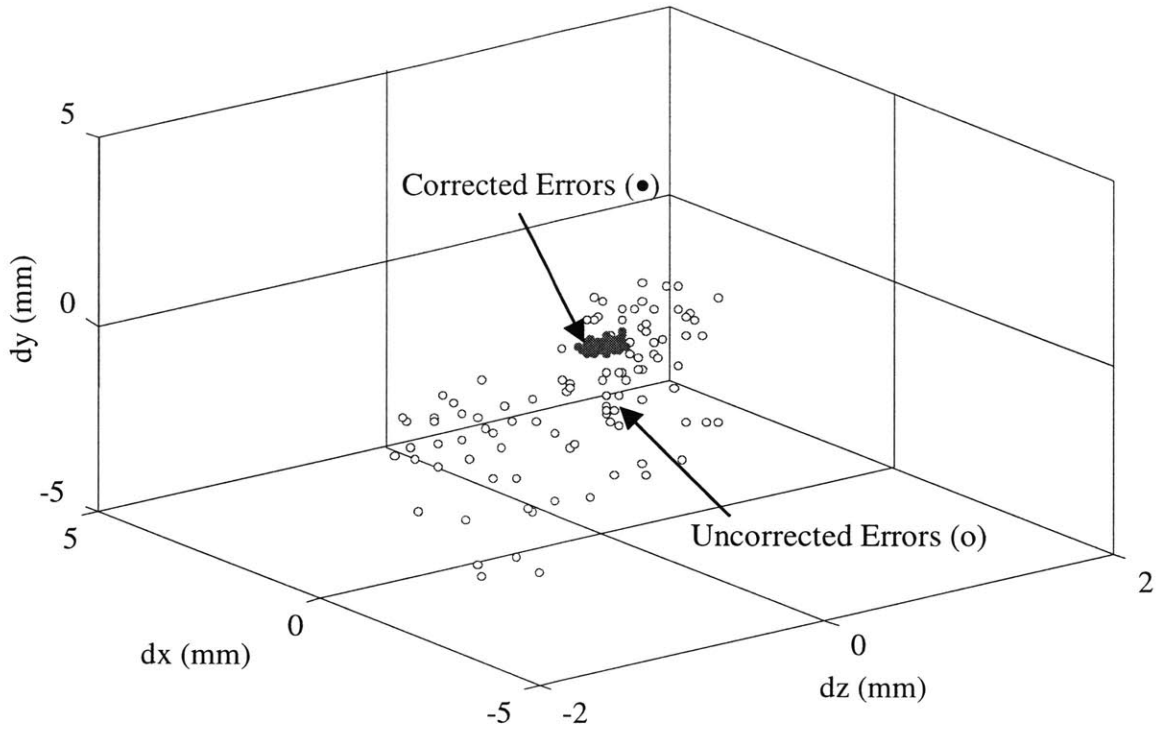


**Figure 4.5(a) - Measured and Residual Errors After Compensation**

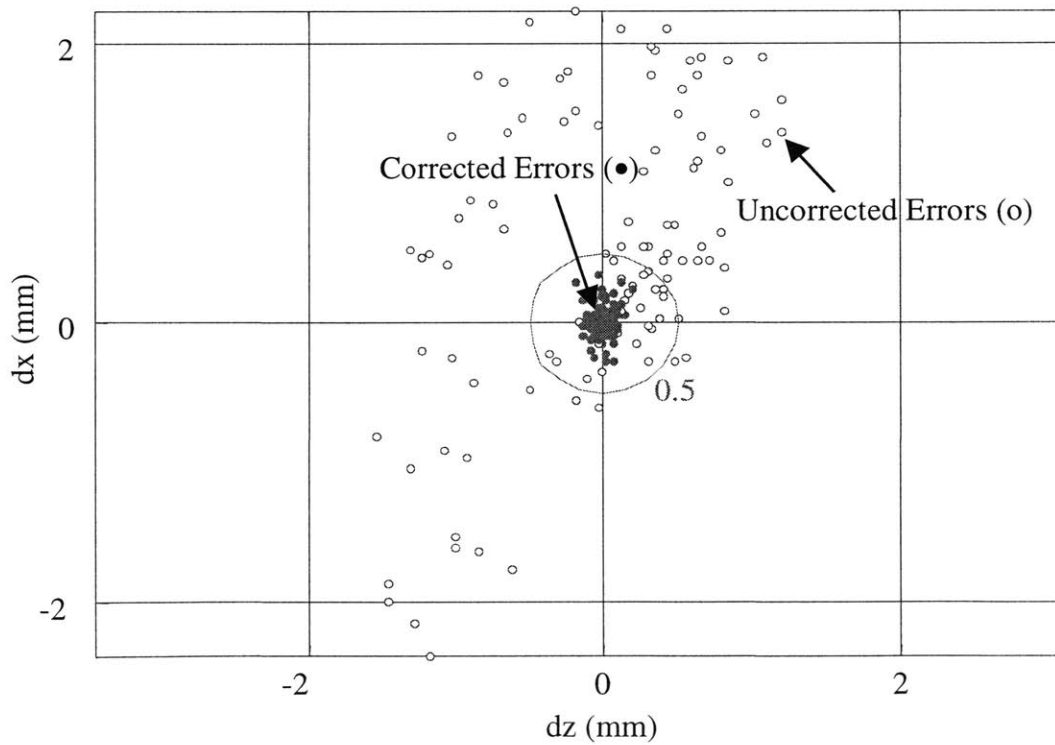
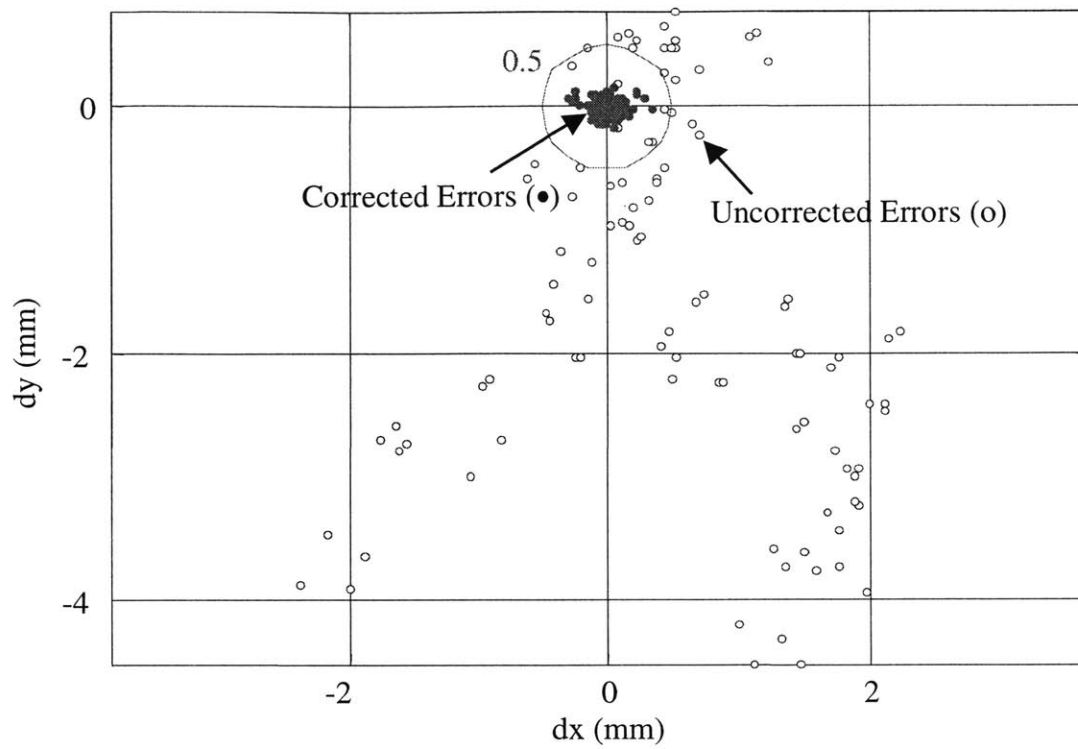


**Figure 4.5(b) - Measured and Residual Errors After Compensation**

Part of the uncompensated error is the repeatability errors. This error is due to the random system errors, and it cannot be compensated by a model based technique. They represent the accuracy limit of any error compensation algorithm and it also shows how well an error compensation technique performs. Here the system repeatability is based on how well the system would return the NTP to certain arbitrary configurations. A total of 270 measurements were taken with zero payload weight. Figure 4.6 shows the distributions of the repeatability errors for each axis. The repeatability error can be seen to be less than 0.15mm ( $3\sigma$ ). Thus this system is a good candidate for model based error correction methods, since the repeatability errors are relatively small compared to the  $\pm 0.50\text{mm}$  accuracy requirement.

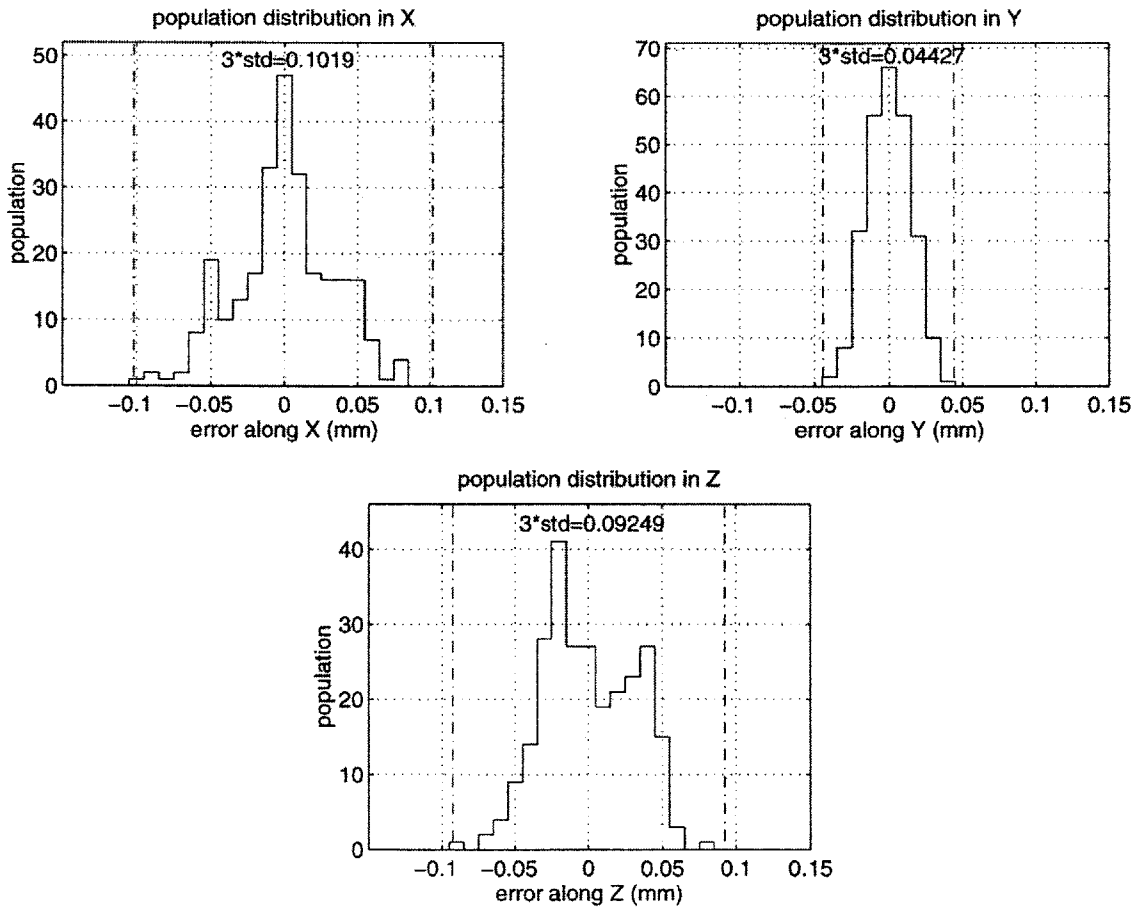


**Figure 4.6 - Repeatability Distribution**

In implementing the computation method a general nonlinear function of the wrench  $\mathbf{w}$  can be used. To help establish this function, the behavior of the PPS positioning errors for different payload weights was examined with measurements made at the home (zero) configuration. The weights ranged from 0 to 300 lbs in steps of approximately 25 lbs. The positioning errors of the PPS are nearly linear with the payload weight, and the least-square error is less than 0.1mm for the linear fit. Hence the generalized errors were taken as linear functions of the system wrench in Equation (4.1).

The redundant error parameters are eliminated from the error model using Equations (3.2-3.5). The generalized errors are then calculated with Equation (2.9) using the configurations of set (b) (independent motion of its axes) and half of the treatment volume data (set a). For a Pentium PC 300MHz, the computing time was less than one minute. Figures 4.7-4.9 show the measured and the GEC predicted errors at the NTP when each axis is moved independently. The PPS is then commanded to move to compensated points for the remaining configurations of set (a). The residual positioning errors of the PPS after compensation are shown in Figures 4.5(a-b). The residual errors are enclosed in a sphere of 0.38 mm radius which is smaller than the sphere of 0.5 mm radius that represents the accuracy specification. The required number of data points for this calculation was less than 400. The error distribution along each axis is shown in Figure 4.10. Hence the compensation method used in this paper enables the system to meet its specification and is now a key element in MGH's operational software.

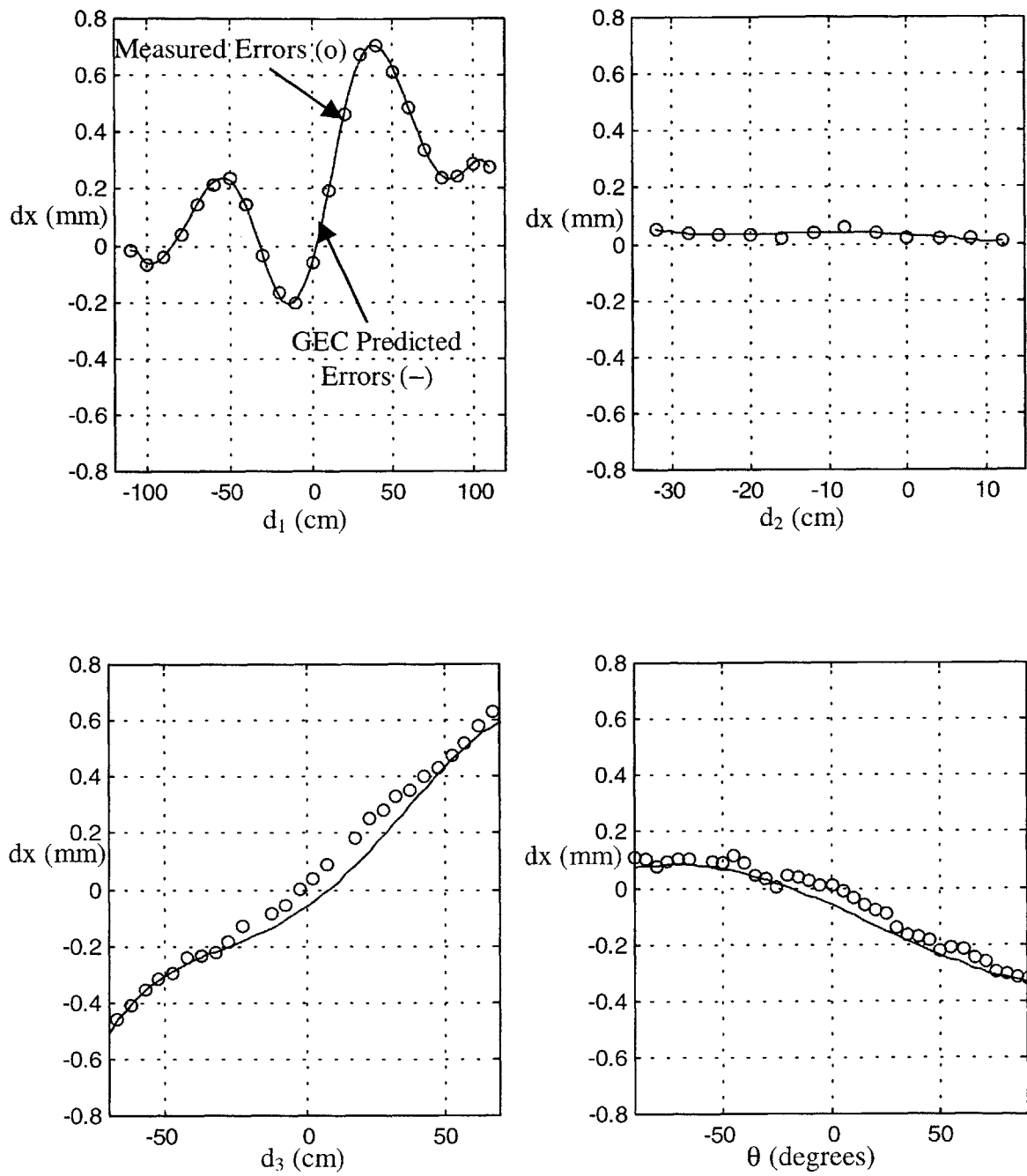


**Figure 4.7 - Measured and GEC Predicted Errors along the X Axis at NTP**



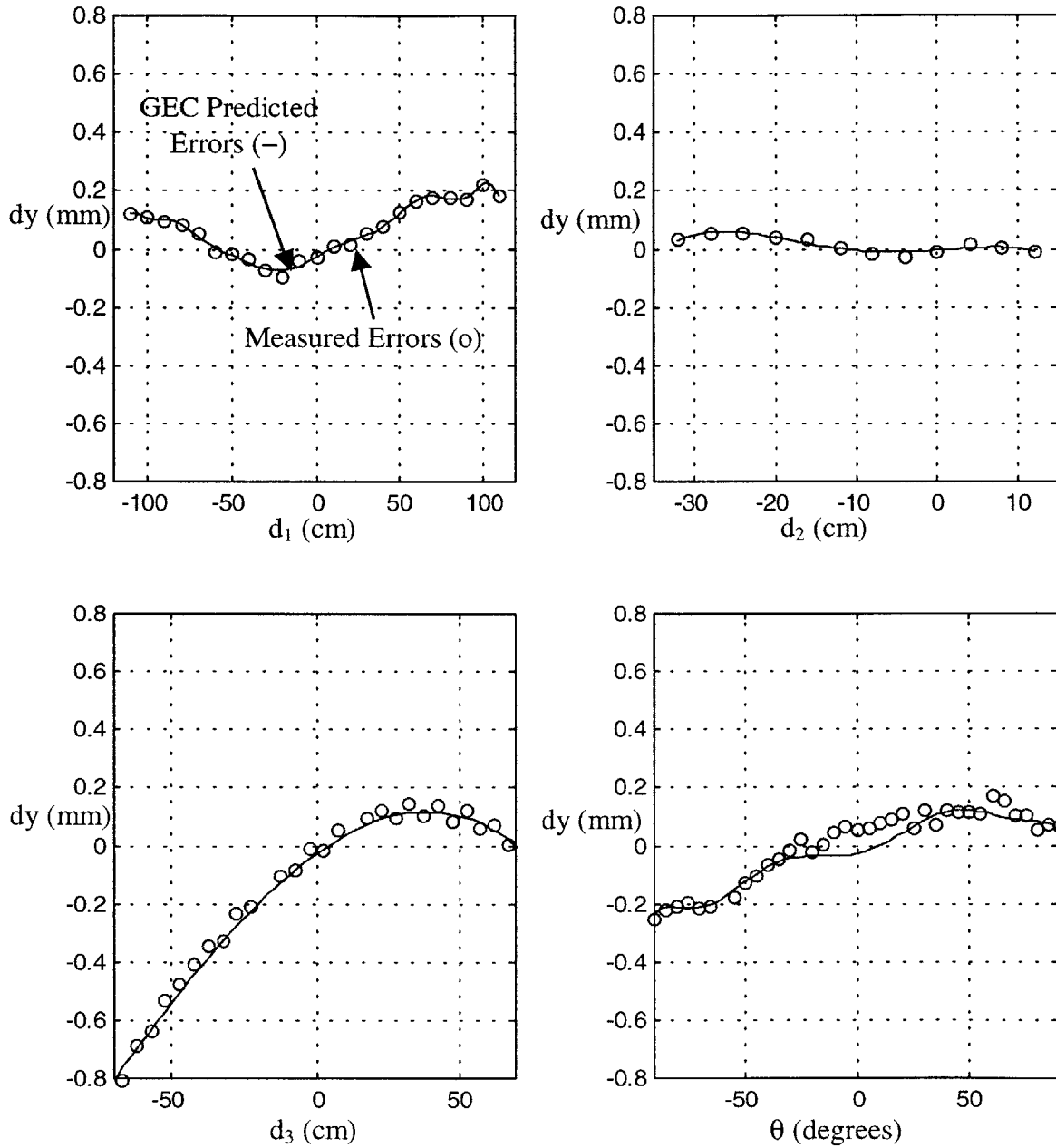


**Figure 4.8 - Measured and GEC Predicted Errors along the Y Axis at NTP**

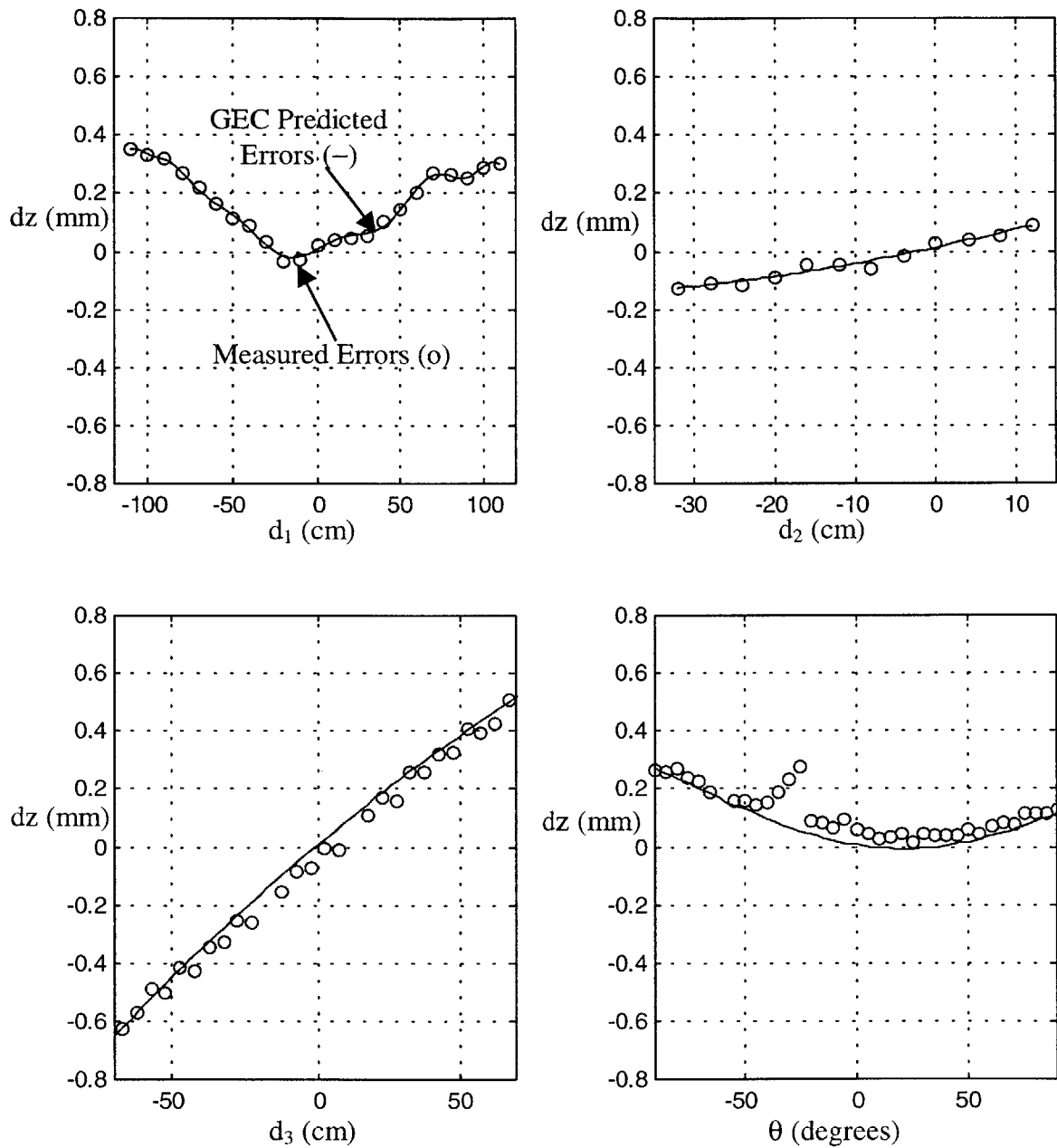


**Figure 4.9 - Measured and GEC Predicted Errors along the Z Axis at NTP**

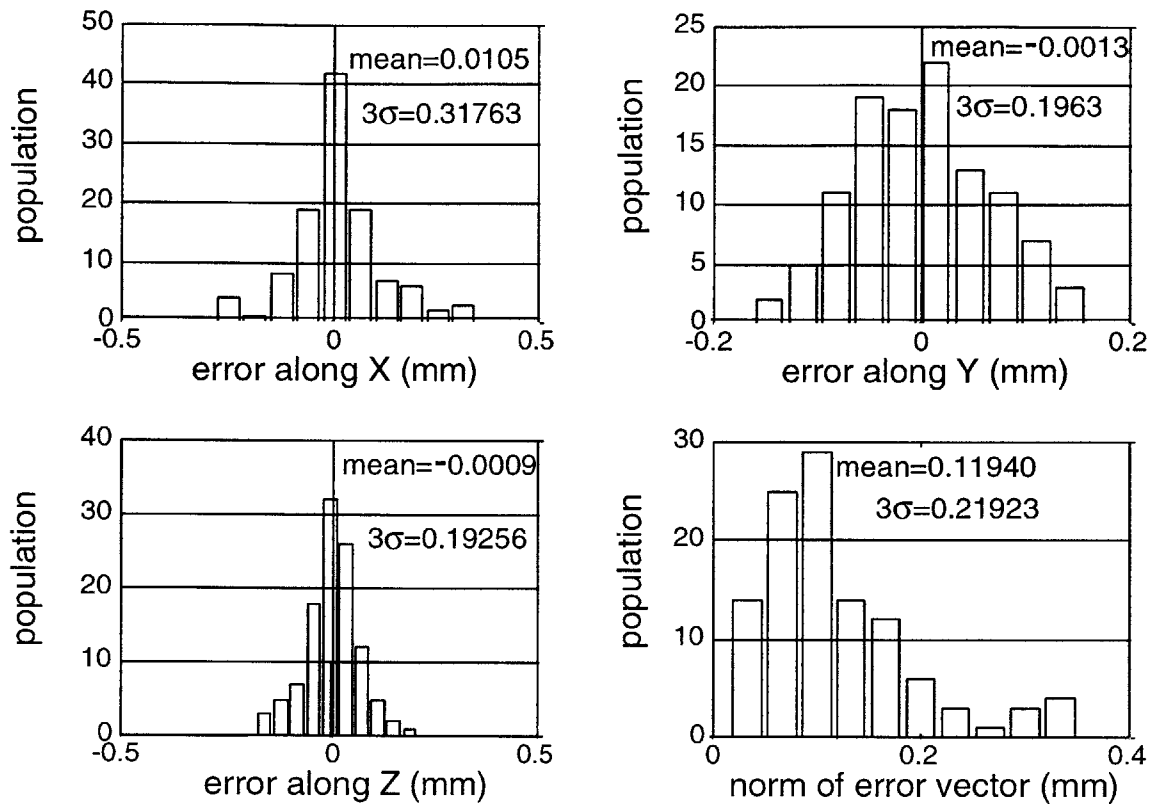


**Figure 4.10 - Statistics of the Compensated PPS Errors at NTP**

#### 4.4 Application to the Nozzle Dam Task

In this section, the GEC method is applied together with Base Sensor Control (see Section 2.2). The combined GEC/BSC method is experimentally evaluated for the nozzle dam application. In this application, unlike the PPS, the system repeatability is poor due to joint friction. The BSC method improves the repeatability as required by GEC. The nozzle dam insertion task requires the use of a strong manipulator to transport the heavy nozzle dam payload within the harsh radioactive environment of the steam generator. The manipulator chosen for this system is a Schilling Titan II, a six DOF hydraulic robot

widely used for remote manipulation in hostile environments such as deep-ocean, toxic-chemical, high-voltage, and radioactive environments (see Figure 4.11). The Schilling is well-suited for these tasks because of its large workspace (a 194 cm maximum reach) and its high load bearing capacity in excess of 100 kg at full extension (Tomcat Manipulator System Technical Manual, 1991).

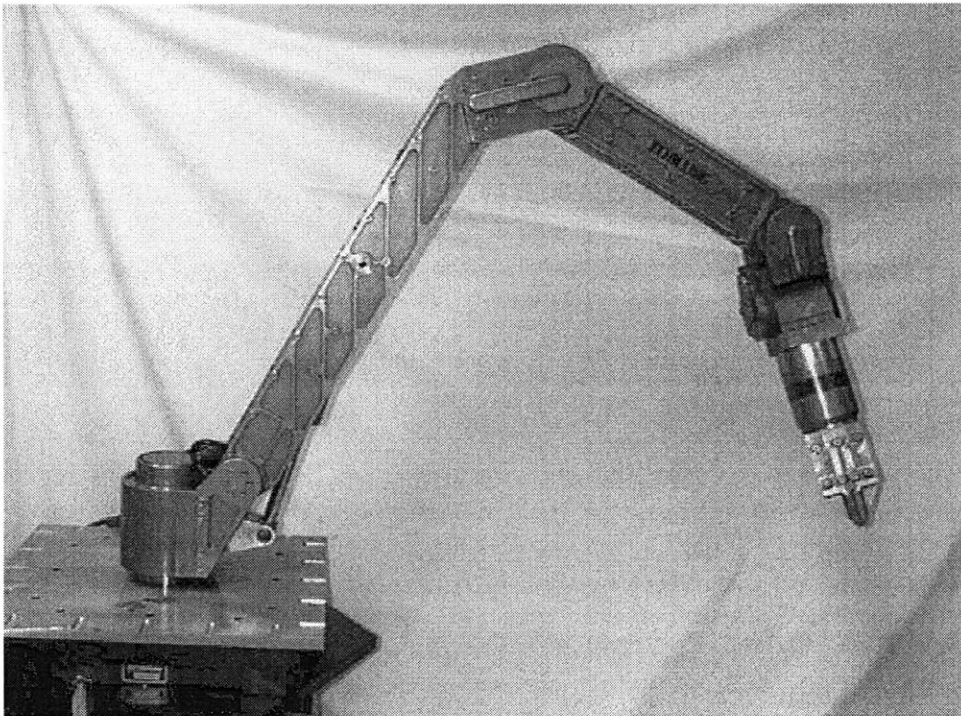


**Figure 4.11 - Schilling Titan II Manipulator**

Like many strong, powerful manipulators, the Schilling does not inherently have fine repeatability due to high friction in its joints. However, the nozzle dam task requires extremely accurate positioning for fine motions. Also, absolute accuracy is sacrificed as a result of the poor repeatability and significant geometric errors. Its absolute position accuracy is approximately 40 mm (RMS), many times the nozzle dam specification.

The objective of the experiment is to see if the combined GEC/BSC method outlined in Figure 4.12 can be applied to the experimental system to improve its repeatability and its absolute accuracy, while minimizing the implementation cost to keep the solution practical for the nuclear industry. For this experimental system, the achievable repeatability is limited by the particular control electronics used. The joint resolver signals, standard on the Schilling, are converted to quadrature encoder waveforms using a special purpose Delta Tau Data/PMAC controller design. The joint angle resolution of this configuration is limited to  $\pm 0.087$  degree, which leads to as much as  $\pm 5$  mm errors in the end-effector positioning.

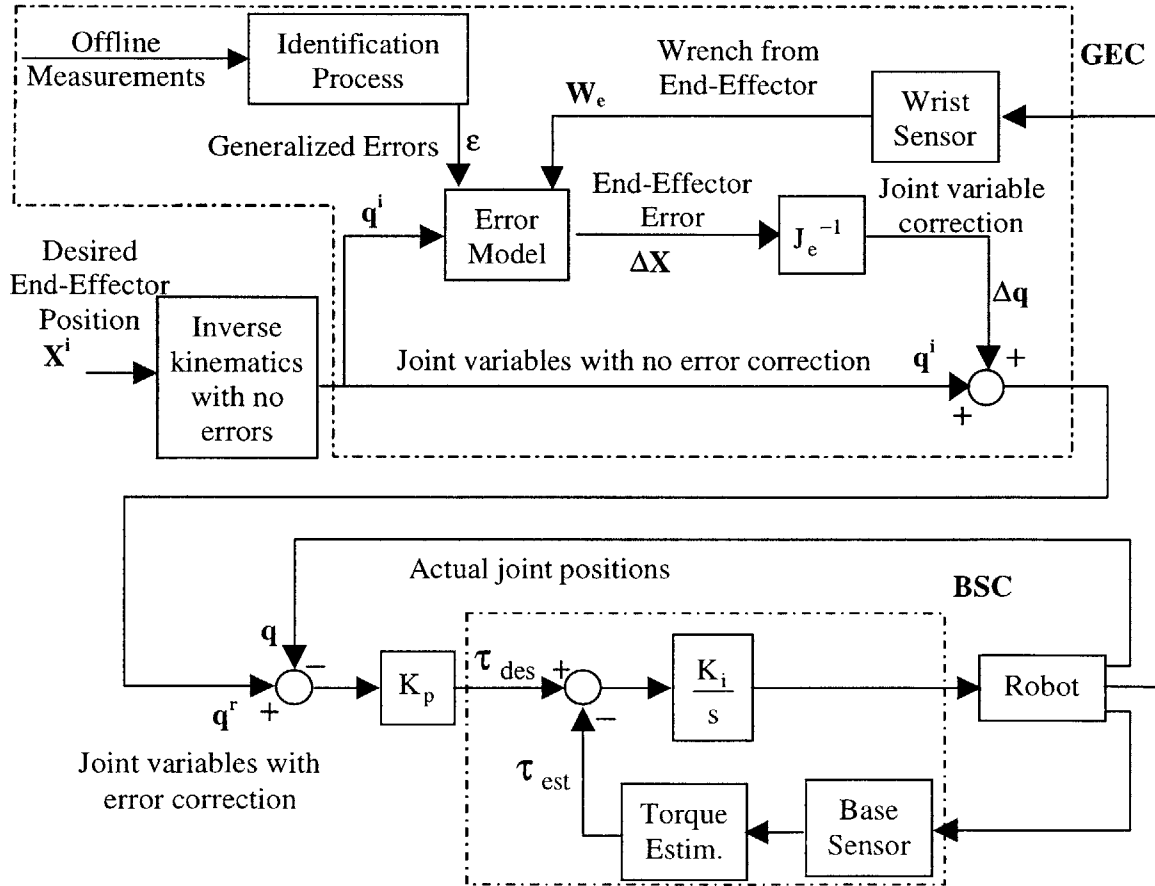


**Figure 4.12 - Base Sensor Control and Error Compensation Scheme**

Figure 4.13 shows the experimental test-bed constructed for this study. A six-axis Advanced Mechanical Technology, Inc. (AMTI) force/torque sensor is mounted under the manipulator base to provide wrench measurements for the BSC algorithm. A 15 kg replica of the nozzle dam center-plate was built along with an adjustable plate receptacle that permits the clearances to be varied from interference to several cm. An algorithm to successfully place the rectangular center plate within the receptacle would be easily extendable to perform the other high precision tasks necessary to complete the entire nozzle dam installation, either through teleoperation or as an autonomous subtask.

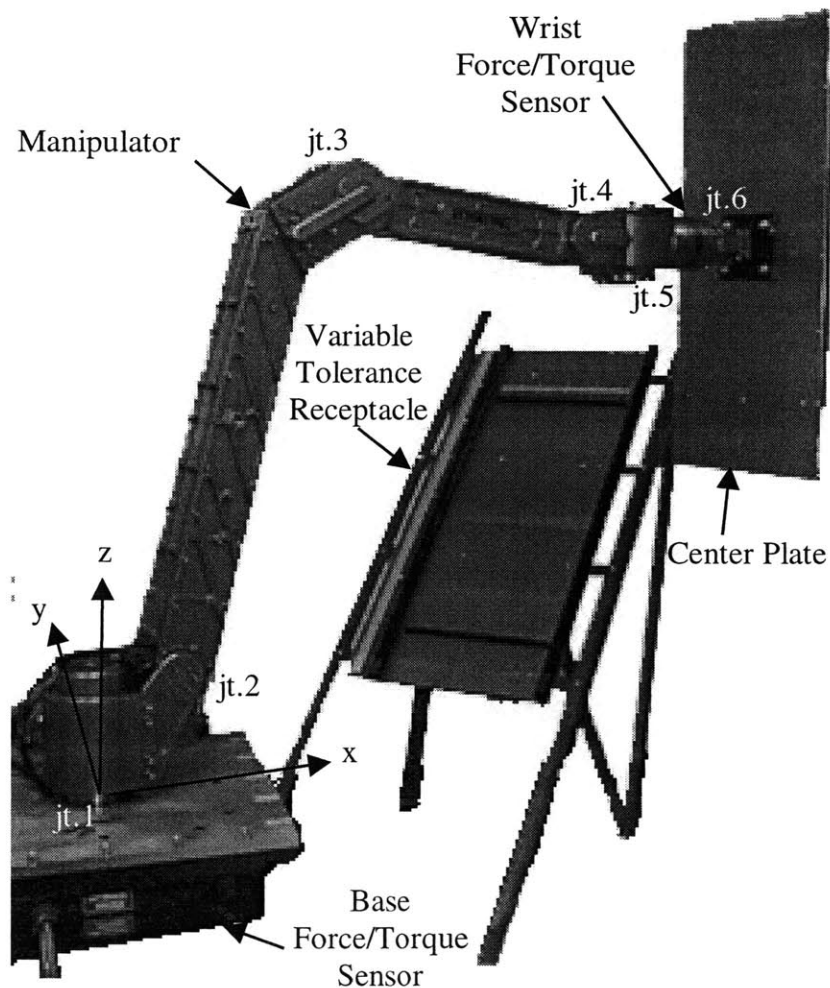


**Figure 4.13 - Nozzle Dam Experimental System**

A pair of Pentax optical theodolites was used to accurately measure the 3D position of the end-effector to generate the correction matrix, evaluate weight dependent deflections, and verify the algorithm performance. The resolution of the theodolites was 30 arc seconds, leading to measurement errors of 0.29 mm.

A fixed reference frame,  $F_0$ , is used to express the coordinates of all points. The origin of this reference lies at the intersection of the top of the base sensor and the joint 1 axis. Its z-axis is vertical and its x-axis is defined by a specific horizontal reference direction.

A PC-based graphical user interface provides the operator with workspace visualization as well as manipulator control functionality. The sampling rate was ten milliseconds, which was sufficiently fast for the experiments.

In this work, 400 measurements were used to evaluate the basic accuracy of the Schilling. Different payloads were used, with weights up to 45 kg. Most of the measurements focused on two specific payloads: one with no weight and another with an 18 kg weight (the replica nozzle dam plate).

End-effector measurements of the manipulator under PI control determined the baseline uncompensated system repeatability and accuracy. The relative positioning root mean square error was used as a measure of the system repeatability. The 12-bit discretization of the Schilling's resolver signal leads to random errors up to 5.0 mm, imposing a lower limit of 2.0 mm (RMS) on the system repeatability. This repeatability value sets the accuracy limit of any error compensation algorithm.

The results show that the BSC algorithm was able to reduce the repeatability errors by a factor of 4.73 over PI control. Data was taken by moving the manipulator an

arbitrary distance from the test point and then commanding it back to its original position. Figure 4.14 shows the distributions of the repeatability error with and without BSC. The maximum errors without BSC were 21.0 mm, and the repeatability was 14.3 mm (RMS). BSC reduced the maximum errors to 5.5 mm with a repeatability of only 2.7 mm (RMS).

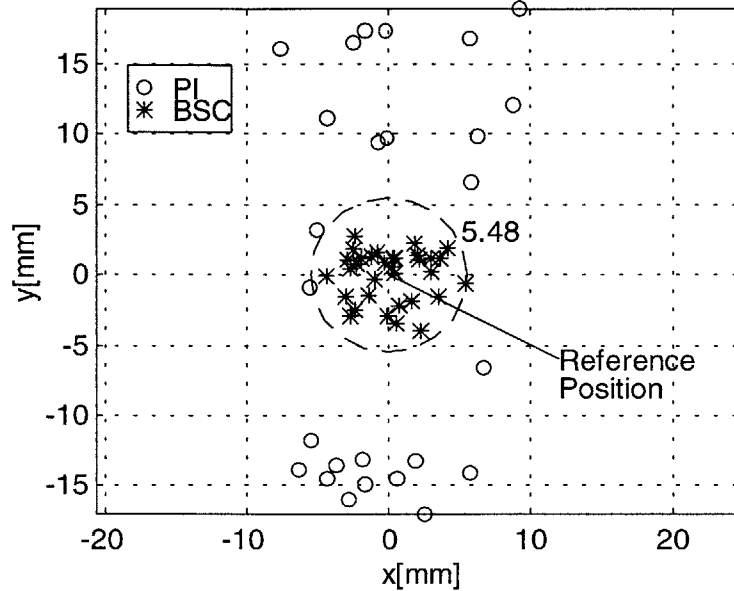


**Figure 4.14 - Repeatability with and without BSC**

Although the BSC algorithm greatly reduced repeatability errors to about 2.7mm (RMS), a 35 mm (RMS) error remained in absolute accuracy. Thus, a model-based error correction method can be applied to reduce the accuracy errors.

In order to implement GEC, the geometric and elastic deformation correction matrix was calculated using approximately 350 measurements of the end-effector in different configurations and with different payloads. The remaining points were used to verify the efficiency of the GEC method.

From the ideal system kinematic model, the ideal coordinates of the end-effector were calculated and subtracted from the experimentally measured values to yield the



vector  $\Delta\mathbf{X}(\mathbf{q},\mathbf{w})$  in Equation (2.7). By treating generalized errors as constant in their respective frames, the system absolute accuracy was improved to 13.4 mm (RMS). Since the GEC method allows for the use of polynomials to describe each generalized error, second order polynomials achieved an absolute accuracy of 7.3 mm (RMS), an additional 100% improvement.

Figure 4.15 shows the convergence of original positioning errors as large as 55.1 mm (34.3 mm RMS) to corrected errors of less than 10.7 mm (7.3 mm RMS) with respect to the base frame  $F_0$ . This demonstrates an overall factor of nearly 4.7 improvement in absolute accuracy by using the GEC algorithm.

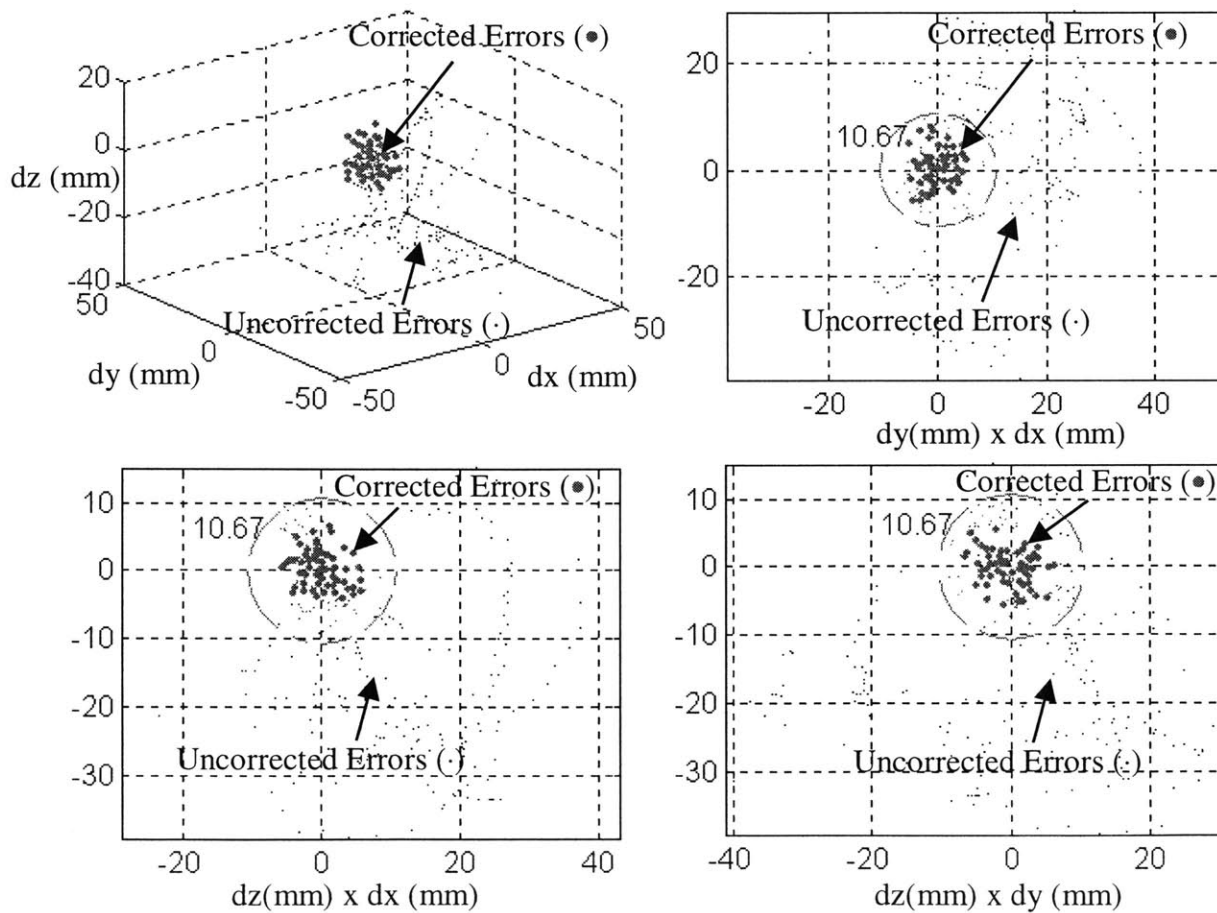


**Figure 4.15 - Measured and Residual Errors After Compensation**

An experiment was conducted to demonstrate the application of the joint GEC and BSC algorithm. The Schilling was commanded to a series of 11 points in the same plane under pure BSC control and then with the addition of two forms of the GEC method. The uncorrected data showed absolute accuracy errors of 29.5 mm (RMS), which are of the same order as the 34.3 mm (RMS) error found from the theodolite measurements. The implementation of GEC with constant generalized errors in their frames resulted in errors being reduced to 11.4 mm (RMS). By expanding the GEC algorithm to include second order polynomials, absolute positioning errors were reduced even further to a RMS value of 8.2 mm. With this improvement in performance, it should make feasible such tasks as the nozzle dam insertion.

## **4.5 Summary and Conclusions**

In this chapter, a method was presented to compensate for the positioning end-effector errors of large manipulators with significant task loads. Both geometric and elastic errors are considered without requiring any explicit elastic model of the system. The method has been applied experimentally to a high-accuracy large medical manipulator (PPS) and to a Schilling Titan II manipulator. The results showed that the basic accuracy of these manipulators exceeded their specifications, but after applying the method to compensate for end-effector errors the accuracy specifications are met. The method is now a key element of the PPS software used to treat cancer patients (Flanz, 1996).

## Single Endpoint Contact Calibration (SEC)

---

### 5.1 Introduction

This chapter investigates the SEC (Single Endpoint Contact) calibration method, where the robot endpoint is constrained to a single contact point. Section 5.2 presents the theoretical background for the SEC method. Section 5.3 contains simulations and experimental results for SEC applied to a Schilling Titan II manipulator.

### 5.2 SEC Theory

In Single Endpoint Contact calibration, instead of moving the end-effector to different positions to obtain the calibration measurements, the endpoint position is kept fixed with changes only in its orientation. Using an end-effector fixture equivalent to a ball joint, the robot executes self-motions to move to different configurations. At each configuration, manipulator joint sensors provide data that is used in an SEC identification algorithm to estimate the robot's parameters. A least squares optimization procedure is used to improve the calibration accuracy.

The advantage of this method is that it does not require measurements of the robot position using external sensors, requiring only an inexpensive and compact device such as a ball joint. Only one endpoint location needs to be known, along with the joint angle measurements. The kinematic loop closure equations are then used to calibrate the manipulator. In order to calibrate the system, the closed chain must have some mobility. So, a spatial manipulator must have 4 DOF's or more to be calibrated using this method. For planar manipulators, the point contact condition provides 2 constraints, so a planar manipulator with as few as 3 DOF's may be calibrated using SEC.

In addition to geometric errors, this calibration method is able to identify elastic structural deformation errors due to task loads and gravity, since arbitrary forces can be applied to the SEC fixture. In this case, a wrist force/torque sensor is added to the manipulator to measure the endpoint wrenches.

Also, to use the method for applications without significant task loads, it is necessary to minimize the forces between the manipulator and the calibration point fixture. Large forces could result in significant elastic deformations on the SEC fixture and the manipulator, compromising the identification accuracy. Section 5.2.2 shows how to keep endpoint forces small while moving a manipulator under endpoint constraint.

The calibration method is applied experimentally to a 6 DOF hydraulic manipulator. The error parameters of the robot are identified and used to predict, and compensate for, the endpoint errors as a function of configuration. Results presented here show that the location selected for endpoint contact significantly affects SEC calibration performance. A technique to find the optimal calibration point is presented in Section 5.2.3 with simulation results. The experimental results show that the method is

able to effectively and significantly improve the manipulator's accuracy without requiring special and expensive metrology equipment.

### 5.2.1 Analytical Development

Consider a manipulator gripping an end-effector fixture at a constant location  $(x_0, y_0, z_0)$ , and define  $\mathbf{q}^{\text{real}}$  as the measured vector of joint variables. The end-effector error is the difference between the actual position of the end-effector, at the SEC fixture, and the ideal position calculated from the kinematic equations applied to the measured  $\mathbf{q}^{\text{real}}$ . This ideal position is the end-effector position that an ideal manipulator would achieve if it was moved to the measured joint readings of the actual robot. As both ideal and real manipulator positions are evaluated at the same configuration  $\mathbf{q}^{\text{real}}$ , the resulting end-effector error  $\Delta\mathbf{X}$  is only due to the generalized errors. From Equations (2.6) and (2.7), the end-effector position error  $\Delta\mathbf{X}$  is

$$\Delta\mathbf{X} = \mathbf{X}^{\text{real}}(\mathbf{q}^{\text{real}}) - \mathbf{X}^{\text{ideal}}(\mathbf{q}^{\text{real}}) = [x_0, y_0, z_0]^T - \mathbf{X}^{\text{ideal}} = \mathbf{J}_e(\mathbf{q}^{\text{real}}) \boldsymbol{\varepsilon} \quad (5.1)$$

Here the three end-effector reference frame orientations are eliminated from the error model, as they are not measured. The three position components of the end-effector reference frame in the inertial reference system are represented by the 3x1 endpoint vectors  $\mathbf{X}^{\text{real}}$  and  $\mathbf{X}^{\text{ideal}}$ .

Since both  $\mathbf{J}_e$  and  $\mathbf{X}^{\text{ideal}}$  can be calculated at each point using the measured joint positions and ideal direct kinematics, the only remaining unknown in Equation (5.1) is the generalized error vector  $\boldsymbol{\varepsilon}$ .

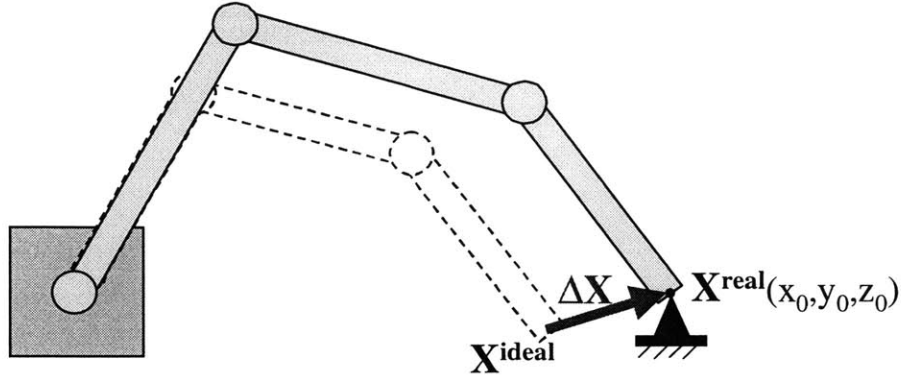


**Figure 5.1 - Real and Ideal Positions of a Manipulator End-Effector**

As the robot executes self-motions to different configurations, the real robot parameters can be estimated from the readings of the internal position sensors and from the identification model. A least squares optimization procedure, shown in Equation (2.9), is then used to improve the calibration accuracy.

As in every calibration method not having *a priori* knowledge of the task constraint dimensions, the scale of the mechanism must be set, i.e., one link length or other length parameter has to be measured by independent means (Bennett and Hollerbach, 1991). In the SEC method, if any of the coordinates  $x_0$ ,  $y_0$  or  $z_0$  of the end-effector fixture is known, then this scaling requirement is already satisfied. However, if none of these coordinates is known, then one length parameter needs to be independently measured. Note that it is not necessary to know *a priori* the location of the end-effector fixture, since its location can be introduced as an unknown. In this case, Equation (5.1) is rewritten as:

$$-\mathbf{X}^{\text{ideal}} = \begin{bmatrix} \mathbf{J}_\varepsilon & \begin{bmatrix} -1 & 0 & 0 \\ 0 & -1 & 0 \\ 0 & 0 & -1 \end{bmatrix} \end{bmatrix} \cdot \begin{bmatrix} \boldsymbol{\varepsilon} \\ x_0 \\ y_0 \\ z_0 \end{bmatrix} = \mathbf{J}_\varepsilon^* \boldsymbol{\varepsilon}^* \quad (5.2)$$

where the unknown vector  $\boldsymbol{\varepsilon}^*$  contains both generalized errors and the coordinates of the end-effector fixture.

In addition to geometric errors, this calibration method is able to identify elastic structural deformation errors, since arbitrary forces can be applied to the SEC fixture (see Figure 5.2). In this case, an extended error model must be used to identify the elastic errors as a function of the payload wrench at the end-effector, as discussed in Chapter 4. Defining  $\mathbf{F}$  as the desired force applied to the end-effector and  $\mathbf{J}$  as the robot Jacobian, then the vector  $\boldsymbol{\tau}$  of applied joint torques/forces to the manipulator is

$$\boldsymbol{\tau} = \mathbf{J}^T (-\mathbf{F}) \quad (5.3)$$

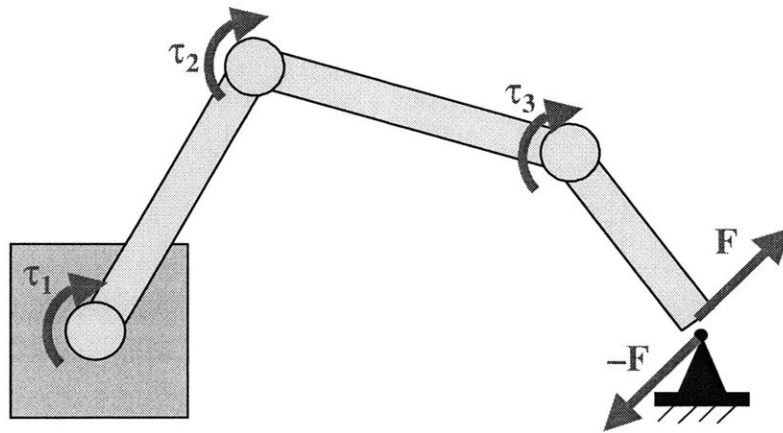


**Figure 5.2 - Calibration of Elastic Errors due to an Arbitrary Force**

### 5.2.2 Control

To use the SEC method, the manipulator must be controlled to move the joint variables while keeping the end-effector still (see Figure 5.3). To accomplish this without causing large and unknown forces on the end-effector that would deform the SEC fixture or the manipulator, a projection approach is adopted (Oriolo, 1994). In the method the control input is a projected error proportional feedback of the form:

$$\mathbf{u} = (\mathbf{I} - \mathbf{J}^\# \cdot \mathbf{J}) \cdot [\mathbf{K} \cdot (\mathbf{q}_r - \mathbf{q})] \quad (5.4)$$

where  $\mathbf{J}$  is the robot Jacobian,  $\mathbf{J}^\#$  is the Jacobian pseudoinverse,  $\mathbf{K}$  is a positive definite matrix, and  $\mathbf{q}_r$  is the desired manipulator configuration. The matrix  $(\mathbf{I} - \mathbf{J}^\# \cdot \mathbf{J})$  is the orthogonal projection operator in the Jacobian null space, which guarantees that joint velocities do not result in any end-effector velocity. Note that the above control scheme is equivalent to using the classical Projected Gradient method to solve redundancy (Oriolo, 1994). It has been shown that the reference configuration  $\mathbf{q}_r$  is globally stable for this control scheme. Thus, this control approach is used to steer the manipulator into different configurations during the offline calibration measurements.

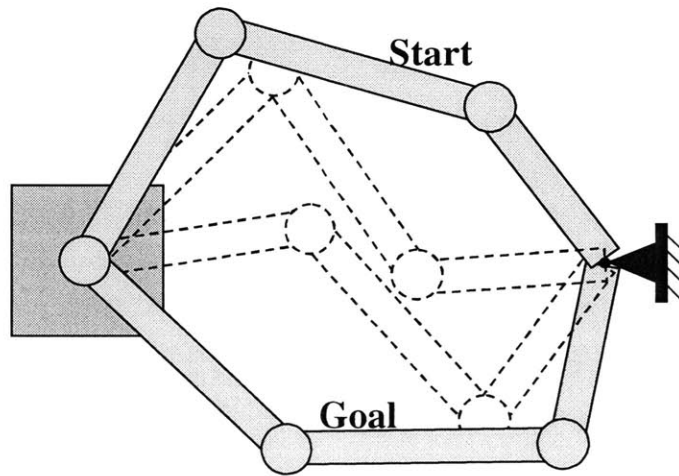


Figure 5.3 - Stabilization of the Arm Self-Motions



### 5.2.3 Optimization of the Fixture Location

In this section a technique to find the optimal location of the calibration fixture is presented. The optimization method has been developed by Guglielmo Scriffignano, a visiting scholar from Politecnico di Milano, Italy.

In SEC calibration, the location of the endpoint fixture can significantly affect the calibration performance. Ideally, generalized errors are constant in their frames, and errors identified at an arbitrary configuration can be used to compensate for errors at any other configuration. In this case, the endpoint fixture location used during SEC does not influence the calibration accuracy, since any configuration would lead to the same constant generalized errors. However, generalized errors are in general functions of configuration, especially in systems with significant elastic deformation. Therefore, interpolating functions must be chosen to model each generalized error, and its coefficients must be identified (see Chapter 4).

Furthermore, depending on the chosen set of measurement points, the error compensation process involves interpolation or extrapolation of the generalized error functions. As a general mathematical result, interpolation accuracy can be improved to the limit of the measurement noise by performing enough measurements in the desired range. However, extrapolation accuracy depends on how well the chosen set of functions model the actual system. So, poorly chosen functions may give a reasonable precision in the interpolation range, but poor precision in configurations outside the measured range. As a result, the choice of the measurement ranges at each joint is critical to the calibration accuracy. The optimization method presented here calculates a fixture location used by the SEC method that maximizes the measurement ranges of each joint.

In the SEC calibration, the measurement ranges of each joint are uniquely defined by the location of the calibration point. For a general manipulator, it is necessary to use numerical methods to find the measurement ranges. If the manipulator inverse kinematic equations can be written, then it is possible to find analytical solutions for the joint ranges. For an ideal 3R planar manipulator, with full-range of all 3 joints and no interference between links, an analytical solution of the measurement ranges for each calibration point  $\mathbf{P}$  has been found, as given below.

Defining  $l_i$  as the length of link  $i$  and  $\mathbf{P} = [r \cos \varphi, r \sin \varphi]$  as the calibration point, the joint angles  $q_i$  must satisfy:

$$k_{11} \equiv \frac{r^2 + l_1^2 - (l_2 + l_3)^2}{2l_1 r} \leq \cos(q_1 - \varphi) \leq \frac{r^2 + l_1^2 - (l_2 - l_3)^2}{2l_1 r} \equiv k_{12} \quad (5.5)$$

$$k_{21} \equiv \frac{(r - l_3)^2 - l_1^2 - l_2^2}{2l_1 l_2} \leq \cos(q_2) \leq \frac{(r + l_3)^2 - l_1^2 - l_2^2}{2l_1 l_2} \equiv k_{22} \quad (5.6)$$

$$k_{31} \equiv \frac{(r - l_1)^2 - l_2^2 - l_3^2}{2l_2 l_3} \leq \cos(q_3) \leq \frac{(r + l_1)^2 - l_2^2 - l_3^2}{2l_2 l_3} \equiv k_{32} \quad (5.7)$$

The measurement range of a joint  $j$  can then be written as:

$$q_j \in [q_{j0} - q_{j1}, q_{j0} - q_{j2}] \cup [q_{j0} + q_{j2}, q_{j0} + q_{j1}] \quad (5.8)$$

where

$$q_{ji} \equiv \begin{cases} \pi & \text{if } k_{ji} \leq -1 \\ 0 & \text{if } k_{ji} \geq 1 \\ \arccos(k_{ji}) & \text{if } -1 \leq k_{ji} \leq 1 \end{cases} \quad \text{and} \quad q_{j0} \equiv \begin{cases} \varphi & \text{if } j = 1 \\ 0 & \text{if } j = 2 \\ 0 & \text{if } j = 3 \end{cases} \quad (5.9)$$

For a generic 3R manipulator, it is also necessary to consider the intersection between the ideal solution from Equation (5.8) and the mechanical limits of each joint.

Once the measurement ranges of each joint are calculated and the errors identified using SEC, the calibration can be evaluated by defining a performance index. This index is based on the observation that measurement interpolation results in better accuracy than

extrapolation. First consider the Interpolated Compensation Region (ICR), defined as the workspace region where the compensation algorithm does not require extrapolation of the error functions. It represents the region of the workspace that the manipulator can reach by independently sweeping its joints through their interpolated ranges. Conversely, the Extrapolated Compensation Region (ECR) is the workspace region where any of the generalized error functions needs to be extrapolated, resulting in reduced accuracy.

In order to obtain an ideal location of the calibration point, a performance index for the SEC method needs to be defined and optimized. The volume of the ICR is an example of such index. By maximizing this volume - therefore minimizing the volume of the ECR - the overall accuracy of the compensation algorithm is increased. However, every region of the workspace is given the same importance, even those that are not useful for the task to be performed after calibration. To choose the fixture location that offers the best accuracy in specific workspace regions, a more general index is defined, called the Weighted Volume of the ICR (WV):

$$WV = \iiint_{ICR} \alpha(x, y, z) \cdot dV \quad (5.10)$$

where  $\alpha(x,y,z) \in [0,1]$  is a weight function defined over the entire workspace, representing the importance of each point  $(x,y,z)$  to the chosen task. Note that if  $\alpha(x,y,z)=1$  in the entire workspace, then the WV becomes the geometric volume of the ICR. The choice of the best fixture location for the SEC method is obtained by maximizing the function WV.

### 5.3 Results

Simulations of the SEC calibration and the optimization of the fixture location were performed for two 3R planar manipulators and a 6-DOF manipulator. Experiments

were then performed on a Schilling Titan II manipulator to show the effectiveness of the SEC calibration.

### 5.3.1 Simulation Results

Two different 3R planar manipulators were considered, with link lengths (1, 1, 1) and (5, 4, 3). In both cases an optimal location of the SEC fixture was found using Equations (5.5-5.10). In this simulation the manipulators do not have joint limits, and the weights  $\alpha(x,y,z)$  of the Weighted Volume in Equation (5.10) are equal to 1.0, i.e., every region of the workspace is considered equally important. For the (1, 1, 1) manipulator, the SEC fixture location that maximizes the volume of the interpolated region is at a distance from the robot base equal to 1.0 (see Figure 5.4). By using this fixture location, it is possible to move the manipulator in the full-range of its 3 joints, and the errors along the entire workspace can be compensated without extrapolation.

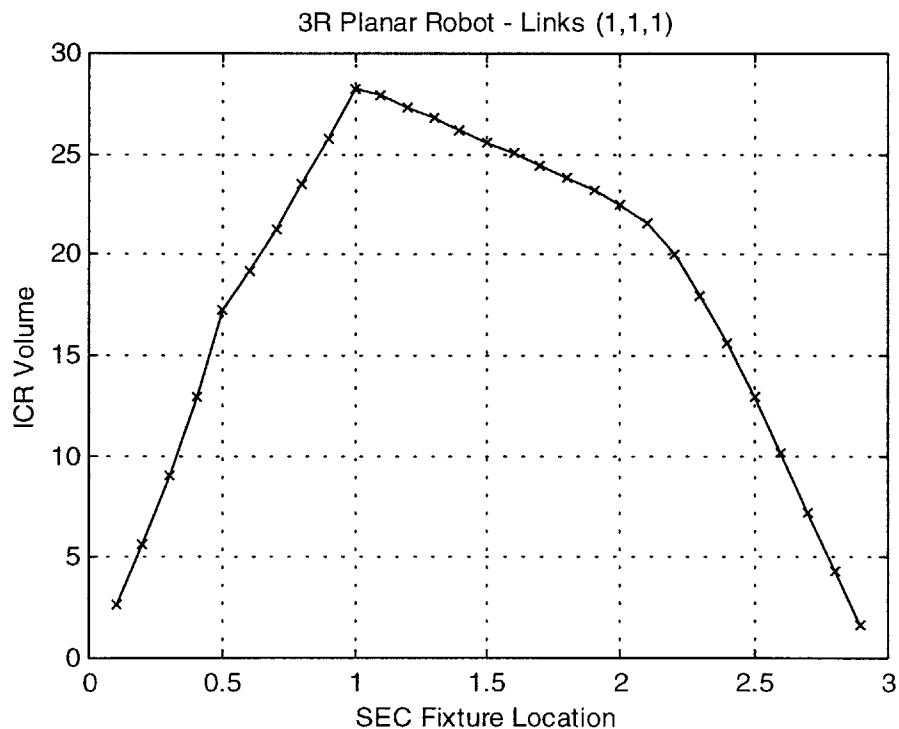


**Figure 5.4 - ICR Volume as a Function of the Fixture Location**

For the (5, 4, 3) planar manipulator, the optimal solution of the fixture location is at a distance from the robot base equal to 6.0 (see Figure 5.5). In this case, however, the ICR is not coincident with the whole workspace. The maximum volume (or area, since it is a planar manipulator) of the ICR is 341.6, while the workspace surface is  $\pi \cdot 12^2 = 452.4$ . So, for even the best choice of the calibration point, 25% of the calibrated workspace relies on extrapolation to compensate for the measured errors. Figure 5.6 shows some of the 3R manipulator configurations corresponding to a fixture location at  $\mathbf{P}(x,y)=(6,0)$ . The Interpolated and Extrapolated Compensation Regions obtained after the calibration process at two different fixture locations are shown in Figures 5.7 and 5.8. Note that the ICR obtained from calibration at the optimal fixture location  $\mathbf{P}=(6,0)$ , shown in Figure 5.7, is much larger than the one obtained using  $\mathbf{P}=(10,0)$ . Thus, from the numerical simulations it is found that SEC calibration using a fixture location at  $\mathbf{P}=(6,0)$  results in better accuracy than at  $\mathbf{P}=(10,0)$ .

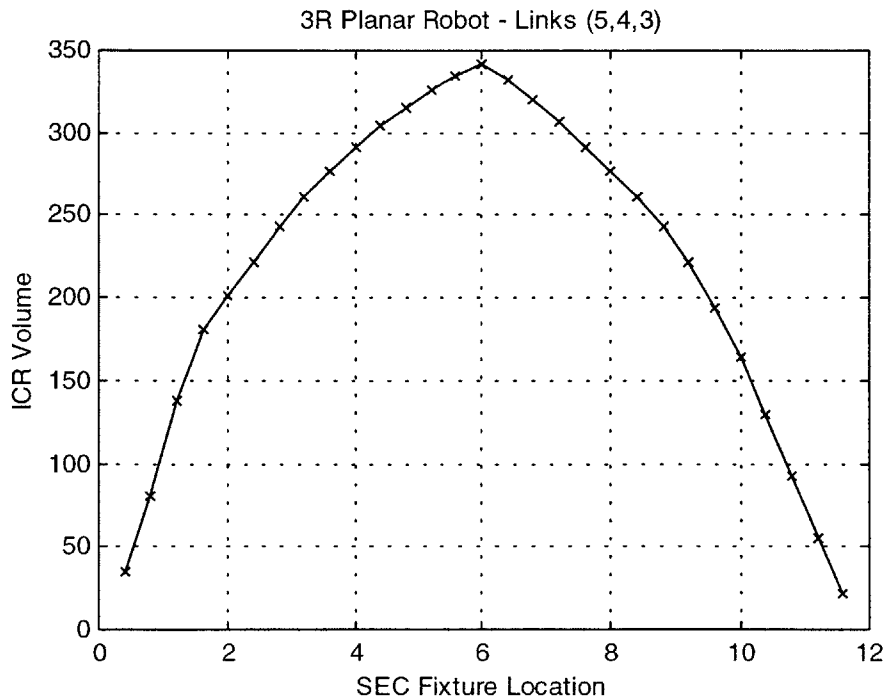


**Figure 5.5 - ICR Volume as a Function of SEC Fixture Location**

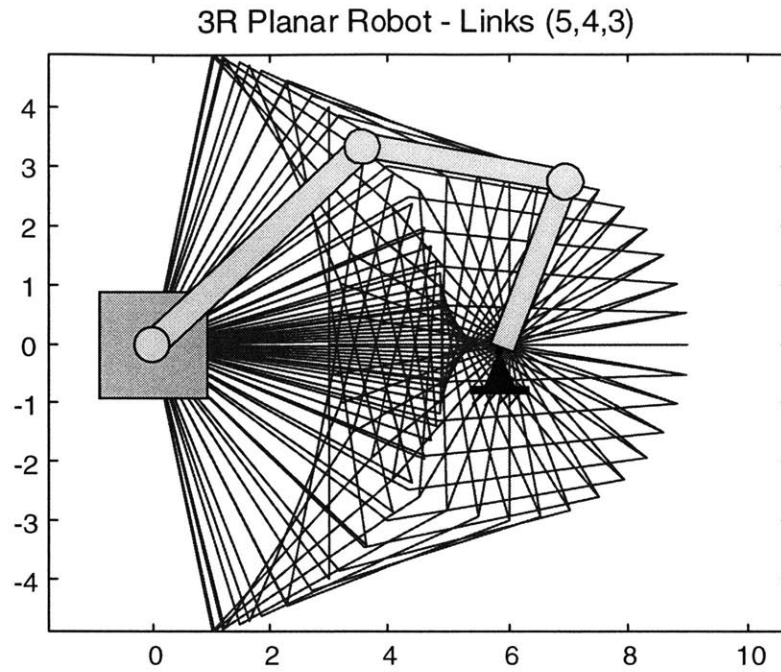


**Figure 5.6 - Measurement Configurations for an SEC Fixture at (6,0)**

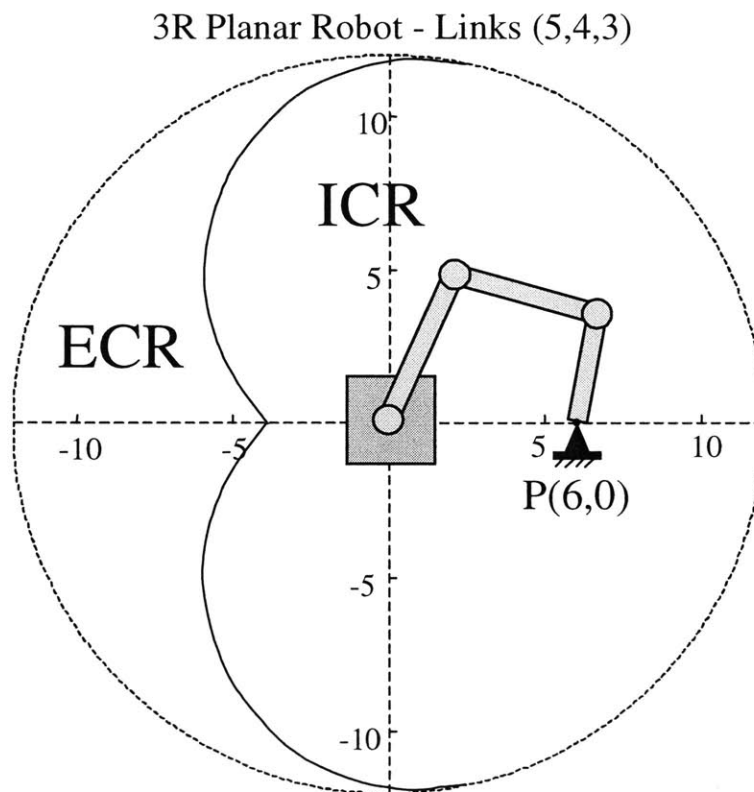


**Figure 5.7 - Extrapolated and Interpolated Regions for an SEC Fixture at (6,0)**

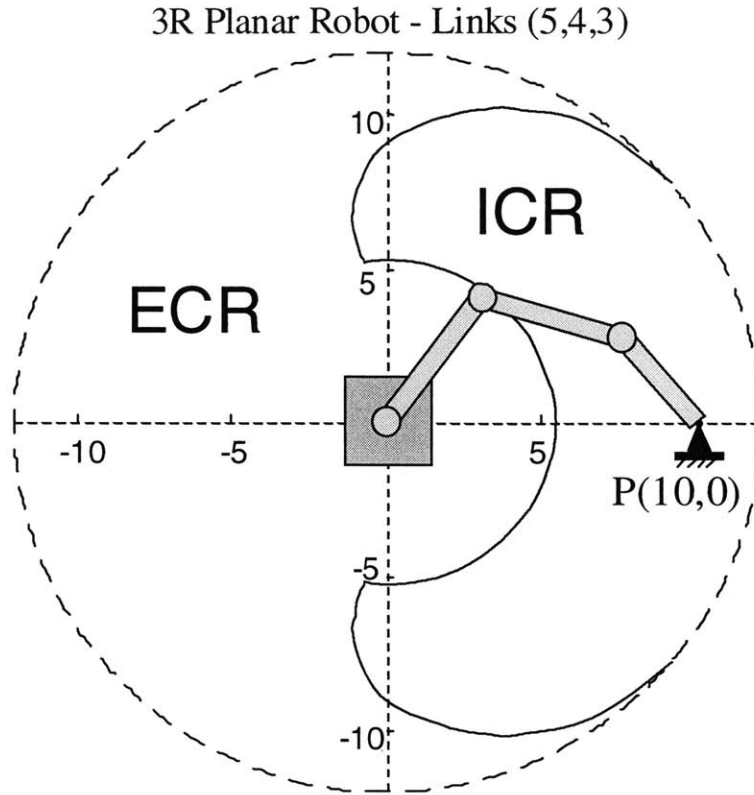


**Figure 5.8 - Extrapolated and Interpolated Regions for an SEC Fixture at (10,0)**

A simulation of the SEC method was applied to a 3R planar manipulator with link lengths (1m, 1m, 1m). The simulation introduced generalized errors that are functions of configuration, reflecting the effects of elastic deformations. To investigate the effects of interpolation and extrapolation on the measured errors, the chosen identification functions were different from the introduced error functions.

Two different fixture locations are used in the calibration, at distances 1.0m (the optimal location in this case) and 2.5m from the manipulator base. The manipulator is moved to 300 measurement configurations, sweeping the joint ranges allowed by each fixture location. An RMS uncorrected error of 8.0mm and a measurement noise of 0.1mm were introduced to both simulations. After the identification process, the end-

effector was released and the compensated manipulator was moved to several configurations in the workspace. The residual error after compensation was then evaluated at each configuration, and its RMS value was calculated.

For the calibration fixture at 1.0m, the full range of the three joints was achieved, and the RMS residual error was 0.16mm. When the fixture location was changed to 2.5m from the robot base, the RMS residual error was 0.49mm, approximately 3 times higher. This poorer accuracy is mainly due to the measurement range of joint 1 being restricted to the interval  $[-49^\circ, 49^\circ]$ . Thus, all configurations outside this range are compensated using extrapolation. Unless the chosen interpolation functions perfectly model the generalized errors, the SEC fixture location plays a critical role in the calibration accuracy.

Figure 5.9 shows the RMS residual error for the (1m, 1m, 1m) planar manipulator as a function of the number of measurement points, for a calibration fixture at 1.0 m, and different RMS measurement noise levels. Note that calibration cannot be made infinitely accurate as the number of measurement points is increased, and a lower bound exists on the calibration error that is dictated by robot repeatability and calibration measurement error (Roth et al., 1987). This is captured by the graph in Figure 5.9, showing residual errors tending to the introduced noise levels as the number of points is increased.



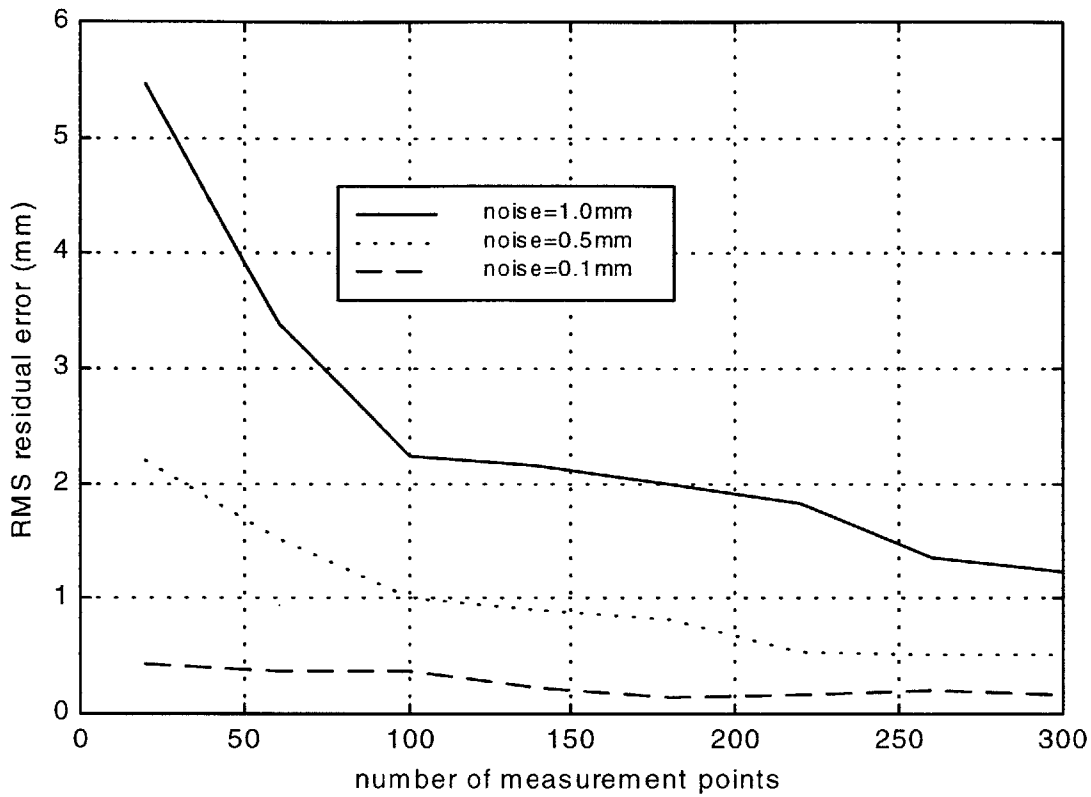


**Figure 5.9 - RMS Residual Error as a Function of the Number of Measurements**

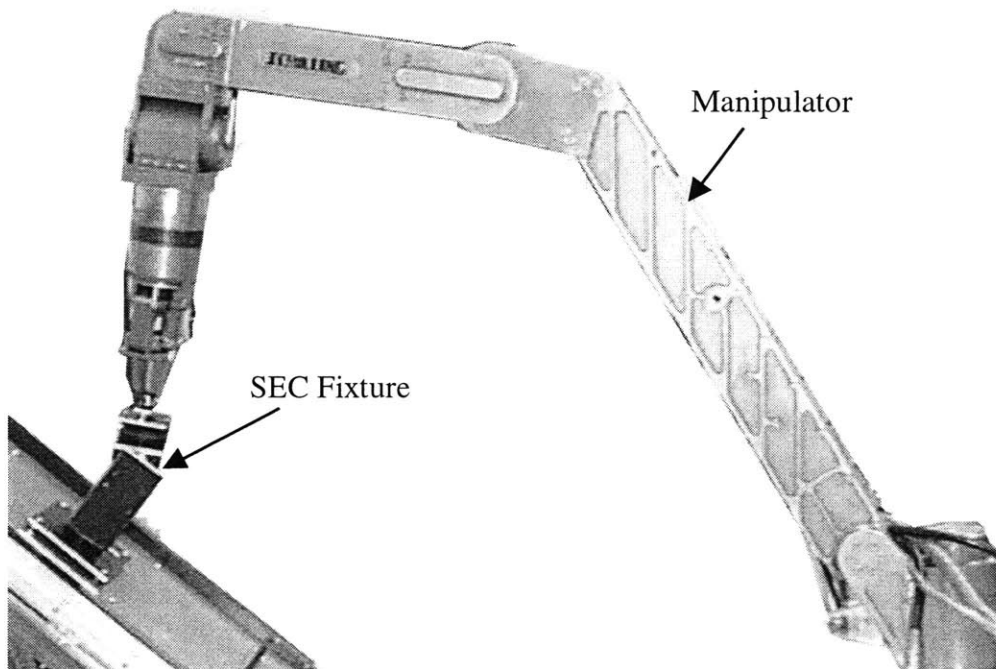
Simulations were also performed for a Schilling Titan II manipulator, a 6-DOF hydraulic robot. The SEC performance was analyzed for two different calibration device lengths: 10 and 50 in (254 and 1270mm). These lengths are the distance between the device gripper, attached to the robot end-effector, and the center of rotation of the spherical joint. The device length plays an important role on the achievable measurement ranges, since it modifies the kinematic equations of the manipulator.

Due to the rotational symmetry of the system around joint 1, the optimal location of the calibration device is on the vertical plane defined by the middle of the mechanical limits of joint 1. The optimal location for the 254mm device is calculated at  $P(x, z) = (550\text{mm}, 1800\text{mm})$ , respectively the horizontal and vertical distances from the

manipulator base along the defined vertical plane. The volume of the ICR in this case is  $8.33\text{m}^3$ . A second maxima for the ICR volume is  $6.66\text{m}^3$ , obtained for a device location at  $P(x, z) = (550\text{mm}, -200\text{mm})$  from the manipulator base. For the 1270mm device, the optimized location is at  $P(x, z) = (1600\text{mm}, 1750\text{mm})$ , resulting in an ICR volume of  $17.8\text{m}^3$ . Note that this volume is twice the ICR volume obtained from the 254mm device, i.e., the 1270mm fixture results in a better calibration accuracy in this case.

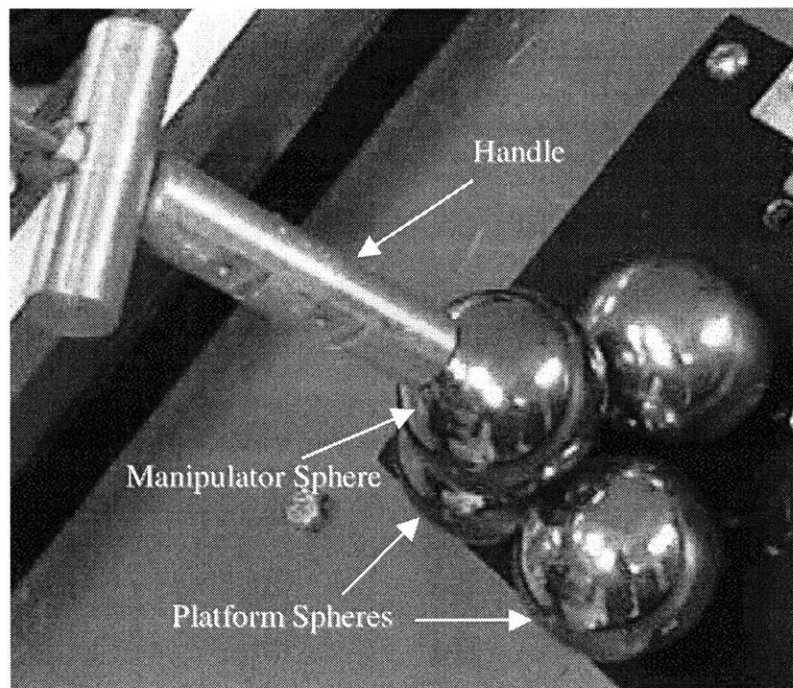
### 5.3.2 Experimental Results

Figure 5.10 shows the laboratory system used to experimentally evaluate the SEC calibration method. The manipulator is a Schilling Titan II, a six DOF hydraulic robot capable of handling payloads in excess of 100 kg. A handle on the SEC fixture provides a repeatable grip for the manipulator.



**Figure 5.10 - Experimental System**

Three different SEC fixtures were evaluated. The first fixture consisted of a single sphere attached to the manipulator end-effector, which seated in a triangular arrangement of three spheres fixed to the platform, see Figure 5.11. All spheres have the same diameter. SEC measurements are performed while the four spheres are in mutual single-point contact. Although simple, this fixture design has a disadvantage: the manipulator must be stopped at each measurement point to guarantee contact among the four balls, significantly increasing calibration time.



**Figure 5.11 - SEC Fixture Using Four Spheres**

The second fixture consists of a system of 3 rotary joints, see Figure 5.12. The axes of rotation of the 3 joints intersect at the same point, resulting in a system equivalent to a spherical joint. This design allows for continuous SEC measurements without

stopping the manipulator. However, the 3 additional joints introduce new error parameters in the loop closure equations, degrading calibration accuracy.

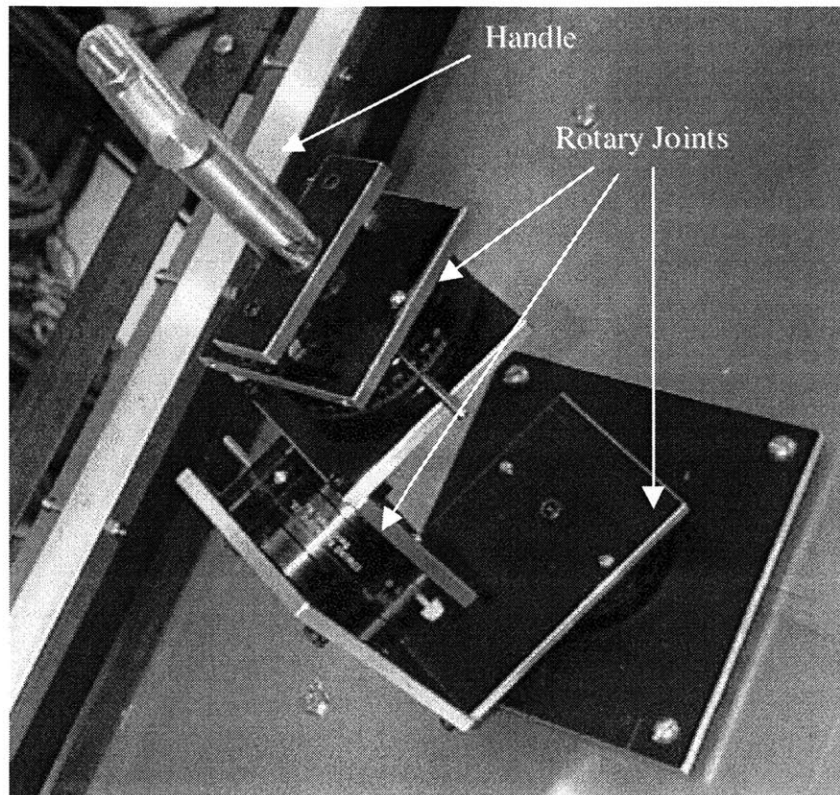


**Figure 5.12 - SEC Fixture Using Three Rotary Joints**

The third fixture considered for SEC measurements consists of a spherical joint attached to the manipulator end-effector, see Figure 5.13. This fixture allows for continuous measurements while moving the manipulator, with the advantage of introducing fewer error parameters in the system. This design was chosen for all SEC measurements presented in this section.

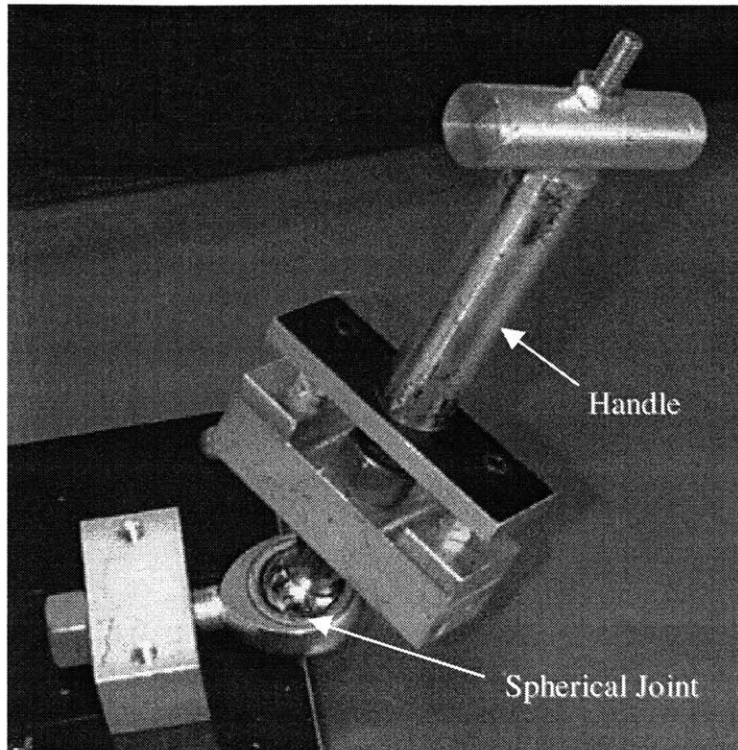


**Figure 5.13 - SEC Fixture Using a Spherical Joint**

The objective of the experiment is to determine if the SEC calibration method can be practically applied to a physical system to improve its absolute accuracy. The goal is to cause the residual error to approach the limit set by the position sensing resolution of the system. The BSC control technique is used to improve the system repeatability by greatly reducing the effects of joint friction (see Section 2.2). This control scheme is applied in concert with the orthogonal projection operator in the Jacobian null space, defined in Equation (5.4), minimizing the resulting forces at the SEC fixture. The relative positioning root mean square error is used as a measure of the system repeatability. Data is taken by moving the manipulator an arbitrary distance from the test point and then commanding it back to its original position. The measured maximum errors are  $\pm 5.5$  mm, and the repeatability of the system is 2.7 mm (RMS).

Although the Base Sensor Control algorithm greatly reduces the repeatability errors, there are still 35 mm (RMS) errors in absolute accuracy (see Section 4.4). Since the system repeatability is relatively small with respect to the absolute errors, a model-based error compensation method can be applied to reduce the accuracy errors, such as the SEC calibration method using the GEC extended error model.

In order to implement SEC, the polynomial generalized error functions defined in Equation (4.1) were interpolated using approximately 800 measurements of the robot configuration. These measurements were performed for an SEC device with length 155mm located at  $\mathbf{P}(x, z) = (1440\text{mm}, 265\text{mm})$  from the manipulator base. Note that the end-effector fixture location was obtained by the SEC calibration, since it was not known *a priori*. After the identification process, the compensated manipulator was moved to 200 different configurations to verify the efficiency of the SEC method.

Figures 5.14(a-b) show the convergence of original positioning errors as large as 98.5mm (34.3mm RMS) to corrected absolute errors of less than 15mm (5.7mm RMS) with respect to the base frame. This demonstrates an overall factor of nearly 6 improvement in absolute accuracy by using the SEC calibration algorithm. This improvement in performance shows that such calibration method is able to effectively identify and correct for the errors in the system.

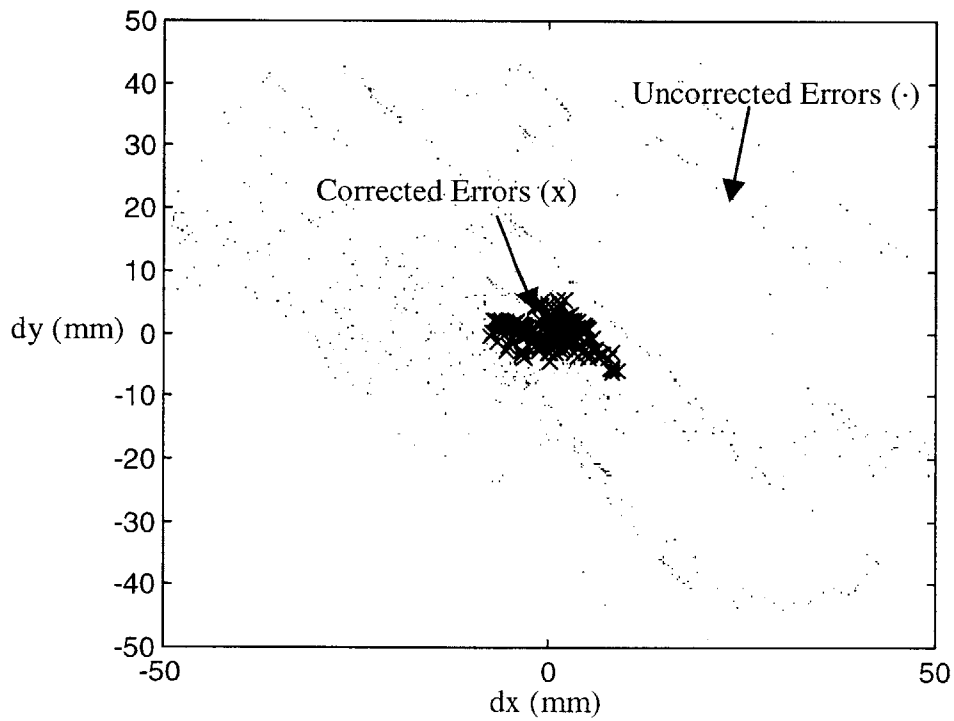
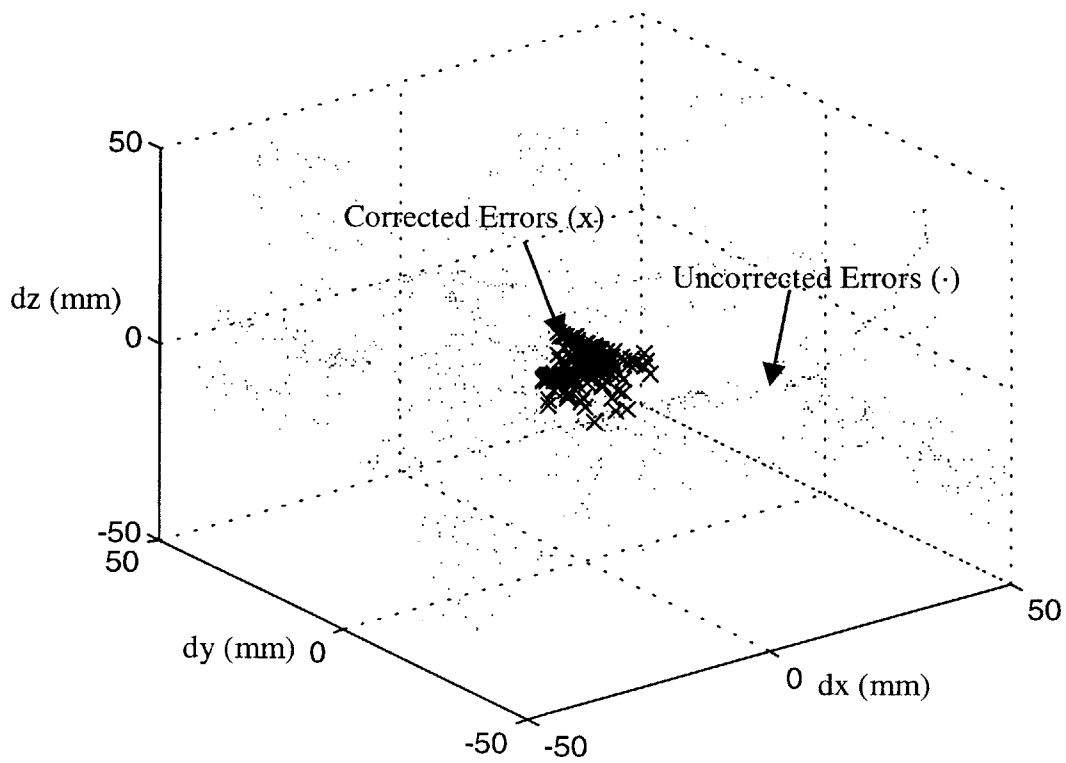


**Figure 5.14(a) - Measured and Residual Errors After Compensation**

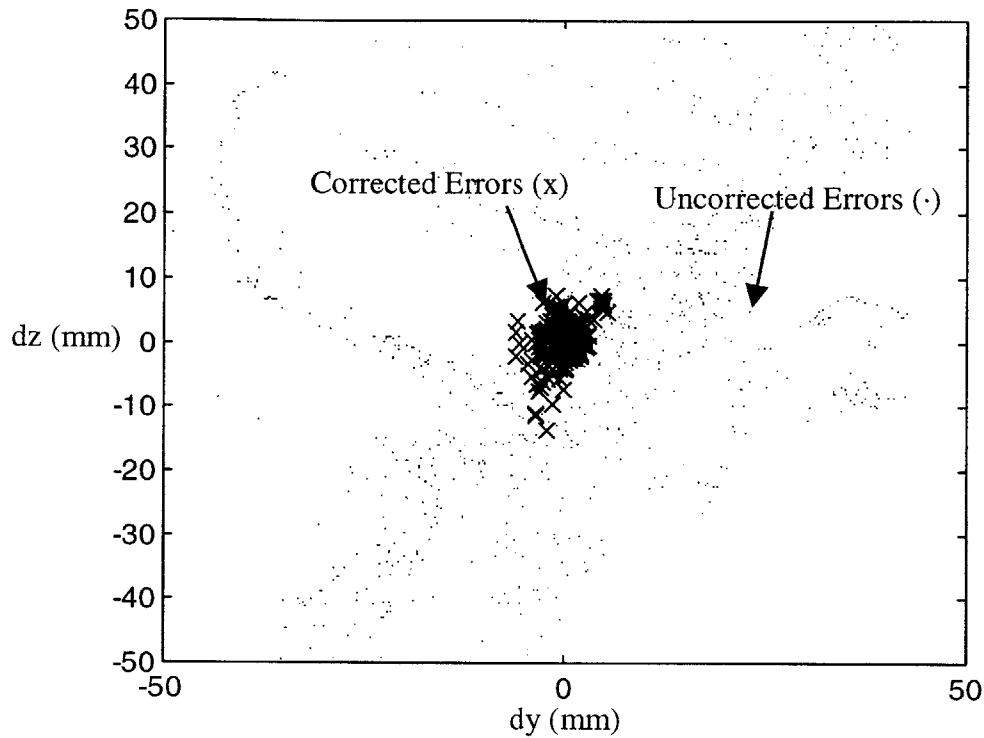


**Figure 5.14(b) - Measured and Residual Errors After Compensation**

## 5.4 Summary and Conclusions

In this chapter, a calibration method that does not require endpoint measurements has been investigated. The method constrains the robot end-effector to a fixture equivalent to a spherical joint. The required fixture has the advantage of being inexpensive and compact when compared to pose measuring devices required by other calibration techniques. By forming the manipulator into a closed kinematic chain, the kinematic loop closure equations are adequate to calibrate the manipulator from joint readings alone. A performance index is introduced to calculate the optimal location of the calibration fixture. The method is evaluated experimentally on a Schilling Titan II



manipulator. Results show that the SEC calibration method is able to effectively identify and correct for errors in the system.

## **Force-Updated Virtual Viewing System**

---

### **6.1 Introduction**

This chapter presents a method to obtain contact force information between the manipulator end-effector and the environment. This method combines wrist force/torque sensor information with knowledge of the end-effector geometry to estimate contact location. These estimates are combined with a custom teleoperator software package developed for the nozzle dam placement task. Section 6.2 presents the theoretical framework for contact force estimation. Section 6.3 introduces a virtual environment teleoperator software package. Section 6.4 presents experiments with a Schilling hydraulic manipulator, showing that successful nozzle dam placements can be performed using the visualization system with contact force estimation.

### **6.2 Contact Force Estimation**

Contact force information between the manipulator end-effector and the environment is fundamental for placement tasks with small tolerances (Bicchi, 1993). Even with the key enabling technologies presented in the previous chapters, the nozzle

dam task may still be impossible to complete due to misalignments. Some geometric uncertainty still exists between the modeled and real environments making teleoperation difficult to perform. Several sources of geometric uncertainty contribute to this. First, the manipulator position relative to the nozzle ring may not be known to high tolerance. Second, placement of the manipulator in the workspace may require mounting it on a gantry system which is often subject to deformations, thereby inducing errors in the absolute position control of the robot (Kuklinski, 1993). Finally, the coupling between the manipulator gripper and the nozzle dam may not be repeatable to within the acceptable insertion errors.

To overcome this, alternate methods must be explored to provide additional information. The method explored in this section uses contact forces measured by a wrist force/torque sensor to aid in the insertion task. The contact forces between the center plate and its receptacle are estimated from wrist sensor information and displayed graphically to the teleoperator.

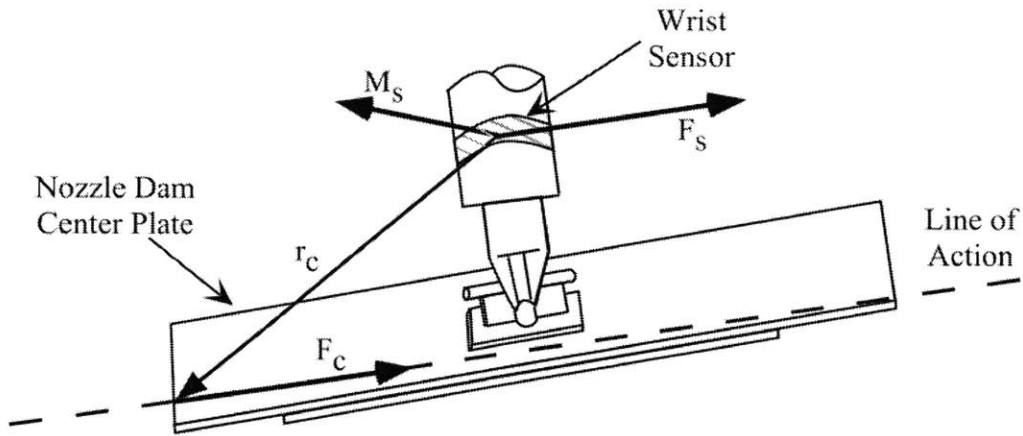
However, a wrist force/torque sensor provides limited information, namely 3 force and 3 torque components, while each contact point is associated with 9 unknowns: the coordinates of the contact point location and the contact wrench components. In the case where there is only one contact point with the environment and where the contact torque is zero, it is possible to calculate the contact information required for control. This can be obtained from wrist force-torque sensor information combined with geometrical knowledge of the mating parts.

Figure 6.1 shows a plate attached to the end-effector of a manipulator. The force exerted by the environment on the plate,  $\mathbf{F}_c$ , and the contact location with respect to the wrist force/torque sensor,  $\mathbf{r}_c$ , can be calculated from:

$$\mathbf{F}_c = \mathbf{F}_s \quad (6.1)$$

$$\mathbf{r}_c = \frac{\mathbf{F}_s \times \mathbf{M}_s}{\|\mathbf{F}_s \times \mathbf{M}_s\|} \frac{\|\mathbf{M}_s\|}{\|\mathbf{F}_s\|} + \alpha \mathbf{F}_s \quad (6.2)$$

where  $\mathbf{F}_s$  and  $\mathbf{M}_s$  are respectively the forces and moments measured from the wrist sensor, and  $\alpha$  is an arbitrary constant. Note that Equation (6.1) has an infinite number of solutions, since two equal forces along the same line of action result in the same wrist sensor reading (see Figure 6.1).



**Figure 6.1 - Contact Force and Wrist Force/Torque Sensor Readings**

To obtain a unique solution to Equation (6.1), the plate geometry must be considered. Defining  $\Gamma$  as a vector function representing the plate surface in the wrist

sensor coordinates, then  $\alpha$  is determined by calculating the intersection between the line of action of the contact force and the plate surface  $\Gamma$ ,

$$\alpha \mathbf{F}_s \equiv \Gamma - \frac{\mathbf{F}_s \times \mathbf{M}_s}{\|\mathbf{F}_s \times \mathbf{M}_s\|} \frac{\|\mathbf{M}_s\|}{\|\mathbf{F}_s\|} \quad (6.3)$$

Due to the nature of contact forces, which are directed toward the interior of the plate, the calculated values of  $\mathbf{r}_c$  must also satisfy

$$\mathbf{n}(\mathbf{r}_c) \cdot \mathbf{F}_c \leq 0 \quad (6.4)$$

where  $\mathbf{n}(\mathbf{r}_c)$  is the normal vector to the plate surface at the point  $\mathbf{r}_c$ .

If  $\Gamma$  represents a convex surface, then the solution to Equations (6.3) and (6.4) is either unique or non-existent. Otherwise, multiple solutions exist for certain configurations. For the particular case shown in Figure 6.1,  $\Gamma$  is not convex, but it can be represented by a set of simple equations of the planes of the plate. Frequently, as in the case of the nozzle dam insertion plate, a single solution for the contact point can be determined by considering the contact friction as well as the geometry of the mating parts.

Based on Equations (6.3) and (6.4) and models of the plate and receptacle, a force vector and contact point is calculated from the measured wrist wrench and displayed to the teleoperator.

### 6.3 Virtual Environment Teleoperator Software

Even with contact force information, the nozzle dam placement task is still very difficult to perform due to restricted teleoperator visibility and tight geometric tolerances between the nozzle dam and its receptacle.

The most common solution is to position a camera in the workspace, thereby providing the teleoperator with a real-time video feed showing the current state of the manipulator and the task. Yet, this allows very limited visualization of the workspace. The large nozzle dam in the confined environment is likely to obscure necessary mating features. Adding more cameras can improve operator visibility, but an increased number of cameras makes it harder for the teleoperator to process the expanding amount of visual data.

A more versatile teleoperation solution is a virtual, 3D representation of the environment. This could dramatically improve visual capabilities with arbitrary camera angles, unlimited panning and zooming, as well as the ability to make objects transparent that obscure crucial visual features. For this purpose, a custom teleoperator software package has been developed. The system contains 3-D kinematic models of the manipulator and the workspace, reflecting the actual system configuration based on the joint resolvers. The interface provides improved operator visibility by allowing virtual viewing of the workspace using arbitrarily positioned "virtual cameras" (Cho, 1998). The virtual cameras also allow for unrestricted panning and magnification of mating edges or other crucial features to aid in teleoperated insertion. Virtual objects can also be made transparent revealing otherwise physically obscured regions. The virtual cameras also allow for magnifying the mating edges in order to aid in teleoperated insertion. A

Cartesian end-point controller is embedded in the software to provide full teleoperation functionality. Figure 6.2 shows the manipulator and experimental testbed for both real and simulated systems.

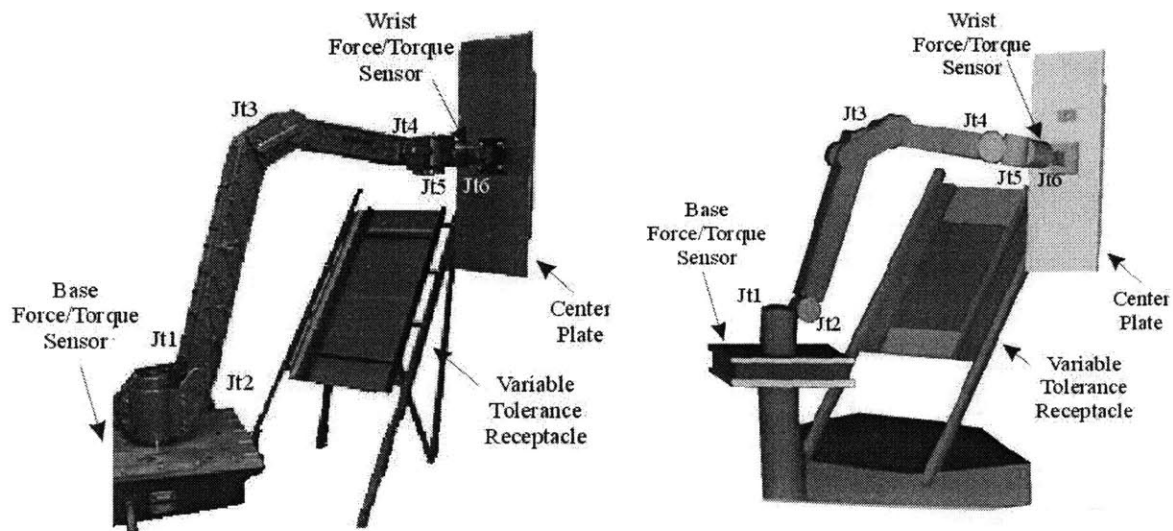


**Figure 6.2 - Real (a) and Simulated (b) Experimental System**

The ideal operator environment is an integration of visualization software with a control system. Once the visualization package was ported to the control PC, the virtual environment could be linked to the actual experimental system. The interface was achieved in two stages.

First, optical theodolites were used to measure the experimental system's position in 3D space with respect to the base of the Schilling manipulator. The optical theodolites had a measurement accuracy of 0.3mm, putting the alignment of the virtual and real environments within the limits of the mating tolerances. Therefore, successful positioning of the virtual nozzle dam within the virtual nozzle ring could correspond to successful insertion in the real system.

The second stage allows active control of the Schilling from the teleoperator package. The forward and inverse kinematic relations in the visualization software were used to implement Cartesian end-point control of the robot (Asada and Slotine, 1986). Based on a desired end-effector position, the desired joint angles are calculated based on a higher level trajectory planner. The desired joint angles are compared to the current joint positions read from the resolvers. The control loop was embedded in an Interrupt Service Routine (ISR) triggered by an interrupt signal originating from a timer card. This guaranteed a consistent sample of 10 ms.

Once the control shell was in place, the control algorithm could be expanded as needed. The tight tolerances of the task require the teleoperator to command fine position adjustments, therefore BSC was implemented to improve the manipulator repeatability through accurate joint torque control using the base force/torque sensor (see Section 2.2). To improve the correlation of the commanded Cartesian position of the Schilling and the actual position of the Schilling end-effector, GEC (Geometric and Elastic Error Compensation) was included to improve the absolute accuracy, using offline measurements provided by the SEC (Single Endpoint Contact) method (see Chapters 4 and 5). Figure 6.3 summarizes how a force-updated operator interface is combined with the high accuracy GEC/BSC position controller using SEC measurements to perform the nozzle dam placement task.



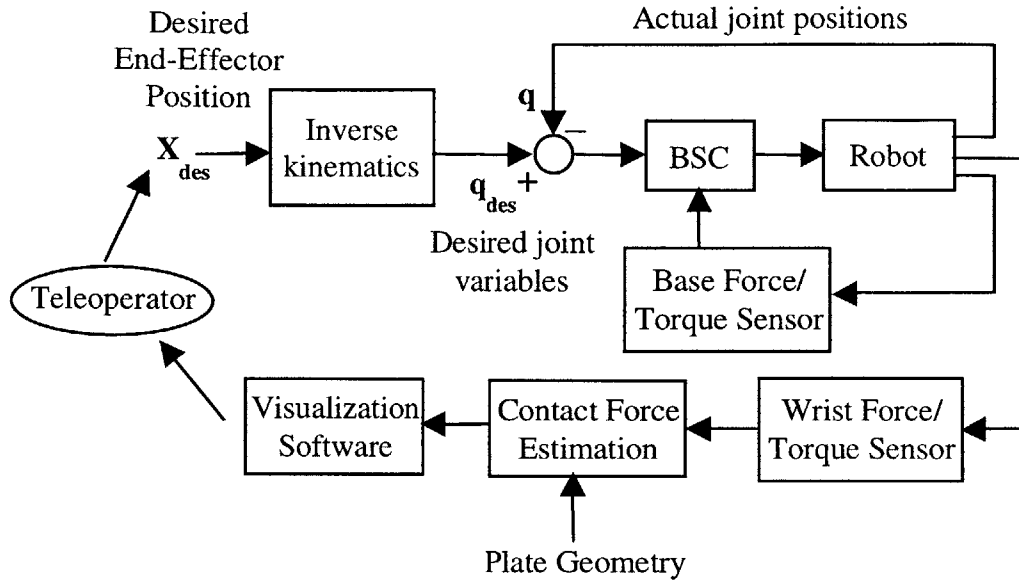


**Figure 6.3 - Base Sensor Control and Contact Force Estimation Scheme**

## 6.4 Experimental Verification

Representative nozzle dam placements were conducted to demonstrate the effectiveness of the force-updated virtual viewing system with contact estimation.

Figure 6.4 shows a sequence of screenshots from the teleoperator display during a typical placement. Each figure shows the center plate contacting the mating receptacle as well as visual feedback of the estimated contact force. The contact vector identifies misalignments in the insertion process, providing the necessary information to command small corrective motions.

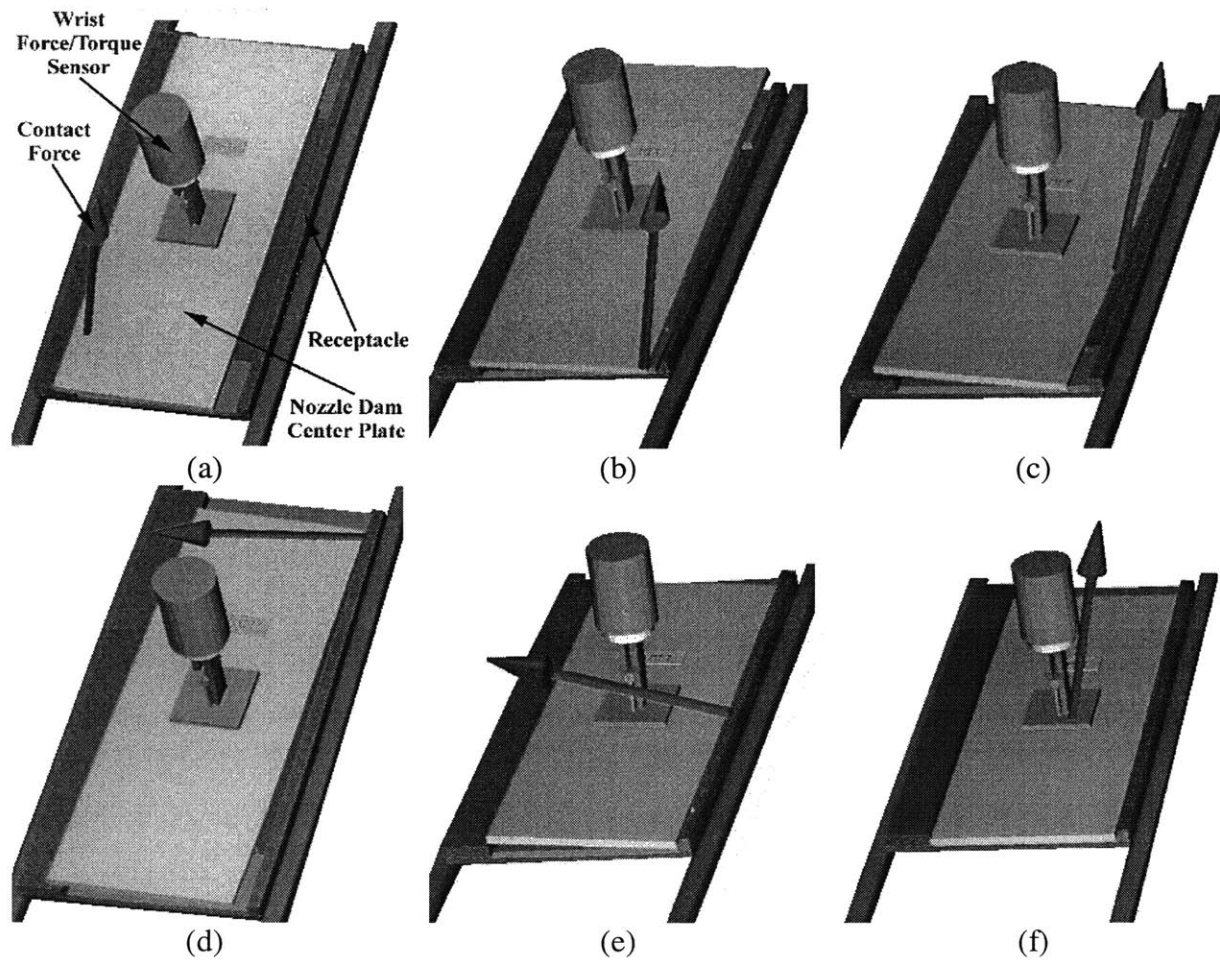


**Figure 6.4 – Typical Placement Steps Using Contact Force Visualization**

Figure 6.4a suggests translational motions are necessary to align the plate. The next four screenshots shown in Figure 6.4 indicate rotational alignment errors. Finally, the contact force in Figure 6.4f suggests that successful placement was achieved.

The experimental insertions show that the force-updated virtual viewing system outlined in Figure 6.3 allows a conventional hydraulic manipulator to successfully perform the nozzle dam placement task. This approach is made practical by the means of BSC and GEC control using SEC offline measurements.

## 6.5 Summary and Conclusions

In this chapter, a robotic visualization system for successfully placing a nuclear power plant steam generator nozzle dam is presented. A teleoperator software package has been developed containing 3-D kinematic models of a Schilling Titan II hydraulic manipulator and the workspace. Contact force information between the center plate and its receptacle is obtained from wrist sensor wrench measurements and geometric models of the mating geometries. The contact force vector is displayed to the teleoperator and allows for real-time recognition of misalignments in the insertion process. This aids in successfully achieving insertion using a position control algorithm. Experiments demonstrated that the nozzle dam placement task can be successfully performed by combining a high repeatability position controller, such as BSC and GEC, and a force-updated operator interface.

## Conclusions and Suggestions for Future Work

---

### 7.1 Contributions of This Work

This thesis described methodologies to substantially improve the absolute accuracy in strong powerful manipulators lacking good repeatability and having significant geometric and elastic errors.

A general analytical method to eliminate the redundant error parameters in robot calibration was presented. These errors, often non-intuitive, must be eliminated from the error model prior to the identification process, since otherwise the robustness of the calibration can be compromised. The analytical expressions and physical interpretation of the linear combinations present in the generalized error parameterization were developed. The non-redundant form of the Identification Jacobian matrix was obtained using these expressions, allowing for the systematic calibration of any serial link manipulator with improved accuracy.

A method to compensate the positioning end-effector errors of large manipulators with significant task loads was presented. Both geometric and elastic errors were considered without requiring any explicit elastic model of the system. The method has been applied experimentally to a high-accuracy large medical manipulator (PPS) and to a

Schilling Titan II manipulator. The results showed that the basic accuracy of these manipulators exceeded their specifications, but after applying the method to compensate for end-effector errors the accuracy specifications are met. The method is now a key element of the PPS software used to treat cancer patients at the Massachusetts General Hospital (Flanz, 1996).

A calibration method that does not require endpoint measurements or precision points has been investigated. The method constrained the robot end-effector to a fixture equivalent to a spherical joint. The required fixture had the advantage of being inexpensive and compact when compared to pose measuring devices required by other calibration techniques. By forming the manipulator into a mobile closed kinematic chain, the kinematic loop closure equations were adequate to calibrate the manipulator from joint readings alone. A performance index was introduced to calculate the optimal location of the calibration device. The method was evaluated experimentally on a Schilling Titan II manipulator. The results showed that the calibration method was able to effectively identify and correct for the errors in the system.

Finally, a robotic visualization system for successfully placing a nuclear power plant steam generator nozzle dam was presented. A teleoperator software package has been developed containing 3-D kinematic models of a Schilling Titan II hydraulic manipulator and the workspace. Contact force information between the center plate and its receptacle was obtained from wrist sensor wrench measurements and geometric models of the mating geometries. The contact force vector was displayed to the teleoperator and allowed for real-time recognition of misalignments in the insertion process. This aided in successfully achieving insertion using a position control

algorithm. An experimental system was developed that employed a Schilling hydraulic manipulator, mechanical fixturing that embodied the crucial task criteria of the nozzle dam placement. Experiments demonstrated that the nozzle dam placement task could be achieved by combining a high repeatability position controller, such as BSC and GEC, and a force-updated operator interface.

## **7.2 Suggestions for Further Work**

This thesis has shown that fine absolute positioning accuracy could be achieved in large powerful manipulators lacking good repeatability and having significant geometric and elastic errors. Although substantial work has been completed in this area, some improvements can be achieved in the presented methodologies.

In this work, a general analytical method to eliminate the redundant error parameters in robot calibration was presented. The analytical expressions presented here were only valid for serial link manipulators. Methods to eliminate redundant errors in parallel manipulators have yet to be developed.

In the GEC (Geometric and Elastic Error Compensation) method, generalized errors are represented by polynomial series expansions. The minimum order of each of the polynomials to achieve a desired absolute accuracy depends on the manipulator being calibrated. For instance, third order polynomials are in general sufficient to model elastic deflections, but higher order polynomials are required to identify rail curvatures in linear joints. An optimization method to calculate the minimum order of the generalized error polynomials could be developed, resulting in a reduced number of required measurement points for a given absolute accuracy.

# References

- Abdel-Malek, K. and Yeh, H.J., "Analytical Boundary of the Workspace for General 3-DOF Mechanisms", *International Journal of Robotics Research*, Vol. 16, No. 2, pp. 198-213, 1997.
- Asada, H. and Hirai S. "Towards a symbolic-level force feedback: recognition of assembly process states," *Robotics Research Fifth International Symposium*, pp.341-346, MIT Press, Cambridge, MA, 1990.
- Asada, H. and Slotine, J.-J., *Robot Analysis and Control*, Wiley, New York, 1986.
- Bennett, D.J. and Hollerbach, J.M., "Autonomous Calibration of Single-Loop Closed Kinematic Chains Formed by Manipulators with Passive Endpoint Constraints", *IEEE Trans. Robotics and Automation*, Vol. 7, No. 5, pp.597-606, 1991.
- Bicchi, A., Salisbury, J., and Brock, D., "Contact Sensing from Force Measurements," *International Journal of Robotics Research*, Vol. 12, No. 3, pp 249-262, 1993.
- Borm, J.H. and Menq, C.H., "Determination of Optimal Measurement Configurations for Robot Calibration Based on Observability Measure", *International Journal of Robotics Research*, Vol. 10, No. 1, pp. 51-63, 1991.
- Broderick, P. and Cirpa, R., "A Method for Determining and Correcting Robot Position and Orientation Errors Due to Manufacturing", *Transactions of the ASME, Journal of Mechanisms, Transmissions and Automation in Design*, Vol. 10, pp. 3-10, 1988.
- Burdick, J.W., "On the Inverse Kinematics of Redundant Manipulators: Characterization of the Self-Motion Manifolds", *Proceedings of the IEEE International Conference on Robotics and Automation*, Vol.1, pp. 264-270, 1989.

- Canudas-de-Wit, C., Olsson, H, Astrom, K.J. and Lischinsky, P., "A New Model for Control of Systems with Friction," *IEEE Transactions on Automatic Control* Vol. 40, No. 3, pp. 419-425, 1995.
- Cho, B.H., "Maintenance Procedure: Nozzle Dam Installation and Removal," KEPCO Internal Report, 1997.
- Cho, B.H., "Simulation Studies on Robot System Applied to Nozzle Dam Installation," Technical Report to KEPRI, 1998.
- Craig, J., *Introduction to Robotics*, Addison-Wesley Publishing Company, Massachusetts, 1989.
- Dakin, G.A., *Fine-Motion Planning for Robotic Assembly in Local Contact Space*, PhD thesis, Department of Computer Science, University of Massachusetts Amherst, Amherst, Massachusetts, 1994.
- Drouet, P., Dubowsky, S. and Mavroidis, C., "Compensation of Geometric and Elastic Deflection Errors in Large Manipulators Based on Experimental Measurements: Application to a High Accuracy Medical Manipulator," *Proceedings of the 6th International Symposium on Advances in Robot Kinematics*, Austria, pp. 513-522, 1998.
- Drouet, P., *Modeling, Identification and Compensation of Positioning Errors in High Accuracy Manipulators under Variable Loading: Application to a Medical Patient Positioning System*, Ph.D. Thesis, Université de Poitiers, France, 1999.
- Dubowsky, S., Maatuk, J. and Perreira, N.D., "A Parametric Identification Study of Kinematic Errors in Planar Mechanisms," *Transactions of the ASME, Journal of Engineering for Industry*, pp. 635-642, 1975.



- Everett, L.J., Lei, J., "Improved Manipulator Performance Through Local D-H Calibration", *Journal of Robotics Systems*, Vol. 12, No. 7, pp. 505-514, 1995.
- Everett, L.J., Lin, C.Y., "Kinematic Calibration of Manipulators with Closed Loop Actuated Joints", *Proceedings of the 1988 IEEE International Conference of Robotics and Automation*, pp. 792-797, 1988.
- Everett, L.J., Suryohadiprojo, A.H., "A Study of Kinematic Models for Forward Calibration of Manipulators," *Proc. IEEE International Conference of Robotics and Automation*, Philadelphia, pp.798-800, 1988.
- Flanz, J. et al., "Overview of the MGH-Northeast Proton Therapy Center: Plans and Progress", *Nuclear Instruments and Methods in Physics Research B*, Vol. 99, pp. 830-834, 1995.
- Flanz, J. et al., "Design Approach for a Highly Accurate Patient Positioning System for NPTC." *Proceedings of the PTOOG XXV and Hadrontherapy Symposium*, Belgium, 1996.
- General Atomics, Patient Positioner Preliminary Design Documents, 1995.
- Gorinevsky, D., Formalsky, A. and Schneider, A., *Force Control of Robotics Systems*, CRC Press, New York, NY, 1997.
- Gullapalli, V., Grupen, R., and Barto, A., "Learning Reactive Admittance Control," *Proceedings of the IEEE International Conference on Robotics and Automation*, pp. 1475-1480, 1992.
- Habibi, S.R., Richards, R.J., and Goldenberg, A.A., "Hydraulic Actuator Analysis for Industrial Robot Multivariable Control," *Proceedings of the American Control Conference*, Vol. 1, pp. 1003-1007, 1994.

- Hamel W., Marland S. and Widner T., "A Model-Based Concept for Telerobotic Control of Decontamination and Dismantlement Tasks," *Proceedings of the 1997 IEEE International Conference of Robotics and Automation*, Albuquerque, New Mexico, 1997.
- Hayati, S.A., "Robot Arm Geometry Link Parameter Estimation," *Proc. 22nd IEEE Conference Decision and Control*, San Antonio, pp. 1477-1483, 1983.
- Hayati, S.A., Tso, K., Roston, G., "Robot Geometry Calibration," *Proceedings of the IEEE International Conference of Robotics and Automation*, pp. 947-951, 1988.
- Hollerbach, J.M., "A Survey of Kinematic Calibration," *Robotics Review*, Khatib O. et al editors, Cambridge, MA, MIT Press, 1988.
- Hollerbach, J.M., Wampler, C.W., "The Calibration Index and Taxonomy for Robot Kinematic Calibration Methods", *International Journal of Robotics Research*, Vol. 15, No. 6, pp. 573-591, 1996.
- Hsu, T.W., Everett, L.J., "Identification of the Kinematic Parameters of a Robot Manipulator for Positional Accuracy Improvement," *Proceedings of Computation in Engineering Conference*, Boston, pp. 263-267, 1985.
- Huang, Q., "Study on the Workspace of a R-Robot", Published by SME, Dearborn, MI, Robots 8, Conference Proceedings, Detroit, MI, Vol. 1, pp. 4.55-4.66, 1984.
- Iagnemma, K., Morel, G. and Dubowsky, S., 1997, "A Model-Free Fine Position Control System Using the Base-Sensor: With Application to a Hydraulic Manipulator," *Symposium on Robot Control (SYROCO '97)*, Vol. 2, pp. 359-365, 1997.

- Ikits, M., Hollerbach, J.M., "Kinematic Calibration Using a Plane Constraint," *IEEE International Conference on Robotics and Automation*, Albuquerque, New Mexico, pp.3191-3196, 1997.
- Johnson, D.R., "An Approach to Large-Scale, Non-Contact Coordinate Measurements," Hewlett Packard Journal, 1980.
- Khalil, W., Gautier, M., Enguehard, Ch., "Identifiable Parameters and Optimum Configurations for Robots Calibration," *Robotica*, Vol. 9, pp. 63-70, 1991.
- Kuklinski, A., *The Practical Implementation of an Experiment Tool for the Dynamic Interactions in Mobile Manipulator Systems*, S.M. Thesis, Department of Mechanical Engineering, Massachusetts Institute of Technology, Cambridge, Massachusetts, 1993.
- Lau, K., Dagalakis, N. and Myers, D., "Testing," in *International Encyclopedia Robotics: Applications in Automation*, New York: Wiley, 1984.
- Lee, J.H., Kim, S., Kim, D., Kang, H. and Park, J.O., "Teleoperation system for sensitive task manipulation," *Proceedings of the 3rd Asian Conference on Robotics and its Applications*, pp.257-64, 1997.
- Leon, S., *Linear algebra with applications*. Indianapolis; Macmillian College Publishing Company, 1994.
- Mavroidis, C., Dubowsky, S., Drouet, P., Hintersteiner, J. and Flanz, J., "A Systematic Error Analysis of Robotic Manipulators: Application to a High Performance Medical Robot," *Proceedings of the 1997 IEEE International Conference of Robotics and Automation*, Vol.2, pp.980-985, 1997.

- Meggiolaro, M., Dubowsky, S., "An Analytical Method to Eliminate the Redundant Parameters in Robot Calibration," *Proceedings of the International Conference on Robotics and Automation (ICRA '2000)*, IEEE, San Francisco, pp. 3609-3615, 2000.
- Meggiolaro, M., Dubowsky, S. and Mavroidis, C., "Calibrating for Geometric and Elastic Errors in Large Manipulators Including Elimination of Redundant Error Parameters", submitted to the *International Journal of Robotics Research*, 2000.
- Meggiolaro, M., Jaffe, P., Dubowsky, S., "Achieving Fine Absolute Positioning Accuracy in Large Powerful Manipulators," *Proceedings of the International Conference on Robotics and Automation (ICRA '99)*, pp.2819-2824, IEEE, Detroit, 1999.
- Meggiolaro, M., Jaffe, P., Iagnemma, K. and Dubowsky, S., "A Force-Updated Kinematic Virtual Viewing System With Application To Nuclear Power Plant Maintenance," *Proceedings of the Tenth World Congress on The Theory of Machine and Mechanisms (IFTOMM)*, Finland, 1999.
- Meggiolaro, M., Mavroidis, C. and Dubowsky, S., "Identification and Compensation of Geometric and Elastic Errors in Large Manipulators: Application to a High Accuracy Medical Robot," *Proceedings of the 1998 ASME Design Engineering Technical Conference*, Atlanta, 1998.
- Meggiolaro, M., Scriffignano, G. and Dubowsky, S., "Manipulator Calibration Using A Single Endpoint Contact Constraint," *Proceedings of the 2000 ASME Design Engineering Technical Conference*, Maryland, 2000.
- Merritt, H., *Hydraulic Control Systems*, John Wiley and Sons, New York, 1967.

- Ming, O.Y., Beard, D.V., and Brooks, F.P., "Force display performs better than visual display in a simple 6-D docking task," *Proceedings of the 1989 IEEE International Conference on Robotics and Automation*, Vol. 3, pp.1462-1466, Washington, DC, 1989.
- Minsky, M., Ming, O., Steele, O., Brooks F.P. and Behensky, M., "Feeling and seeing: issues in force display," *Computer Graphics*, Vol.24, No.2, pp.235-43, 1990.
- Mirman, C. and Gupta, K., "Identification of Position Independent Robot Parameter Errors Using Special Jacobian Matrices," *International Journal of Robotics Research*, Vol. 12, No. 3, pp. 288-298, 1993.
- Morel, G. and Dubowsky, S., "The Precise Control of Manipulators with Joint Friction: A Base Force/Torque Sensor Method," *Proceedings of the IEEE International Conference on Robotics and Automation*, Vol. 1, pp. 360-365, 1996.
- Morel, G., Iagnemma, K. and Dubowsky, S., "The Precise Control of Manipulators with High Joint Friction Using Base Force/Torque Sensing," *Automatica*, pp. 931-941, 2000.
- Nevins, J.L. and Whitney, D.E., "The Force Vector Assembler Concept," *1st CISM-IFTOMM Symposium on Theory and Practice of Robots and Manipulators*, p. 21, 1973.
- Oriolo, G., "Stabilization of Self-Motions in Redundant Robots", *Proceedings of the IEEE International Conference on Robotics and Automation*, pp. 704-709, 1994.
- Ottaviano, E., Ceccarelli, M. and Lanni, C., "A Characterization of Ring Void in Workspace of Three-Revolute Manipulators", *Proc. of the 10th World Congress on the Theory of Machines and Mechanisms*, pp. 1039-1044, Oulu, Finland, 1999.

- Pfeffer, L.E., Khatib, O. and Hake, J., "Joint Torque Sensory Feedback of a PUMA Manipulator," *IEEE Transactions on Robotics and Automation*, Vol. 5, No. 4, pp. 418-425, 1989.
- Popovic, M.R., Shimoga, K.B. Goldenberg, A.A. and Hui, R.C., "Model-Based Compensation of Friction in Direct Drive Robotic Arms," *Journal of Studies in Information and Control*, Vol.3, No.1, pp. 75-88, 1994.
- Qiao, H., Dalay, B. S., and Parkin, R. M., "Fine Motion Strategies for Robotic Peg-Hole Insertion," *Proceedings of the Institution of Mechanical Engineers*, Part C, Vol. 209, pp. 429-448, 1995.
- Rabinowitz, I. et al, "Accuracy of Radiation Field Alignment in Clinical Practice." *International Journal of Radiation Oncology, Biology and Physics*, Vol. 11, pp. 1857-1867, 1985.
- Roth, B., "Performance Evaluation of Manipulators from a Kinematic Viewpoint," *Performance Evaluation of Programmable Robots and Manipulators*, National Bureau of Standards, Special Publ. 459, pp. 39-61, 1976.
- Roth, Z.S., Mooring, B.W. and Ravani, B., "An Overview of Robot Calibration," *IEEE Southcon Conference*, Vol.RA-3, No.5, pp.377-85, 1987.
- Scheffer, B., "Geometric Control and Calibration Methods of Industrial Robots," *12<sup>th</sup> International Symposium on Industrial Robotics*, Renault, France, 1976.
- Schilling Development, Inc., *Tomcat Manipulator System*, Technical Manual, 1991.
- Schneider, J.L., "Automated Tactile Sensing for Object Recognition and Localization," PhD Thesis, Department of Mechanical Engineering, Massachusetts Institute of Technology, Cambridge, Massachusetts, 1986.

- Schröer, K., "Theory of Kinematic Modelling and Numerical Procedures for Robot Calibration." In Bernhardt, R., Albright, S.L. (eds.): Robot Calibration. London: Chapman & Hall, pp.157-196, 1993.
- Simunovic, S.N., *An Information Approach to Parts Mating*, PhD thesis, Department of Mechanical Engineering, Massachusetts Institute of Technology, Cambridge, Massachusetts, 1979.
- Slocum, A., *Precision Machine Design*, Prentice Hall, Englewood Cliffs, 1992.
- Vaillancourt, C. and Gosselin, G., "Compensating for the Structural Flexibility of the SSRMS with the SPDM," *Proceedings of the International Advanced Robotics Program, Second Workshop on Robotics in Space*, Canadian Space Agency, Montreal, Canada, 1994.
- Vaishnav, R. and Magrab, E., "A General Procedure to Evaluate Robot Positioning Errors," *International Journal of Robotics Research*, Vol. 6, No. 1, pp. 59-74, 1987.
- Vira, K. and Lau, K., "Design and Testing of an Extensible Ball Bar for Measuring the Positioning Accuracy and Repeatability of Industrial Robots," *Proceedings of the NAMRAC Conference*, pp. 583-590, 1986.
- Volpe, R. and Khosla, P., "An Analysis of Manipulator Force Control Strategies Applied to an Experimentally Derived Model," *Proceedings of the 1992 IEEE/RSJ International Conference on Intelligent Robots and Systems*, pp.1989-1997, 1992.
- Waldron, K. and Kumar, V., "Development of a Theory of Errors for Manipulators," *Proceedings of the Fifth World Congress on the Theory of Machines and Mechanisms*, pp. 821-826, 1979.

- Warnecke, H.J., Weck, M. and Brodbeck, B., "Assessment of Industrial Robots," *General Assembly of CIRP*, 30<sup>th</sup> Proceeding, 1980.
- Whitney, D.E., "Historical Perspective and State of the Art in Robot Force Control," *International Journal of Robotics Research*, Vol. 6, No. 1, pp.3-14, 1987.
- Whitney, D.E., Lozinski, C.A., Rourke, J.M., "Industrial Robot Forward Calibration Method and Results," *Transactions of the ASME, Journal of Dynamic Systems, Measurement and Control*, Vol. 108, pp. 1-8, 1986.
- Wu, C., "A Kinematic CAD Tool for the Design and Control of a Robot Manipulator," *International Journal of Robotics Research*, Vol.3, No. 1, pp. 58-67, 1984.
- Yang, D.C.H. and Lee, T.W., "On the Workspace of Mechanical Manipulators," *Transactions of the ASME, Journal of Mechanical Design*, Vol. 105, pp. 62-69, 1983.
- Zeza, L.J., "Steam Generator Nozzle Dam System," *Transactions of the American Nuclear Society*, Vol. 50, pp. 412-413, 1985.
- Zhuang, H., "Self Calibration of Parallel Mechanisms with a Case Study on Stewart Platforms", *IEEE Trans. Robotics and Automation*, Vol. 13, No. 3, pp.387-397, 1997.
- Zhuang, H., Motaghedi, S.H., Roth, Z.S., "Robot Calibration with Planar Constraints," *Proc. IEEE International Conference of Robotics and Automation*, Detroit, Michigan, pp.805-810, 1999.
- Zhuang, H., Roth, Z. and Hamano, F., "A Complete and Parametrically Continuous Kinematic Model for Robot Manipulators," *IEEE Transaction in Robotics and Automation*, Vol. 8, No. 4, pp. 451-462, 1992.



- Zhuang, H., Roth, Z., "A Linear Solution to the Kinematic Parameter Identification of Robot Manipulators," *IEEE Transactions in Robotics and Automation*, Vol. 9, No. 2, pp. 174-185, 1993.
- Zhuang, H., Roth, Z., Hamano, F., "Observability Issues in Kinematic Identification of Manipulators," *Journal of Dynamic Systems, Measurement, and Control*, Vol. 114, pp. 319-322, 1992.
- Zhuang, H., Wang, L.K., Roth, Z., "Optimal Selection of Measurement Configurations for Robot Calibration Using Simulated Annealing," *Proceedings of the IEEE International Conference in Robotics and Automation*, pp. 393-398, San Diego, CA, 1994.
- Zhuang, H., Wang, L.K., Roth, Z., "Error-Model-Based Robot Calibration Using a Modified CPC Model," *Robotics and Computer Integrated Manufacturing*, Vol. 10, No. 4, pp. 287-299, Great Britain, 1993.
- Zhuang, H., Wu, J., Huang, W., "Optimal Planning of Robot Calibration Experiments by Genetic Algorithms," *Proceedings of the IEEE International Conference in Robotics and Automation*, pp. 981-986, Minneapolis, Minnesota, 1996.
- Ziegert, J., Datseris, P., "Basic Considerations for Robot Calibration," *Proc. IEEE Int. Conf. Robotics and Automation*, Philadelphia, pp. 932-938, 1988.

# Appendix A

## Linear Dependency Calculations

This appendix contains proof of the linear combination expressions of the columns of the Identification Jacobian matrix  $\mathbf{J}_e$ . These combinations are obtained from the symbolic form of  $\mathbf{J}_e$ , expressed through the manipulator's Denavit-Hartenberg parameters. It is shown that the general expressions can be broken down into combinations of the columns associated with each pair of consecutive links. This allows for great simplification of the proof.

Define the position and orientation of a reference frame  $F_i$  with respect to the previous reference frame  $F_{i-1}$  as a 4x4 matrix  $\mathbf{A}_i$  using the D.H. parameters (see Figure 2.3):

$$\mathbf{A}_i = \begin{bmatrix} \cos\theta_i & -\sin\theta_i \cos\alpha_i & \sin\theta_i \sin\alpha_i & a_i \cos\theta_i \\ \sin\theta_i & \cos\theta_i \cos\alpha_i & -\cos\theta_i \sin\alpha_i & a_i \sin\theta_i \\ 0 & \sin\alpha_i & \cos\alpha_i & d_i \\ 0 & 0 & 0 & 1 \end{bmatrix} \quad (\text{A.1})$$

When the generalized errors defined in Section 2.3 are considered in the model, the manipulator loop closure equation takes the form:

$$\mathbf{A}_{LC} = \mathbf{E}_0 \mathbf{A}_1 \mathbf{E}_1 \mathbf{A}_2 \mathbf{E}_2 \dots \mathbf{A}_n \mathbf{E}_n \quad (\text{A.2})$$

where  $\mathbf{A}_{LC}$  is a 4x4 homogeneous matrix that describes the position and orientation of the end-effector frame  $F_n$  with respect to the inertial reference frame  $F_0$ , and after a first order approximation the error matrix  $\mathbf{E}_i$  has the form:

$$\mathbf{E}_i = \begin{bmatrix} 1 & -\epsilon_{r,i} & \epsilon_{s,i} & \epsilon_{x,i} \\ \epsilon_{r,i} & 1 & -\epsilon_{p,i} & \epsilon_{y,i} \\ -\epsilon_{s,i} & \epsilon_{p,i} & 1 & \epsilon_{z,i} \\ 0 & 0 & 0 & 1 \end{bmatrix} \quad (\text{A.3})$$

The Identification Jacobian matrix  $\mathbf{J}_e$  is determined by taking the derivative of the loop closure matrix  $\mathbf{A}_{LC}$  with respect to each generalized error  $\epsilon_{j,i}$ , resulting in 4x4 sensitivity matrices  $\mathbf{L}_{j,i}$

$$\mathbf{L}_{j,i} \equiv \left. \frac{\partial (\mathbf{E}_0 \mathbf{A}_1 \mathbf{E}_1 \cdots \mathbf{A}_i \mathbf{E}_i \cdots \mathbf{A}_n \mathbf{E}_n)}{\partial \epsilon_{j,i}} \right|_{\epsilon=0} \quad (\text{A.4})$$

Clearly, the linear combinations of the columns  $\mathbf{J}_{j,i}$  of the Identification Jacobian matrix (defined in Section 3.2) are the same as the ones of the  $\mathbf{L}_{j,i}$  matrices. Since  $\mathbf{E}_i$  is the only matrix that depends on the generalized error  $\epsilon_{j,i}$  then  $\mathbf{L}_{j,i}$  can be simplified to

$$\mathbf{L}_{j,i} = \mathbf{A}_1 \cdots \mathbf{A}_{i-2} \cdot \mathbf{M}_{j,i} \cdot \mathbf{A}_{i+1} \cdots \mathbf{A}_n, \quad \mathbf{M}_{j,i} \equiv \mathbf{A}_{i-1} \mathbf{A}_i \frac{\partial \mathbf{E}_i}{\partial \epsilon_{j,i}} \quad (\text{A.5})$$

Applying the same result for joint  $i-1$ ,

$$\mathbf{L}_{j,(i-1)} = \mathbf{A}_1 \cdots \mathbf{A}_{i-2} \cdot \mathbf{M}_{j,(i-1)} \cdot \mathbf{A}_{i+1} \cdots \mathbf{A}_n, \quad \mathbf{M}_{j,(i-1)} \equiv \mathbf{A}_{i-1} \frac{\partial \mathbf{E}_{i-1}}{\partial \epsilon_{j,(i-1)}} \mathbf{A}_i \quad (\text{A.6})$$

Since both products  $\mathbf{A}_1 \cdots \mathbf{A}_{i-2}$  and  $\mathbf{A}_{i+1} \cdots \mathbf{A}_n$  do not depend on the coordinates of frames  $i-1$  and  $i$ , Equations (A.5) and (A.6) show that the linear combinations of the  $\mathbf{L}_{j,i}$  matrices are also the same as the ones of the  $\mathbf{M}_{j,i}$  matrices. Hence, it is not necessary to develop the lengthy Equations (A.4-A.6), since the desired linear combinations can be

obtained from the much simpler  $\mathbf{M}_{j,i}$  matrices. In addition, all linear combination expressions can then be broken down into expressions involving the generalized errors of each consecutive link pair, since the considered system is a serial link manipulator.

Consider the following general expression for the linear combinations associated with two consecutive links, represented by the unknown coefficients  $c_1, \dots, c_{12}$ :

$$\begin{aligned} c_1 \mathbf{J}_{x,(i-1)} + c_2 \mathbf{J}_{y,(i-1)} + c_3 \mathbf{J}_{z,(i-1)} + c_4 \mathbf{J}_{s,(i-1)} + c_5 \mathbf{J}_{r,(i-1)} + c_6 \mathbf{J}_{p,(i-1)} \equiv \\ c_7 \mathbf{J}_{x,i} + c_8 \mathbf{J}_{y,i} + c_9 \mathbf{J}_{z,i} + c_{10} \mathbf{J}_{s,i} + c_{11} \mathbf{J}_{r,i} + c_{12} \mathbf{J}_{p,i} \end{aligned} \quad (\text{A.7})$$

To determine the unknown coefficients, the column vectors  $\mathbf{J}_{j,i}$  can be replaced by the matrices  $\mathbf{M}_{j,i}$  in the above expression, since it was shown that both  $\mathbf{J}_{j,i}$  and  $\mathbf{M}_{j,i}$  have the same linear combinations. The  $\mathbf{M}_{j,i}$  matrices are obtained by substituting Equations (A.1) and (A.3) into Equations (A.5) and (A.6). Equation (A.7) then results in

$$\left\{ \begin{aligned} & c_4 (\mathbf{w}_i \cos \theta_i) + c_5 (\mathbf{v}_i \cos \theta_i - \mathbf{u}_i \sin \theta_i) + c_6 (\mathbf{w}_i \sin \theta_i) \\ & + c_{10} (\mathbf{u}_i \sin \theta_i \sin \alpha_i - \mathbf{v}_i \cos \theta_i \sin \alpha_i + \mathbf{w}_i \cos \alpha_i) \\ & - c_{11} (-\mathbf{u}_i \sin \theta_i \cos \alpha_i + \mathbf{v}_i \cos \theta_i \cos \alpha_i + \mathbf{w}_i \sin \alpha_i) \equiv 0 \\ & c_4 (-\mathbf{w}_i \sin \theta_i \cos \alpha_i + \mathbf{u}_i \sin \alpha_i) - c_5 \cos \alpha_i (\mathbf{v}_i \sin \theta_i + \mathbf{u}_i \cos \theta_i) \\ & + c_6 (\mathbf{w}_i \cos \theta_i \cos \alpha_i - \mathbf{v}_i \sin \alpha_i) + c_{11} (\mathbf{u}_i \cos \theta_i + \mathbf{v}_i \sin \theta_i) \\ & + c_{12} (\mathbf{u}_i \sin \theta_i \sin \alpha_i - \mathbf{v}_i \cos \theta_i \sin \alpha_i + \mathbf{w}_i \cos \alpha_i) \equiv 0 \\ & c_4 (\mathbf{w}_i \sin \theta_i \sin \alpha_i + \mathbf{u}_i \cos \alpha_i) + c_5 \sin \alpha_i (\mathbf{v}_i \sin \theta_i + \mathbf{u}_i \cos \theta_i) \\ & - c_6 (\mathbf{w}_i \cos \theta_i \sin \alpha_i - \mathbf{v}_i \cos \alpha_i) - c_{10} (\mathbf{u}_i \cos \theta_i + \mathbf{v}_i \sin \theta_i) \\ & + c_{12} (-\mathbf{u}_i \sin \theta_i \cos \alpha_i + \mathbf{v}_i \cos \theta_i \cos \alpha_i + \mathbf{w}_i \sin \alpha_i) \equiv 0 \\ & c_1 \mathbf{u}_i + c_2 \mathbf{v}_i + c_3 \mathbf{w}_i + c_4 (\mathbf{w}_i a_i \cos \theta_i + \mathbf{u}_i d_i) \\ & + c_5 (\mathbf{v}_i a_i \cos \theta_i - \mathbf{u}_i a_i \sin \theta_i) \\ & + c_6 (\mathbf{w}_i a_i \sin \theta_i - \mathbf{v}_i d_i) - c_7 (\mathbf{u}_i \cos \theta_i + \mathbf{v}_i \sin \theta_i) \\ & - c_8 (-\mathbf{u}_i \sin \theta_i \cos \alpha_i + \mathbf{v}_i \cos \theta_i \cos \alpha_i + \mathbf{w}_i \sin \alpha_i) \\ & - c_9 (\mathbf{u}_i \sin \theta_i \sin \alpha_i - \mathbf{v}_i \cos \theta_i \sin \alpha_i + \mathbf{w}_i \cos \alpha_i) \equiv 0 \end{aligned} \right. \quad (\text{A.8})$$

where

$$\mathbf{u}_i \equiv \begin{bmatrix} \cos \theta_{i-1} \\ \sin \theta_{i-1} \\ 0 \\ 0 \end{bmatrix}, \quad \mathbf{v}_i \equiv \begin{bmatrix} -\sin \theta_{i-1} \cos \alpha_{i-1} \\ \cos \theta_{i-1} \cos \alpha_{i-1} \\ \sin \alpha_{i-1} \\ 0 \end{bmatrix}, \quad \mathbf{w}_i \equiv \begin{bmatrix} \sin \theta_{i-1} \sin \alpha_{i-1} \\ -\cos \theta_{i-1} \sin \alpha_{i-1} \\ \cos \alpha_{i-1} \\ 0 \end{bmatrix} \quad (\text{A.9})$$

Solving Equation (A.8) results in

$$\begin{cases} c_4 = c_6 = c_{12} = 0 \\ c_1 = c_7 \\ c_{10} = c_5 \sin \alpha_i \\ c_{11} = c_5 \cos \alpha_i \\ c_8 = c_3 \sin \alpha_i + (c_2 + c_5 a_i) \cdot \cos \alpha_i \\ c_9 = c_3 \cos \alpha_i - (c_2 + c_5 a_i) \cdot \sin \alpha_i \end{cases} \quad (\text{A.10})$$

Then, substituting Equation (A.10) in (A.8) results in Equations (3.2) and (3.3). If joint  $i$  is revolute, then  $c_1 = c_2 = c_7 = 0$ , and no other combinations are present. However, if joint  $i$  is prismatic, then Equation (A.10) results in Equations (3.4) and (3.5).

In the particular case where only the end-effector position is measured, only the last equation in (A.8) must hold, resulting in

$$\begin{cases} c_1 = c_4 = c_6 = c_7 \\ c_8 = c_3 \sin \alpha_n + (c_2 + c_5 \cdot a_n) \cdot \cos \alpha_n \\ c_9 = c_3 \cos \alpha_n - (c_2 + c_5 \cdot a_n) \cdot \sin \alpha_n \end{cases} \quad (\text{A.11})$$

Substituting Equation (A.11) in (A.7) results in

$$\begin{aligned} c_3 \mathbf{J}_{z,(n-1)} + c_5 \mathbf{J}_{r,(n-1)} &\equiv (c_3 \sin \alpha_n + c_5 \cdot a_n \cos \alpha_n) \mathbf{J}_{y,n} + \\ &(c_3 \cos \alpha_n - c_5 \cdot a_n \sin \alpha_n) \mathbf{J}_{z,n} + c_{10} \mathbf{J}_{s,n} + c_{11} \mathbf{J}_{r,n} + c_{12} \mathbf{J}_{p,n} \end{aligned} \quad (\text{A.12})$$

Equation (A.12) must hold for all values of  $c_3$ ,  $c_5$ ,  $c_{10}$ ,  $c_{11}$ ,  $c_{12}$ , resulting in Equation (3.9).

If joint  $n$  is prismatic, then  $c_4$  and  $c_6$  are always zero (even if  $a_n \equiv 0$ ) and no other combinations are present. However, if joint  $n$  is revolute and the link length  $a_n$  is zero,

then  $c_4$  and  $c_6$  are different than zero, and two other linear combinations are present, namely

$$\begin{cases} c_1 + c_4 \cdot d_n = 0 \\ c_2 - c_6 \cdot d_n = 0 \end{cases} \Rightarrow \begin{cases} (-c_4 \cdot d_n) \mathbf{J}_{x,(n-1)} + c_4 \mathbf{J}_{s,(n-1)} = 0 \\ (c_6 \cdot d_n) \mathbf{J}_{y,(n-1)} + c_6 \mathbf{J}_{p,(n-1)} = 0 \end{cases} \Rightarrow \begin{cases} \mathbf{J}_{s,(n-1)} = d_n \mathbf{J}_{x,(n-1)} \\ \mathbf{J}_{p,(n-1)} = -d_n \mathbf{J}_{y,(n-1)} \end{cases} \quad (\text{A.13})$$

Equations (3.3) and (3.9) also imply that  $\mathbf{J}_{r,(n-1)} \equiv \mathbf{0}$  for this case. If the joint offset  $d_n$  is also zero, then reference frames  $n$  and  $n-1$  have common origins at the manipulator end-effector, and Equations (3.3) and (3.10-3.12) imply that

$$\mathbf{J}_{s,(n-1)} \equiv \mathbf{J}_{r,(n-1)} \equiv \mathbf{J}_{p,(n-1)} \equiv \mathbf{0} \quad (\text{A.14})$$

Equations (3.9-3.12) are then recursively applied for link  $n-1$ .

Once the linear combinations of the columns of the Jacobian matrix  $\mathbf{J}_e$  are calculated, the independent generalized error set is obtained. From Equation (3.2),

$$\begin{aligned} \mathbf{J}_{z,(i-1)} \epsilon_{z,(i-1)} + \mathbf{J}_{y,i} \epsilon_{y,i} + \mathbf{J}_{z,i} \epsilon_{z,i} &\equiv \mathbf{J}_{y,i} (\epsilon_{y,i} + \epsilon_{z,(i-1)} \sin \alpha_i) + \\ \mathbf{J}_{z,i} (\epsilon_{z,i} + \epsilon_{z,(i-1)} \cos \alpha_i) &\equiv \mathbf{J}_{y,i} \epsilon_{y,i}^* + \mathbf{J}_{z,i} \epsilon_{z,i}^* \end{aligned} \quad (\text{A.15})$$

showing that the generalized error  $\epsilon_{z,(i-1)}$  can be incorporated into  $\epsilon_{y,i}$  and  $\epsilon_{z,i}$  if joint  $i$  is revolute, resulting in the combined generalized errors  $\epsilon_{y,i}^*$  and  $\epsilon_{z,i}^*$ . Using Equations (3.2) and (3.3) and the approach described above, the combined generalized errors are obtained:

$$\begin{cases} \epsilon_{y,i}^* \equiv \epsilon_{y,i} + \epsilon_{z,(i-1)} \sin \alpha_i + \epsilon_{r,(i-1)} \cdot a_i \cos \alpha_i \\ \epsilon_{z,i}^* \equiv \epsilon_{z,i} + \epsilon_{z,(i-1)} \cos \alpha_i - \epsilon_{r,(i-1)} \cdot a_i \sin \alpha_i \\ \epsilon_{s,i}^* \equiv \epsilon_{s,i} + \epsilon_{r,(i-1)} \sin \alpha_i \\ \epsilon_{r,i}^* \equiv \epsilon_{r,i} + \epsilon_{r,(i-1)} \cos \alpha_i \end{cases} \quad (\text{A.16})$$

which holds for both revolute and prismatic joints.

If joint  $i$  is prismatic, then Equations (3.4) and (3.5) are combined with Equation (A.16), resulting in

$$\begin{cases} \epsilon_{x,i}^* \equiv \epsilon_{x,i} + \epsilon_{x,(i-1)} \\ \epsilon_{y,i}^* \equiv \epsilon_{y,i} + \epsilon_{y,(i-1)} \cos \alpha_i + \epsilon_{z,(i-1)} \sin \alpha_i + \epsilon_{r,(i-1)} \cdot a_i \cos \alpha_i \\ \epsilon_{z,i}^* \equiv \epsilon_{z,i} - \epsilon_{y,(i-1)} \sin \alpha_i + \epsilon_{z,(i-1)} \cos \alpha_i - \epsilon_{r,(i-1)} \cdot a_i \sin \alpha_i \\ \epsilon_{s,i}^* \equiv \epsilon_{s,i} + \epsilon_{r,(i-1)} \sin \alpha_i \\ \epsilon_{r,i}^* \equiv \epsilon_{r,i} + \epsilon_{r,(i-1)} \cos \alpha_i \end{cases} \quad (\text{A.17})$$

In the particular case where the end-effector orientation is not considered, Equation (3.9) implies that the generalized errors  $\epsilon_{s,n}$ ,  $\epsilon_{r,n}$  and  $\epsilon_{p,n}$  do not affect the end-effector measurements. Furthermore, if the last joint is revolute and  $a_n \equiv 0$  then Equation (A.13) results in the combined generalized errors

$$\begin{cases} \epsilon_{x,(n-1)}^* = \epsilon_{x,(n-1)} + \epsilon_{s,(n-1)} \cdot d_n \\ \epsilon_{y,(n-1)}^* = \epsilon_{y,(n-1)} - \epsilon_{p,(n-1)} \cdot d_n \end{cases} \quad (\text{A.18})$$

and also implies that  $\epsilon_{r,(n-1)}$  does not influence the end-effector position.

## Appendix B

### Patient Positioning System Kinematic Description

This appendix contains the PPS direct kinematic equations, as well as the Identification Jacobian matrices for the generalized error formulation.

Consider the D.H. parameters  $q_1, q_2, q_3, q_4, q_5$  and  $q_6$  of the PPS, defined in Figure B.1. The parameters  $x_i, y_i$  and  $z_i$  are constant offsets in the X, Y and Z directions of the D.H. frame  $i$ .

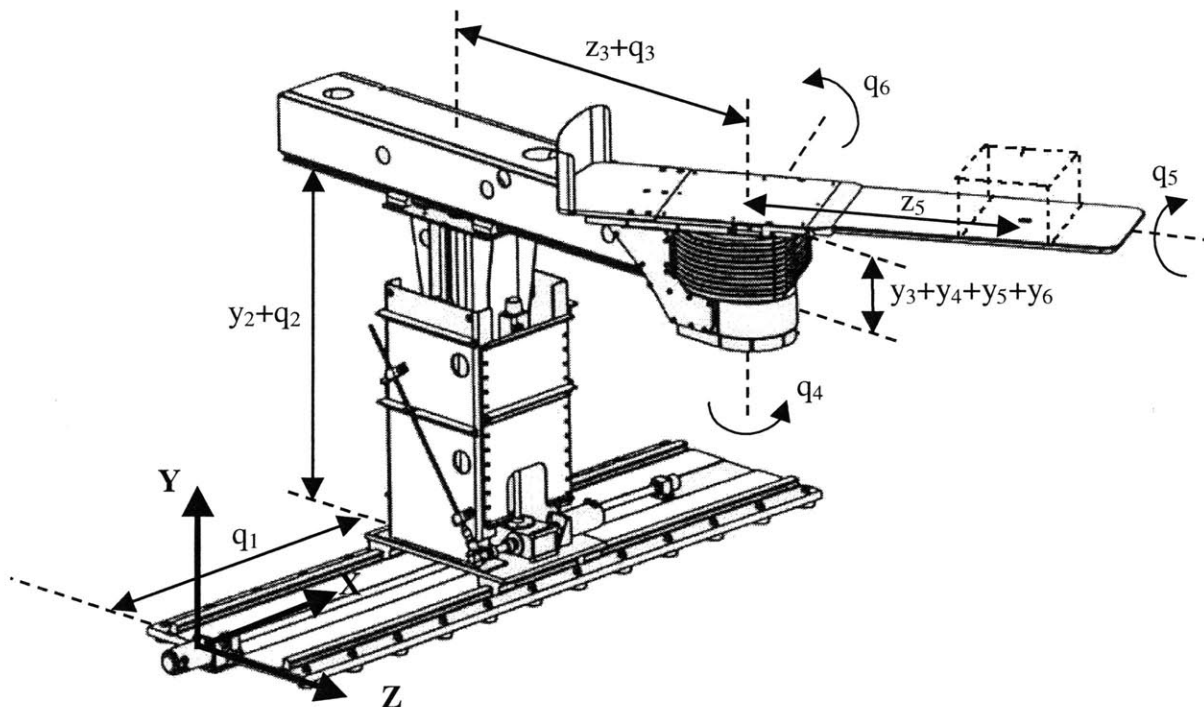


Figure B.1 - Parameter Definitions for the PPS [Ref. Flanz, 1996]



The end-effector position with respect to the fixed coordinate system defined in Figure B.1 is:

$$\begin{aligned} x = & q_1 - y_5 \cos(q_4) \sin(q_5) + z_5 \sin(q_4) - z_5 \cos(q_4) \sin(q_5) \sin(q_6) \\ & - z_5 \sin(q_4) \cos(q_6) + y_6 \sin(q_4) \sin(q_6) - y_6 \cos(q_4) \sin(q_5) \cos(q_6) \end{aligned} \quad (B.1)$$

$$y = q_2 + y_2 + y_3 + y_4 + y_5 \cos(q_5) + z_5 \cos(q_5) \sin(q_6) + y_6 \cos(q_5) \cos(q_6) \quad (B.2)$$

$$\begin{aligned} z = & z_2 + z_3 + q_3 + y_5 \sin(q_4) \sin(q_5) + z_5 \cos(q_4) + z_5 \sin(q_4) \sin(q_5) \sin(q_6) \\ & - z_5 \cos(q_4) \cos(q_6) + y_6 \cos(q_4) \sin(q_6) + y_6 \sin(q_4) \sin(q_5) \cos(q_6) \end{aligned} \quad (B.3)$$

The Identification Jacobian Matrix of the PPS is

$$\mathbf{J}_e = [\mathbf{J}_{x,1}, \dots, \mathbf{J}_{x,i}, \mathbf{J}_{y,i}, \mathbf{J}_{z,i}, \mathbf{J}_{s,i}, \mathbf{J}_{r,i}, \mathbf{J}_{p,i}, \dots, \mathbf{J}_{p,6}] \quad (B.4)$$

where

$$\mathbf{J}_{x,1} = [1, 0, 0, 0, 0, 0]^T$$

$$\mathbf{J}_{y,1} = [0, 1, 0, 0, 0, 0]^T$$

$$\mathbf{J}_{z,1} = [0, 0, 1, 0, 0, 0]^T$$

$$\begin{aligned} \mathbf{J}_{s,1} = & [0, -z_3 - q_3 - z_2 - \cos(q_4) \cdot z_5 + \sin(q_4) \cdot x_4 - \sin(q_4) \cdot \sin(q_5) \cdot \cos(q_6) \cdot y_6 - \sin(q_4) \\ & \cdot \sin(q_5) \cdot \sin(q_6) \cdot z_5 - \cos(q_4) \cdot \sin(q_6) \cdot y_6 + \cos(q_4) \cdot \cos(q_6) \cdot z_5 - \sin(q_4) \cdot \cos(q_5) \\ & \cdot x_4 - \sin(q_4) \cdot \sin(q_5) \cdot y_5, \cos(q_5) \cdot y_5 - \sin(q_5) \cdot x_4 + \cos(q_5) \cdot \cos(q_6) \cdot y_6 + \cos(q_5) \cdot \\ & \sin(q_6) \cdot z_5 + y_4 + y_3 + y_2 \cdot \cos(q_5) \cdot y_5 - \sin(q_5) \cdot x_4 + \cos(q_5) \cdot \cos(q_6) \cdot y_6 + \cos(q_5) \cdot \\ & \sin(q_6) \cdot z_5 + y_4 + y_3 + y_2 + q_2, 1, 0, 0]^T \end{aligned}$$

$$\begin{aligned} \mathbf{J}_{r,1} = & [z_3 + q_3 + z_2 + \cos(q_4) \cdot z_5 - \sin(q_4) \cdot x_4 + \sin(q_4) \cdot \sin(q_5) \cdot \cos(q_6) \cdot y_6 + \sin(q_4) \cdot \\ & \sin(q_5) \cdot \sin(q_6) \cdot z_5 + \cos(q_4) \cdot \sin(q_6) \cdot y_6 - \cos(q_4) \cdot \cos(q_6) \cdot z_5 + \sin(q_4) \cdot \cos(q_5) \cdot \\ & x_4 + \sin(q_4) \cdot \sin(q_5) \cdot y_5, 0, -\sin(q_4) \cdot z_5 + \cos(q_4) \cdot \sin(q_5) \cdot \cos(q_6) \cdot y_6 + \cos(q_4) \cdot \\ & \sin(q_5) \cdot \sin(q_6) \cdot z_5 - \sin(q_4) \cdot \sin(q_6) \cdot y_6 + \sin(q_4) \cdot \cos(q_6) \cdot z_5 + \cos(q_4) \cdot \cos(q_5) \cdot \\ & x_4 + \cos(q_4) \cdot \sin(q_5) \cdot y_5 - \cos(q_4) \cdot x_4, 0, 1, 0]^T \end{aligned}$$

$$\mathbf{J}_{p,1} = [-y_4 - y_3 - y_2 - q_2 + \sin(q_5) \cdot x_4 - \cos(q_5) \cdot y_5 - \cos(q_5) \cdot \cos(q_6) \cdot y_6 - \cos(q_5) \cdot \sin(q_6) \cdot z_5, -\cos(q_4) \cdot \sin(q_5) \cdot \sin(q_6) \cdot z_5 - \sin(q_4) \cdot \cos(q_6) \cdot z_5 - \cos(q_4) \cdot \cos(q_5) \cdot x_4 - \cos(q_4) \cdot \sin(q_5) \cdot y_5 - \cos(q_4) \cdot \sin(q_5) \cdot \cos(q_6) \cdot y_6 + \sin(q_4) \cdot \sin(q_6) \cdot y_6 + \sin(q_4) \cdot z_5 + \cos(q_4) \cdot x_4, 0, 0, 0, 1]^T$$

$$\mathbf{J}_{x,2} = [1, 0, 0, 0, 0, 0]^T$$

$$\mathbf{J}_{y,2} = [0, 1, 0, 0, 0, 0]^T$$

$$\mathbf{J}_{z,2} = [0, 0, 1, 0, 0, 0]^T$$

$$\mathbf{J}_{s,2} = [0, -\sin(q_4) \cdot \sin(q_5) \cdot \cos(q_6) \cdot y_6 - \sin(q_4) \cdot \sin(q_5) \cdot \sin(q_6) \cdot z_5 - \cos(q_4) \cdot \sin(q_6) \cdot y_6 + \cos(q_4) \cdot \cos(q_6) \cdot z_5 - \sin(q_4) \cdot \cos(q_5) \cdot x_4 - \sin(q_4) \cdot \sin(q_5) \cdot y_5 - z_3 - q_3 - \cos(q_4) \cdot z_5 + \sin(q_4) \cdot x_4, \cos(q_5) \cdot y_5 - \sin(q_5) \cdot x_4 + \cos(q_5) \cdot \cos(q_6) \cdot y_6 + \cos(q_5) \cdot \sin(q_6) \cdot z_5 + y_3 + y_4, 1, 0, 0]^T$$

$$\mathbf{J}_{r,2} = [\sin(q_4) \cdot \sin(q_5) \cdot \sin(q_6) \cdot z_5 + \cos(q_4) \cdot \sin(q_6) \cdot y_6 - \cos(q_4) \cdot \cos(q_6) \cdot z_5 + \sin(q_4) \cdot \cos(q_5) \cdot x_4 + \sin(q_4) \cdot \sin(q_5) \cdot y_5 + z_3 + q_3 + \cos(q_4) \cdot z_5 - \sin(q_4) \cdot x_4 + \sin(q_4) \cdot \sin(q_5) \cdot \cos(q_6) \cdot y_6, 0, -\sin(q_4) \cdot z_5 + \cos(q_4) \cdot \sin(q_5) \cdot \cos(q_6) \cdot y_6 + \cos(q_4) \cdot \sin(q_5) \cdot \sin(q_6) \cdot z_5 - \sin(q_4) \cdot \sin(q_6) \cdot y_6 + \sin(q_4) \cdot \cos(q_6) \cdot z_5 + \cos(q_4) \cdot \cos(q_5) \cdot x_4 + \cos(q_4) \cdot \sin(q_5) \cdot y_5 - \cos(q_4) \cdot x_4, 0, 1, 0]^T$$

$$\mathbf{J}_{p,2} = [-\cos(q_5) \cdot \cos(q_6) \cdot y_6 - \cos(q_5) \cdot \sin(q_6) \cdot z_5 - y_4 - y_3 + \sin(q_5) \cdot x_4 - \cos(q_5) \cdot y_5, -\cos(q_4) \cdot \sin(q_5) \cdot \sin(q_6) \cdot z_5 - \sin(q_4) \cdot \cos(q_6) \cdot z_5 - \cos(q_4) \cdot \cos(q_5) \cdot x_4 - \cos(q_4) \cdot \sin(q_5) \cdot y_5 - \cos(q_4) \cdot \sin(q_5) \cdot \cos(q_6) \cdot y_6 + \sin(q_4) \cdot \sin(q_6) \cdot y_6 + \sin(q_4) \cdot z_5 + \cos(q_4) \cdot x_4, 0, 0, 0, 1]^T$$

$$\mathbf{J}_{x,3} = [1, 0, 0, 0, 0, 0]^T$$

$$\mathbf{J}_{y,3} = [0, 1, 0, 0, 0, 0]^T$$

$$\mathbf{J}_{z,3} = [0, 0, 1, 0, 0, 0]^T$$

$$\begin{aligned} \mathbf{J}_{s,3} = [0, & -\sin(q_4) \cdot \sin(q_5) \cdot \cos(q_6) \cdot y_6 - \sin(q_4) \cdot \sin(q_5) \cdot \sin(q_6) \cdot z_5 - \cos(q_4) \cdot \sin(q_6) \cdot \\ & y_6 + \cos(q_4) \cdot \cos(q_6) \cdot z_5 - \sin(q_4) \cdot \cos(q_5) \cdot x_4 - \sin(q_4) \cdot \sin(q_5) \cdot y_5 + \sin(q_4) \cdot x_4 \\ & - \cos(q_4) \cdot z_5, \cos(q_5) \cdot \cos(q_6) \cdot y_6 + \cos(q_5) \cdot \sin(q_6) \cdot z_5 - \sin(q_5) \cdot x_4 + \cos(q_5) \cdot y_5 \\ & + y_4, 1, 0, 0]^T \end{aligned}$$

$$\begin{aligned} \mathbf{J}_{r,3} = [\sin(q_4) \cdot \sin(q_5) \cdot \cos(q_6) \cdot y_6 + \sin(q_4) \cdot \sin(q_5) \cdot \sin(q_6) \cdot z_5 + \cos(q_4) \cdot \sin(q_6) \cdot y_6 \\ - \cos(q_4) \cdot \cos(q_6) \cdot z_5 + \sin(q_4) \cdot \cos(q_5) \cdot x_4 + \sin(q_4) \cdot \sin(q_5) \cdot y_5 + \cos(q_4) \cdot z_5 \\ - \sin(q_4) \cdot x_4, 0, -\sin(q_4) \cdot z_5 + \cos(q_4) \cdot \sin(q_5) \cdot \cos(q_6) \cdot y_6 + \cos(q_4) \cdot \sin(q_5) \cdot \\ \sin(q_6) \cdot z_5 - \sin(q_4) \cdot \sin(q_6) \cdot y_6 + \sin(q_4) \cdot \cos(q_6) \cdot z_5 + \cos(q_4) \cdot \cos(q_5) \cdot x_4 \\ + \cos(q_4) \cdot \sin(q_5) \cdot y_5 - \cos(q_4) \cdot x_4, 0, 1, 0]^T \end{aligned}$$

$$\begin{aligned} \mathbf{J}_{p,3} = [-\cos(q_5) \cdot \cos(q_6) \cdot y_6 - \cos(q_5) \cdot \sin(q_6) \cdot z_3 - y_4 + \sin(q_5) \cdot x_4 - \cos(q_5) \cdot y_5, \\ - \cos(q_4) \cdot \sin(q_5) \cdot \sin(q_6) \cdot z_5 - \sin(q_4) \cdot \cos(q_6) \cdot z_5 - \cos(q_4) \cdot \cos(q_5) \cdot x_4 \\ - \cos(q_4) \cdot \sin(q_5) \cdot y_5 - \cos(q_4) \cdot \sin(q_5) \cdot \cos(q_6) \cdot y_6 + \sin(q_4) \cdot \sin(q_6) \cdot y_6 + \sin(q_4) \\ \cdot z_5 + \cos(q_4) \cdot x_4, 0, 0, 0, 1]^T \end{aligned}$$

$$\mathbf{J}_{x,4} = [\cos(q_4), 0, -\sin(q_4), 0, 0, 0]^T$$

$$\mathbf{J}_{y,4} = [0, 1, 0, 0, 0, 0]^T$$

$$\mathbf{J}_{z,4} = [\sin(q_4), 0, \cos(q_4), 0, 0, 0]^T$$

$$\begin{aligned} \mathbf{J}_{s,4} = [\sin(q_4) \cdot (\cos(q_5) \cdot \cos(q_6) \cdot y_6 + \cos(q_5) \cdot \sin(q_6) \cdot z_5 - \sin(q_5) \cdot x_4 + \cos(q_5) \cdot y_5), \\ - \sin(q_6) \cdot y_6 + \cos(q_6) \cdot z_5 - z_5, \cos(q_4) \cdot (\cos(q_5) \cdot \cos(q_6) \cdot y_6 + \cos(q_5) \cdot \sin(q_6) \cdot z_5 \\ - \sin(q_5) \cdot x_4 + \cos(q_5) \cdot y_5), \cos(q_4), 0, -\sin(q_4)]^T \end{aligned}$$

$$\begin{aligned} \mathbf{J}_{r,4} = [\sin(q_4) \cdot \sin(q_5) \cdot y_5 + \sin(q_4) \cdot \sin(q_5) \cdot \sin(q_6) \cdot z_5 + \sin(q_4) \cdot \cos(q_5) \cdot x_4 + \sin(q_4) \cdot \\ \sin(q_5) \cdot \cos(q_6) \cdot y_6 + \cos(q_4) \cdot z_5 + \cos(q_4) \cdot \sin(q_6) \cdot y_6 - \cos(q_4) \cdot \cos(q_6) \cdot z_5 \end{aligned}$$

$$\begin{aligned} & -\cos(q_4) \cdot (\cos(q_5) \cdot \cos(q_6) \cdot y_6 + \cos(q_5) \cdot \sin(q_6) \cdot z_5 - \sin(q_5) \cdot \cos(q_6) \cdot z_5, 0, \\ & \sin(q_4) \cdot \cos(q_6) \cdot z_5 - \sin(q_4) \cdot \sin(q_6) \cdot y_6 - \sin(q_4) \cdot z_5 + \cos(q_4) \cdot \sin(q_5) \cdot \cos(q_6) \cdot \\ & y_6 + \cos(q_4) \cdot \sin(q_5) \cdot \sin(q_6) \cdot z_5 + \cos(q_4) \cdot \cos(q_5) \cdot x_4 + \cos(q_4) \cdot \sin(q_5) \cdot y_5, 0, 1, \\ & 0]^T \end{aligned}$$

$$\begin{aligned} \mathbf{J}_{p,4} = & [-\cos(q_4) \cdot (\cos(q_5) \cdot \cos(q_6) \cdot y_6 + \cos(q_5) \cdot \sin(q_6) \cdot z_5 - \sin(q_5) \cdot x_4 + \cos(q_5) \cdot y_5), \\ & -\sin(q_5) \cdot \cos(q_6) \cdot y_6 - \sin(q_5) \cdot \sin(q_6) \cdot z_5 - \cos(q_5) \cdot x_4 - \sin(q_5) \cdot y_5, \sin(q_4) \cdot \\ & (\cos(q_5) \cdot \cos(q_6) \cdot y_6 + \cos(q_5) \cdot \sin(q_6) \cdot z_5 - \sin(q_5) \cdot x_4 + \cos(q_5) \cdot y_5), \sin(q_4), 0, \\ & \cos(q_4)]^T \end{aligned}$$

$$\mathbf{J}_{x,5} = [\cos(q_4) \cdot \cos(q_5), \sin(q_5), -\sin(q_4) \cdot \cos(q_5), 0, 0, 0]^T$$

$$\mathbf{J}_{y,5} = [-\cos(q_4) \cdot \sin(q_5), \cos(q_5), \sin(q_4) \cdot \sin(q_5), 0, 0, 0]^T$$

$$\mathbf{J}_{z,5} = [\sin(q_4), 0, \cos(q_4), 0, 0, 0]^T$$

$$\begin{aligned} \mathbf{J}_{s,5} = & [\sin(q_4) \cdot \cos(q_6) \cdot y_6 + \sin(q_4) \cdot \sin(q_6) \cdot z_5 + \cos(q_4) \cdot \sin(q_5) \cdot \sin(q_6) \cdot y_6 - \cos(q_4) \cdot \\ & \sin(q_5) \cdot \cos(q_6) \cdot z_5, \cos(q_5) \cdot (-\sin(q_6) \cdot y_6 + \cos(q_6) \cdot z_5), \cos(q_4) \cdot \cos(q_6) \cdot y_6 + \\ & \cos(q_4) \cdot \sin(q_6) \cdot z_5 - \sin(q_4) \cdot \sin(q_5) \cdot \sin(q_6) \cdot y_6 + \sin(q_4) \cdot \sin(q_5) \cdot \cos(q_6) \cdot z_5, \\ & \cos(q_4) \cdot \cos(q_5), \sin(q_5), -\sin(q_4) \cdot \cos(q_5)]^T \end{aligned}$$

$$\begin{aligned} \mathbf{J}_{r,5} = & [-\cos(q_4) \cdot \cos(q_5) \cdot (-\sin(q_6) \cdot y_6 + \cos(q_6) \cdot z_5), -\sin(q_5) \cdot (-\sin(q_6) \cdot y_6 + \cos(q_6) \cdot \\ & z_5), \sin(q_4) \cdot \cos(q_5) \cdot (-\sin(q_6) \cdot y_6 + \cos(q_6) \cdot z_5), -\cos(q_4) \cdot \sin(q_5), \cos(q_5), \\ & \sin(q_4) \cdot \sin(q_5)]^T \end{aligned}$$

$$\begin{aligned} \mathbf{J}_{p,5} = & [-\cos(q_4) \cdot \cos(q_5) \cdot (\cos(q_6) \cdot y_6 + \sin(q_6) \cdot z_5), -\sin(q_5) \cdot (\cos(q_6) \cdot y_6 + \sin(q_6) \cdot z_5), \\ & \sin(q_4) \cdot \cos(q_5) \cdot (\cos(q_6) \cdot y_6 + \sin(q_6) \cdot z_5), \sin(q_4), 0, \cos(q_4)]^T \end{aligned}$$

$$\mathbf{J}_{x,6} = [\cos(q_4) \cdot \cos(q_5), \sin(q_5), -\sin(q_4) \cdot \cos(q_5), 0, 0, 0]^T$$

$$\mathbf{J}_{y,6} = [-\cos(q_4) \cdot \sin(q_5) \cdot \cos(q_6) + \sin(q_4) \cdot \sin(q_6), \cos(q_5) \cdot \cos(q_6), \sin(q_4) \cdot \sin(q_5) \cdot \cos(q_6) + \cos(q_4) \cdot \sin(q_6), 0, 0, 0]^T$$

$$\mathbf{J}_{z,6} = [\cos(q_4) \cdot \sin(q_5) \cdot \sin(q_6) + \sin(q_4) \cdot \cos(q_6), -\cos(q_5) \cdot \sin(q_6), -\sin(q_4) \cdot \sin(q_5) \cdot \sin(q_6) + \cos(q_4) \cdot \cos(q_6), 0, 0, 0]^T$$

$$\mathbf{J}_{s,6} = [0, 0, 0, \cos(q_4) \cdot \cos(q_5), \sin(q_5), -\sin(q_4) \cdot \cos(q_5)]^T$$

$$\mathbf{J}_{r,6} = [0, 0, 0, -\cos(q_4) \cdot \sin(q_5) \cdot \cos(q_6) + \sin(q_4) \cdot \sin(q_6), \cos(q_5) \cdot \cos(q_6), \sin(q_4) \cdot \sin(q_5) \cdot \cos(q_6) + \cos(q_4) \cdot \sin(q_6)]^T$$

$$\mathbf{J}_{p,6} = [\cos(q_4) \cdot \sin(q_5) \cdot \sin(q_6) + \sin(q_4) \cdot \cos(q_6), -\cos(q_5) \cdot \sin(q_6), -\sin(q_4) \cdot \sin(q_5) \cdot \sin(q_6) + \cos(q_4) \cdot \cos(q_6)]^T$$

## Appendix C

### Schilling Titan II Kinematic Description

This appendix contains the Schilling Titan II direct and inverse kinematic equations, as well as the Identification Jacobian matrices for the generalized error formulation.

Consider the D.H. parameters defined in Figure C.1. The end-effector position with respect to the base sensor coordinates is:

$$x = [a_1 + a_2 \cos\theta_2 + a_3 \cos(\theta_2 + \theta_3) + (a_4 + a_5 \cos\theta_5) \cos(\theta_2 + \theta_3 + \theta_4)] \cos\theta_1 - a_5 \sin\theta_5 \sin\theta_1 \quad (C.1)$$

$$y = [a_1 + a_2 \cos\theta_2 + a_3 \cos(\theta_2 + \theta_3) + (a_4 + a_5 \cos\theta_5) \cos(\theta_2 + \theta_3 + \theta_4)] \sin\theta_1 + a_5 \sin\theta_5 \cos\theta_1 \quad (C.2)$$

$$z = [d_1 + a_2 \sin\theta_2 + a_3 \sin(\theta_2 + \theta_3) + (a_4 + a_5 \cos\theta_5) \sin(\theta_2 + \theta_3 + \theta_4)] \quad (C.3)$$

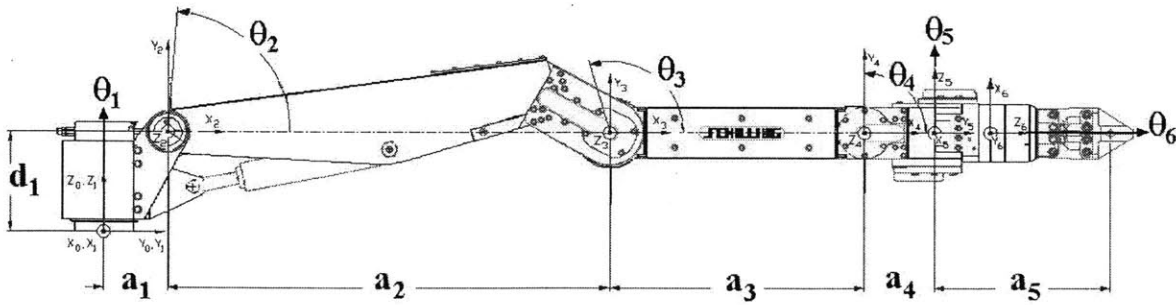
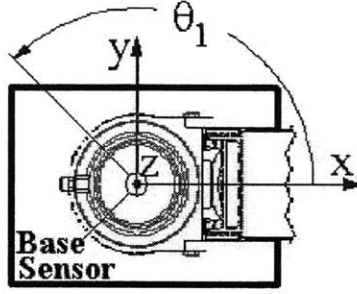


Figure C.1 - Side view of the Schilling Titan II [Ref. Schilling Development, 1991]



**Figure C.2 - Top View showing the Base Force/Torque Sensor Frame**

There are two solutions for the Schilling inverse kinematics given a desired end-effector position  $[p_x \ p_y \ p_z]^T$  (with respect to the base sensor coordinates) and a pair of perpendicular unit vectors  $[b_x \ b_y \ b_z]^T$  and  $[n_x \ n_y \ n_z]^T$  representing the directions of joint six Z and X axes respectively (see Figure C.2). These solutions refer to the case where  $\theta_3 > 0$  and  $\theta_3 < 0$ , denominated respectively as lower and upper arm configurations. Defining the auxiliary variables:

$$w = \sqrt{(b_x \cos\theta_1 + b_y \sin\theta_1)^2 + b_z^2} \quad (C.4)$$

$$x_3 = (p_x - a_5 \cdot b_x) \cos\theta_1 + (p_y - a_5 \cdot b_y) \sin\theta_1 - a_4 \frac{(b_x \cos\theta_1 + b_y \sin\theta_1)}{w} - a_1 \quad (C.5)$$

$$z_3 = p_z - a_5 \cdot b_z - a_4 \cdot b_z / w - d_1 \quad (C.6)$$

then the joint angle solutions are:

$$\theta_1 = \tan^{-1} \left( \frac{p_y - a_5 \cdot b_y}{p_x - a_5 \cdot b_x} \right) \quad (C.7)$$

$$\theta_2 = \tan^{-1} \left( \frac{z_3}{x_3} \right) \pm \cos^{-1} \left( \frac{a_2^2 + x_3^2 + z_3^2 - a_3^2}{2 \cdot a_2 \cdot \sqrt{x_3^2 + z_3^2}} \right) \quad (C.8)$$

$$\theta_3 = \tan^{-1} \left( \frac{z_3 - a_2 \sin \theta_2}{x_3 - a_2 \cos \theta_2} \right) - \theta_2 \quad (C.9)$$

$$\theta_4 = \tan^{-1} \left( \frac{b_z}{b_x \cos \theta_1 + b_y \sin \theta_1} \right) - (\theta_2 + \theta_3) \quad (C.10)$$

$$\theta_5 = \tan^{-1} \left( \frac{-b_x \sin \theta_1 + b_y \cos \theta_1}{w} \right) \quad (C.11)$$

$$\theta_6 = \cos^{-1} \left( \frac{b_x (n_x \cos \theta_1 + n_y \sin \theta_1) - n_z (b_x \cos \theta_1 + b_y \sin \theta_1)}{w} \right) \quad (C.12)$$

The Identification Jacobian Matrix of the Schilling is

$$\mathbf{J}_e = [\mathbf{J}_{x,0}, \dots, \mathbf{J}_{x,i}, \mathbf{J}_{y,i}, \mathbf{J}_{z,i}, \mathbf{J}_{s,i}, \mathbf{J}_{r,i}, \mathbf{J}_{p,i}, \dots, \mathbf{J}_{p,6}] \quad (C.13)$$

where

$$\mathbf{J}_{x,0} = [1, 0, 0]^T$$

$$\mathbf{J}_{y,0} = [0, 1, 0]^T$$

$$\mathbf{J}_{z,0} = [0, 0, 1]^T$$

$$\begin{aligned} \mathbf{J}_{s,0} = & [\cos \theta_5 \cdot d_6 \cdot \cos \theta_4 \cdot \sin \theta_2 \cdot \cos \theta_3 + \cos \theta_5 \cdot d_6 \cdot \cos \theta_4 \cdot \cos \theta_2 \cdot \sin \theta_3 - \cos \theta_5 \cdot d_6 \cdot \sin \theta_4 \cdot \sin \theta_2 \cdot \sin \theta_3 \\ & + \cos \theta_5 \cdot d_6 \cdot \sin \theta_4 \cdot \cos \theta_2 \cdot \cos \theta_3 + a_5 \cdot \cos \theta_5 \cdot \cos \theta_4 \cdot \sin \theta_2 \cdot \cos \theta_3 + \\ & a_5 \cdot \cos \theta_5 \cdot \cos \theta_4 \cdot \cos \theta_2 \cdot \sin \theta_3 - a_5 \cdot \cos \theta_5 \cdot \sin \theta_4 \cdot \sin \theta_2 \cdot \sin \theta_3 + a_5 \cdot \cos \theta_5 \cdot \sin \theta_4 \cdot \cos \theta_2 \cdot \cos \theta_3 \\ & + a_4 \cdot \cos \theta_4 \cdot \sin \theta_2 \cdot \cos \theta_3 + a_4 \cdot \cos \theta_4 \cdot \cos \theta_2 \cdot \sin \theta_3 - a_4 \cdot \sin \theta_4 \cdot \sin \theta_2 \cdot \sin \theta_3 + \\ & a_4 \cdot \sin \theta_4 \cdot \cos \theta_2 \cdot \cos \theta_3 + \sin \theta_2 \cdot a_3 \cdot \cos \theta_3 + \cos \theta_2 \cdot a_3 \cdot \sin \theta_3 + a_2 \cdot \sin \theta_2 + d_1, 0, \\ & - (d_6 \cdot \cos \theta_5 \cdot \cos \theta_4 \cdot \cos \theta_1 \cdot \cos \theta_2 \cdot \cos \theta_3 - d_6 \cdot \cos \theta_5 \cdot \cos \theta_4 \cdot \cos \theta_1 \cdot \sin \theta_2 \cdot \sin \theta_3 - \\ & d_6 \cdot \cos \theta_5 \cdot \sin \theta_4 \cdot \cos \theta_1 \cdot \cos \theta_2 \cdot \sin \theta_3 - d_6 \cdot \cos \theta_5 \cdot \sin \theta_4 \cdot \cos \theta_1 \cdot \sin \theta_2 \cdot \cos \theta_3 + d_6 \cdot \sin \theta_1 \cdot \sin \theta_5 \\ & + a_5 \cdot \cos \theta_5 \cdot \cos \theta_4 \cdot \cos \theta_1 \cdot \cos \theta_2 \cdot \cos \theta_3 - a_5 \cdot \cos \theta_5 \cdot \cos \theta_4 \cdot \cos \theta_1 \cdot \sin \theta_2 \cdot \sin \theta_3 - \\ & a_5 \cdot \cos \theta_5 \cdot \sin \theta_4 \cdot \cos \theta_1 \cdot \cos \theta_2 \cdot \sin \theta_3 - a_5 \cdot \cos \theta_5 \cdot \sin \theta_4 \cdot \cos \theta_1 \cdot \sin \theta_2 \cdot \cos \theta_3 + \sin \theta_1 \cdot a_5 \cdot \sin \theta_5 \\ & + a_4 \cdot \cos \theta_4 \cdot \cos \theta_1 \cdot \cos \theta_2 \cdot \cos \theta_3 - a_4 \cdot \cos \theta_4 \cdot \cos \theta_1 \cdot \sin \theta_2 \cdot \sin \theta_3 - \end{aligned}$$



$$a_4 \cdot \sin\theta_4 \cdot \cos\theta_1 \cdot \cos\theta_2 \cdot \sin\theta_3 - a_4 \cdot \sin\theta_4 \cdot \cos\theta_1 \cdot \sin\theta_2 \cdot \cos\theta_3 + \cos\theta_1 \cdot \cos\theta_2 \cdot a_3 \cdot \cos\theta_3 - \\ \cos\theta_1 \cdot \sin\theta_2 \cdot a_3 \cdot \sin\theta_3 + \cos\theta_1 \cdot a_2 \cdot \cos\theta_2 + a_1 \cdot \cos\theta_1)]^T$$

$$\mathbf{J}_{r,0} = [- (d_6 \cdot \cos\theta_5 \cdot \cos\theta_4 \cdot \sin\theta_1 \cdot \cos\theta_2 \cdot \cos\theta_3 - d_6 \cdot \cos\theta_5 \cdot \cos\theta_4 \cdot \sin\theta_1 \cdot \sin\theta_2 \cdot \sin\theta_3 - \\ d_6 \cdot \cos\theta_5 \cdot \sin\theta_4 \cdot \sin\theta_1 \cdot \cos\theta_2 \cdot \sin\theta_3 - d_6 \cdot \cos\theta_5 \cdot \sin\theta_4 \cdot \sin\theta_1 \cdot \sin\theta_2 \cdot \cos\theta_3 - d_6 \cdot \cos\theta_1 \cdot \sin\theta_5 \\ + a_5 \cdot \cos\theta_5 \cdot \cos\theta_4 \cdot \sin\theta_1 \cdot \cos\theta_2 \cdot \cos\theta_3 - a_5 \cdot \cos\theta_5 \cdot \cos\theta_4 \cdot \sin\theta_1 \cdot \sin\theta_2 \cdot \sin\theta_3 - \\ a_5 \cdot \cos\theta_5 \cdot \sin\theta_4 \cdot \sin\theta_1 \cdot \cos\theta_2 \cdot \sin\theta_3 - a_5 \cdot \cos\theta_5 \cdot \sin\theta_4 \cdot \sin\theta_1 \cdot \sin\theta_2 \cdot \cos\theta_3 - \cos\theta_1 \cdot a_5 \cdot \sin\theta_5 + \\ a_4 \cdot \cos\theta_4 \cdot \sin\theta_1 \cdot \cos\theta_2 \cdot \cos\theta_3 - a_4 \cdot \cos\theta_4 \cdot \sin\theta_1 \cdot \sin\theta_2 \cdot \sin\theta_3 - a_4 \cdot \sin\theta_4 \cdot \sin\theta_1 \cdot \cos\theta_2 \cdot \sin\theta_3 - \\ a_4 \cdot \sin\theta_4 \cdot \sin\theta_1 \cdot \sin\theta_2 \cdot \cos\theta_3 + \sin\theta_1 \cdot \cos\theta_2 \cdot a_3 \cdot \cos\theta_3 - \sin\theta_1 \cdot \sin\theta_2 \cdot a_3 \cdot \sin\theta_3 + \\ \sin\theta_1 \cdot a_2 \cdot \cos\theta_2 + a_1 \cdot \sin\theta_1), d_6 \cdot \cos\theta_5 \cdot \cos\theta_4 \cdot \cos\theta_1 \cdot \cos\theta_2 \cdot \cos\theta_3 - \\ d_6 \cdot \cos\theta_5 \cdot \cos\theta_4 \cdot \cos\theta_1 \cdot \sin\theta_2 \cdot \sin\theta_3 - d_6 \cdot \cos\theta_5 \cdot \sin\theta_4 \cdot \cos\theta_1 \cdot \cos\theta_2 \cdot \sin\theta_3 - \\ d_6 \cdot \cos\theta_5 \cdot \sin\theta_4 \cdot \cos\theta_1 \cdot \sin\theta_2 \cdot \cos\theta_3 + d_6 \cdot \sin\theta_1 \cdot \sin\theta_5 + a_5 \cdot \cos\theta_5 \cdot \cos\theta_4 \cdot \cos\theta_1 \cdot \cos\theta_2 \cdot \cos\theta_3 \\ - a_5 \cdot \cos\theta_5 \cdot \cos\theta_4 \cdot \cos\theta_1 \cdot \sin\theta_2 \cdot \sin\theta_3 - a_5 \cdot \cos\theta_5 \cdot \sin\theta_4 \cdot \cos\theta_1 \cdot \cos\theta_2 \cdot \sin\theta_3 - \\ a_5 \cdot \cos\theta_5 \cdot \sin\theta_4 \cdot \cos\theta_1 \cdot \sin\theta_2 \cdot \cos\theta_3 + \sin\theta_1 \cdot a_5 \cdot \sin\theta_5 + a_4 \cdot \cos\theta_4 \cdot \cos\theta_1 \cdot \cos\theta_2 \cdot \cos\theta_3 - \\ a_4 \cdot \cos\theta_4 \cdot \cos\theta_1 \cdot \sin\theta_2 \cdot \sin\theta_3 - a_4 \cdot \sin\theta_4 \cdot \cos\theta_1 \cdot \cos\theta_2 \cdot \sin\theta_3 - a_4 \cdot \sin\theta_4 \cdot \cos\theta_1 \cdot \sin\theta_2 \cdot \cos\theta_3 \\ + \cos\theta_1 \cdot \cos\theta_2 \cdot a_3 \cdot \cos\theta_3 - \cos\theta_1 \cdot \sin\theta_2 \cdot a_3 \cdot \sin\theta_3 + \cos\theta_1 \cdot a_2 \cdot \cos\theta_2 + a_1 \cdot \cos\theta_1, 0]^T$$

$$\mathbf{J}_{p,0} = [0, - (\cos\theta_5 \cdot d_6 \cdot \cos\theta_4 \cdot \sin\theta_2 \cdot \cos\theta_3 + \cos\theta_5 \cdot d_6 \cdot \cos\theta_4 \cdot \cos\theta_2 \cdot \sin\theta_3 - \\ \cos\theta_5 \cdot d_6 \cdot \sin\theta_4 \cdot \sin\theta_2 \cdot \sin\theta_3 + \cos\theta_5 \cdot d_6 \cdot \sin\theta_4 \cdot \cos\theta_2 \cdot \cos\theta_3 + a_5 \cdot \cos\theta_5 \cdot \cos\theta_4 \cdot \sin\theta_2 \cdot \cos\theta_3 \\ + a_5 \cdot \cos\theta_5 \cdot \cos\theta_4 \cdot \cos\theta_2 \cdot \sin\theta_3 - a_5 \cdot \cos\theta_5 \cdot \sin\theta_4 \cdot \sin\theta_2 \cdot \sin\theta_3 + \\ a_5 \cdot \cos\theta_5 \cdot \sin\theta_4 \cdot \cos\theta_2 \cdot \cos\theta_3 + a_4 \cdot \cos\theta_4 \cdot \sin\theta_2 \cdot \cos\theta_3 + a_4 \cdot \cos\theta_4 \cdot \cos\theta_2 \cdot \sin\theta_3 - \\ a_4 \cdot \sin\theta_4 \cdot \sin\theta_2 \cdot \sin\theta_3 + a_4 \cdot \sin\theta_4 \cdot \cos\theta_2 \cdot \cos\theta_3 + \sin\theta_2 \cdot a_3 \cdot \cos\theta_3 + \cos\theta_2 \cdot a_3 \cdot \sin\theta_3 + \\ a_2 \cdot \sin\theta_2 + d_1), d_6 \cdot \cos\theta_5 \cdot \cos\theta_4 \cdot \sin\theta_1 \cdot \cos\theta_2 \cdot \cos\theta_3 - d_6 \cdot \cos\theta_5 \cdot \cos\theta_4 \cdot \sin\theta_1 \cdot \sin\theta_2 \cdot \sin\theta_3 - \\ d_6 \cdot \cos\theta_5 \cdot \sin\theta_4 \cdot \sin\theta_1 \cdot \cos\theta_2 \cdot \sin\theta_3 - d_6 \cdot \cos\theta_5 \cdot \sin\theta_4 \cdot \sin\theta_1 \cdot \sin\theta_2 \cdot \cos\theta_3 - d_6 \cdot \cos\theta_1 \cdot \sin\theta_5$$

$$\begin{aligned}
& + a_5 \cdot \cos\theta_5 \cdot \cos\theta_4 \cdot \sin\theta_1 \cdot \cos\theta_2 \cdot \cos\theta_3 - a_5 \cdot \cos\theta_5 \cdot \cos\theta_4 \cdot \sin\theta_1 \cdot \sin\theta_2 \cdot \sin\theta_3 - \\
& a_5 \cdot \cos\theta_5 \cdot \sin\theta_4 \cdot \sin\theta_1 \cdot \cos\theta_2 \cdot \sin\theta_3 - a_5 \cdot \cos\theta_5 \cdot \sin\theta_4 \cdot \sin\theta_1 \cdot \sin\theta_2 \cdot \cos\theta_3 - \cos\theta_1 \cdot a_5 \cdot \sin\theta_5 + \\
& a_4 \cdot \cos\theta_4 \cdot \sin\theta_1 \cdot \cos\theta_2 \cdot \cos\theta_3 - a_4 \cdot \cos\theta_4 \cdot \sin\theta_1 \cdot \sin\theta_2 \cdot \sin\theta_3 - a_4 \cdot \sin\theta_4 \cdot \sin\theta_1 \cdot \cos\theta_2 \cdot \sin\theta_3 - \\
& a_4 \cdot \sin\theta_4 \cdot \sin\theta_1 \cdot \sin\theta_2 \cdot \cos\theta_3 + \sin\theta_1 \cdot \cos\theta_2 \cdot a_3 \cdot \cos\theta_3 - \sin\theta_1 \cdot \sin\theta_2 \cdot a_3 \cdot \sin\theta_3 + \\
& \sin\theta_1 \cdot a_2 \cdot \cos\theta_2 + a_1 \cdot \sin\theta_1]^\text{T}
\end{aligned}$$

$$\mathbf{J}_{x,1} = [\cos\theta_1, \sin\theta_1, 0]^\text{T}$$

$$\mathbf{J}_{y,1} = [0, 0, 1]^\text{T}$$

$$\mathbf{J}_{z,1} = [\sin\theta_1, -\cos\theta_1, 0]^\text{T}$$

$$\begin{aligned}
\mathbf{J}_{s,1} = & [((((d_6 + a_5) \cdot \cos\theta_5 + a_4) \cdot \cos\theta_4 + a_3) \cdot \sin\theta_3 + ((d_6 + a_5) \cdot \cos\theta_5 + a_4) \cdot \cos\theta_3 \cdot \sin\theta_4) \cdot \sin\theta_2 \\
& + ((d_6 + a_5) \cdot \cos\theta_5 + a_4) \cdot \cos\theta_2 \cdot \sin\theta_4 \cdot \sin\theta_3 + (((-a_5 - d_6) \cdot \cos\theta_5 - a_4) \cdot \cos\theta_4 - \\
& a_3) \cdot \cos\theta_3 - a_2) \cdot \cos\theta_2) \cdot \sin\theta_1 + (d_6 + a_5) \cdot \cos\theta_1 \cdot \sin\theta_5, (d_6 + a_5) \cdot \sin\theta_5 \cdot \sin\theta_1 + (((-a_5 - \\
& d_6) \cdot \cos\theta_5 - a_4) \cdot \cos\theta_4 - a_3) \cdot \cos\theta_1 \cdot \sin\theta_3 + ((-a_5 - d_6) \cdot \cos\theta_5 - \\
& a_4) \cdot \cos\theta_3 \cdot \cos\theta_1 \cdot \sin\theta_4) \cdot \sin\theta_2 + ((-a_5 - d_6) \cdot \cos\theta_5 - a_4) \cdot \cos\theta_2 \cdot \cos\theta_1 \cdot \sin\theta_4 \cdot \sin\theta_3 + \\
& (((((d_6 + a_5) \cdot \cos\theta_5 + a_4) \cdot \cos\theta_4 + a_3) \cdot \cos\theta_3 + a_2) \cdot \cos\theta_2 \cdot \cos\theta_1, 0)]^\text{T}
\end{aligned}$$

$$\begin{aligned}
\mathbf{J}_{r,1} = & [((((d_6 + a_5) \cdot \cos\theta_5 + a_4) \cdot \cos\theta_1 \cdot \sin\theta_4 \cdot \sin\theta_3 + ((((-a_5 - d_6) \cdot \cos\theta_5 - a_4) \cdot \cos\theta_4 - \\
& a_3) \cdot \cos\theta_3 - a_2) \cdot \cos\theta_1) \cdot \sin\theta_2 + ((((-a_5 - d_6) \cdot \cos\theta_5 - a_4) \cdot \cos\theta_4 - a_3) \cdot \cos\theta_2 \cdot \cos\theta_1 \cdot \sin\theta_3 \\
& + ((-a_5 - d_6) \cdot \cos\theta_5 - a_4) \cdot \cos\theta_3 \cdot \cos\theta_2 \cdot \cos\theta_1 \cdot \sin\theta_4, (((((d_6 + a_5) \cdot \cos\theta_5 + \\
& a_4) \cdot \sin\theta_4 \cdot \sin\theta_3 + ((((-a_5 - d_6) \cdot \cos\theta_5 - a_4) \cdot \cos\theta_4 - a_3) \cdot \cos\theta_3 - a_2) \cdot \sin\theta_2 + ((((-a_5 - \\
& d_6) \cdot \cos\theta_5 - a_4) \cdot \cos\theta_4 - a_3) \cdot \cos\theta_2 \cdot \sin\theta_3 + ((-a_5 - d_6) \cdot \cos\theta_5 - \\
& a_4) \cdot \cos\theta_3 \cdot \cos\theta_2 \cdot \sin\theta_4) \cdot \sin\theta_1, (((((-a_5 - d_6) \cdot \cos\theta_5 - a_4) \cdot \cos\theta_4 - a_3) \cdot \sin\theta_3 + ((-a_5 - \\
& d_6) \cdot \cos\theta_5 - a_4) \cdot \cos\theta_3 \cdot \sin\theta_4) \cdot \sin\theta_2 + ((-a_5 - d_6) \cdot \cos\theta_5 - a_4) \cdot \cos\theta_2 \cdot \sin\theta_4 \cdot \sin\theta_3 + \\
& (((((d_6 + a_5) \cdot \cos\theta_5 + a_4) \cdot \cos\theta_4 + a_3) \cdot \cos\theta_3 + a_2) \cdot \cos\theta_2)]^\text{T}
\end{aligned}$$

$$\mathbf{J}_{p,1} = [((( - a_5 - d_6) \cdot \cos\theta_5 - a_4) \cdot \sin\theta_4 \cdot \sin\theta_3 + (((d_6 + a_5) \cdot \cos\theta_5 + a_4) \cdot \cos\theta_4 + a_3) \cdot \cos\theta_3 + a_2) \cdot \sin\theta_2 + (((d_6 + a_5) \cdot \cos\theta_5 + a_4) \cdot \cos\theta_4 + a_3) \cdot \cos\theta_2 \cdot \sin\theta_3 + ((d_6 + a_5) \cdot \cos\theta_5 + a_4) \cdot \cos\theta_3 \cdot \cos\theta_2 \cdot \sin\theta_4) \cdot \sin\theta_1, (((d_6 + a_5) \cdot \cos\theta_5 + a_4) \cdot \cos\theta_1 \cdot \sin\theta_4 \cdot \sin\theta_3 + ((( - a_5 - d_6) \cdot \cos\theta_5 - a_4) \cdot \cos\theta_4 - a_3) \cdot \cos\theta_3 - a_2) \cdot \cos\theta_1) \cdot \sin\theta_2 + ((( - a_5 - d_6) \cdot \cos\theta_5 - a_4) \cdot \cos\theta_4 - a_3) \cdot \cos\theta_2 \cdot \cos\theta_1 \cdot \sin\theta_3 + (( - a_5 - d_6) \cdot \cos\theta_5 - a_4) \cdot \cos\theta_3 \cdot \cos\theta_2 \cdot \cos\theta_1 \cdot \sin\theta_4, ( - a_5 - d_6) \cdot \sin\theta_5]^T$$

$$\mathbf{J}_{x,2} = [\cos\theta_1 \cdot \cos\theta_2, \sin\theta_1 \cdot \cos\theta_2, \sin\theta_2]^T$$

$$\mathbf{J}_{y,2} = [-\cos\theta_1 \cdot \sin\theta_2, -\sin\theta_1 \cdot \sin\theta_2, \cos\theta_2]^T$$

$$\mathbf{J}_{z,2} = [\sin\theta_1, -\cos\theta_1, 0]^T$$

$$\mathbf{J}_{s,2} = [(((d_6 + a_5) \cdot \cos\theta_5 + a_4) \cdot \sin\theta_4 \cdot \sin\theta_3 + ((( - a_5 - d_6) \cdot \cos\theta_5 - a_4) \cdot \cos\theta_4 - a_3) \cdot \cos\theta_3) \cdot \sin\theta_1 + (d_6 + a_5) \cdot \cos\theta_2 \cdot \cos\theta_1 \cdot \sin\theta_5, (d_6 + a_5) \cdot \cos\theta_2 \cdot \sin\theta_5 \cdot \sin\theta_1 + (( - a_5 - d_6) \cdot \cos\theta_5 - a_4) \cdot \cos\theta_1 \cdot \sin\theta_4 \cdot \sin\theta_3 + (((d_6 + a_5) \cdot \cos\theta_5 + a_4) \cdot \cos\theta_4 + a_3) \cdot \cos\theta_3 \cdot \cos\theta_1, (d_6 + a_5) \cdot \sin\theta_5 \cdot \sin\theta_2]^T$$

$$\mathbf{J}_{r,2} = [(((d_6 + a_5) \cdot \cos\theta_5 + a_4) \cdot \cos\theta_1 \cdot \sin\theta_4 \cdot \sin\theta_3 + ((( - a_5 - d_6) \cdot \cos\theta_5 - a_4) \cdot \cos\theta_4 - a_3) \cdot \cos\theta_3 \cdot \cos\theta_1) \cdot \sin\theta_2 + ((( - a_5 - d_6) \cdot \cos\theta_5 - a_4) \cdot \cos\theta_4 - a_3) \cdot \cos\theta_2 \cdot \cos\theta_1 \cdot \sin\theta_3 + (( - a_5 - d_6) \cdot \cos\theta_5 - a_4) \cdot \cos\theta_3 \cdot \cos\theta_2 \cdot \cos\theta_1 \cdot \sin\theta_4, (((d_6 + a_5) \cdot \cos\theta_5 + a_4) \cdot \sin\theta_4 \cdot \sin\theta_3 + ((( - a_5 - d_6) \cdot \cos\theta_5 - a_4) \cdot \cos\theta_4 - a_3) \cdot \cos\theta_3) \cdot \sin\theta_2 + ((( - a_5 - d_6) \cdot \cos\theta_5 - a_4) \cdot \cos\theta_4 - a_3) \cdot \cos\theta_2 \cdot \sin\theta_3 + (( - a_5 - d_6) \cdot \cos\theta_5 - a_4) \cdot \cos\theta_3 \cdot \cos\theta_2 \cdot \sin\theta_4) \cdot \sin\theta_1, ((( - a_5 - d_6) \cdot \cos\theta_5 - a_4) \cdot \cos\theta_4 - a_3) \cdot \sin\theta_3 + (( - a_5 - d_6) \cdot \cos\theta_5 - a_4) \cdot \cos\theta_3 \cdot \sin\theta_4) \cdot \sin\theta_2 + (( - a_5 - d_6) \cdot \cos\theta_5 - a_4) \cdot \cos\theta_2 \cdot \sin\theta_4 \cdot \sin\theta_3 + (((d_6 + a_5) \cdot \cos\theta_5 + a_4) \cdot \cos\theta_4 + a_3) \cdot \cos\theta_3 \cdot \cos\theta_2]^T$$

$$\mathbf{J}_{p,2} = [(((d_6 + a_5) \cdot \cos\theta_5 + a_4) \cdot \cos\theta_4 + a_3) \cdot \sin\theta_3 + ((d_6 + a_5) \cdot \cos\theta_5 + a_4) \cdot \cos\theta_3 \cdot \sin\theta_4) \cdot \sin\theta_1 \\ + (d_6 + a_5) \cdot \cos\theta_1 \cdot \sin\theta_5 \cdot \sin\theta_2, (d_6 + a_5) \cdot \sin\theta_5 \cdot \sin\theta_2 \cdot \sin\theta_1 + (((-a_5 - d_6) \cdot \cos\theta_5 - \\ a_4) \cdot \cos\theta_4 - a_3) \cdot \cos\theta_1 \cdot \sin\theta_3 + ((-a_5 - d_6) \cdot \cos\theta_5 - a_4) \cdot \cos\theta_3 \cdot \cos\theta_1 \cdot \sin\theta_4, (-a_5 - \\ d_6) \cdot \cos\theta_2 \cdot \sin\theta_5]^T$$

$$\mathbf{J}_{x,3} = [-\cos\theta_1 \cdot \sin\theta_2 \cdot \sin\theta_3 + \cos\theta_1 \cdot \cos\theta_2 \cdot \cos\theta_3, (-\sin\theta_2 \cdot \sin\theta_3 + \cos\theta_2 \cdot \cos\theta_3) \cdot \sin\theta_1, \\ \sin\theta_2 \cdot \cos\theta_3 + \cos\theta_2 \cdot \sin\theta_3]^T$$

$$\mathbf{J}_{y,3} = [-\cos\theta_1 \cdot \sin\theta_2 \cdot \cos\theta_3 - \cos\theta_1 \cdot \cos\theta_2 \cdot \sin\theta_3, (-\sin\theta_2 \cdot \cos\theta_3 - \cos\theta_2 \cdot \sin\theta_3) \cdot \sin\theta_1, \\ -\sin\theta_2 \cdot \sin\theta_3 + \cos\theta_2 \cdot \cos\theta_3]^T$$

$$\mathbf{J}_{z,3} = [\sin\theta_1, -\cos\theta_1, 0]^T$$

$$\mathbf{J}_{s,3} = [((-a_5 - d_6) \cdot \cos\theta_5 - a_4) \cdot \cos\theta_4 \cdot \sin\theta_1 + (-a_5 - d_6) \cdot \cos\theta_1 \cdot \sin\theta_5 \cdot \sin\theta_3 \cdot \sin\theta_2 + (d_6 + \\ a_5) \cdot \cos\theta_3 \cdot \cos\theta_2 \cdot \cos\theta_1 \cdot \sin\theta_5, ((-a_5 - d_6) \cdot \sin\theta_5 \cdot \sin\theta_3 \cdot \sin\theta_2 + (d_6 + \\ a_5) \cdot \cos\theta_3 \cdot \cos\theta_2 \cdot \sin\theta_5) \cdot \sin\theta_1 + ((d_6 + a_5) \cdot \cos\theta_5 + a_4) \cdot \cos\theta_4 \cdot \cos\theta_1, (d_6 + \\ a_5) \cdot \cos\theta_3 \cdot \sin\theta_5 \cdot \sin\theta_2 + (d_6 + a_5) \cdot \cos\theta_2 \cdot \sin\theta_5 \cdot \sin\theta_3]^T$$

$$\mathbf{J}_{r,3} = [(((d_6 + a_5) \cdot \cos\theta_5 + a_4) \cdot \cos\theta_1 \cdot \sin\theta_4 \cdot \sin\theta_3 + ((-a_5 - d_6) \cdot \cos\theta_5 - \\ a_4) \cdot \cos\theta_4 \cdot \cos\theta_3 \cdot \cos\theta_1) \cdot \sin\theta_2 + ((-a_5 - d_6) \cdot \cos\theta_5 - a_4) \cdot \cos\theta_4 \cdot \cos\theta_2 \cdot \cos\theta_1 \cdot \sin\theta_3 + (( \\ -a_5 - d_6) \cdot \cos\theta_5 - a_4) \cdot \cos\theta_3 \cdot \cos\theta_2 \cdot \cos\theta_1 \cdot \sin\theta_4, (((d_6 + a_5) \cdot \cos\theta_5 + a_4) \cdot \sin\theta_4 \cdot \sin\theta_3 + \\ ((-a_5 - d_6) \cdot \cos\theta_5 - a_4) \cdot \cos\theta_4 \cdot \cos\theta_3) \cdot \sin\theta_2 + ((-a_5 - d_6) \cdot \cos\theta_5 - \\ a_4) \cdot \cos\theta_4 \cdot \cos\theta_2 \cdot \sin\theta_3 + ((-a_5 - d_6) \cdot \cos\theta_5 - a_4) \cdot \cos\theta_3 \cdot \cos\theta_2 \cdot \sin\theta_4) \cdot \sin\theta_1, (((-a_5 - \\ d_6) \cdot \cos\theta_5 - a_4) \cdot \cos\theta_4 \cdot \sin\theta_3 + ((-a_5 - d_6) \cdot \cos\theta_5 - a_4) \cdot \cos\theta_3 \cdot \sin\theta_4) \cdot \sin\theta_2 + ((-a_5 - \\ d_6) \cdot \cos\theta_5 - a_4) \cdot \cos\theta_2 \cdot \sin\theta_4 \cdot \sin\theta_3 + ((d_6 + a_5) \cdot \cos\theta_5 + a_4) \cdot \cos\theta_4 \cdot \cos\theta_3 \cdot \cos\theta_2]^T$$

$$\mathbf{J}_{p,3} = [((d_6 + a_5) \cdot \cos\theta_5 + a_4) \cdot \sin\theta_4 \cdot \sin\theta_1 + (d_6 + a_5) \cdot \cos\theta_3 \cdot \cos\theta_1 \cdot \sin\theta_5 \cdot \sin\theta_2 + (d_6 + \\ a_5) \cdot \cos\theta_2 \cdot \cos\theta_1 \cdot \sin\theta_5 \cdot \sin\theta_3, ((d_6 + a_5) \cdot \cos\theta_3 \cdot \sin\theta_5 \cdot \sin\theta_2 + (d_6 +$$

$$\begin{aligned}
& a_5) \cdot \cos\theta_2 \cdot \sin\theta_5 \cdot \sin\theta_3) \cdot \sin\theta_1 + ((-a_5 - d_6) \cdot \cos\theta_5 - a_4) \cdot \cos\theta_1 \cdot \sin\theta_4, (d_6 + \\
& a_5) \cdot \sin\theta_5 \cdot \sin\theta_3 \cdot \sin\theta_2 + (-a_5 - d_6) \cdot \cos\theta_3 \cdot \cos\theta_2 \cdot \sin\theta_5]^T \\
\mathbf{J}_{x,4} = & [(-\cos\theta_1 \cdot \sin\theta_3 \cdot \cos\theta_4 - \cos\theta_1 \cdot \cos\theta_3 \cdot \sin\theta_4) \cdot \sin\theta_2 + \cos\theta_1 \cdot \cos\theta_2 \cdot \cos\theta_3 \cdot \cos\theta_4 - \\
& \cos\theta_1 \cdot \cos\theta_2 \cdot \sin\theta_3 \cdot \sin\theta_4, ((-\cos\theta_3 \cdot \sin\theta_4 - \sin\theta_3 \cdot \cos\theta_4) \cdot \sin\theta_2 - \cos\theta_2 \cdot \sin\theta_3 \cdot \sin\theta_4 + \\
& \cos\theta_2 \cdot \cos\theta_3 \cdot \cos\theta_4) \cdot \sin\theta_1, (\cos\theta_4 \cdot \cos\theta_3 - \sin\theta_4 \cdot \sin\theta_3) \cdot \sin\theta_2 + \cos\theta_4 \cdot \cos\theta_2 \cdot \sin\theta_3 + \\
& \sin\theta_4 \cdot \cos\theta_2 \cdot \cos\theta_3]^T \\
\mathbf{J}_{y,4} = & [\sin\theta_1, -\cos\theta_1, 0]^T \\
\mathbf{J}_{z,4} = & [(-\cos\theta_1 \cdot \sin\theta_3 \cdot \sin\theta_4 + \cos\theta_1 \cdot \cos\theta_3 \cdot \cos\theta_4) \cdot \sin\theta_2 + \cos\theta_1 \cdot \cos\theta_2 \cdot \cos\theta_3 \cdot \sin\theta_4 + \\
& \cos\theta_1 \cdot \cos\theta_2 \cdot \sin\theta_3 \cdot \cos\theta_4, ((\cos\theta_4 \cdot \cos\theta_3 - \sin\theta_4 \cdot \sin\theta_3) \cdot \sin\theta_2 + \cos\theta_4 \cdot \cos\theta_2 \cdot \sin\theta_3 + \\
& \sin\theta_4 \cdot \cos\theta_2 \cdot \cos\theta_3) \cdot \sin\theta_1, (\cos\theta_3 \cdot \sin\theta_4 + \sin\theta_3 \cdot \cos\theta_4) \cdot \sin\theta_2 - \cos\theta_2 \cdot \cos\theta_3 \cdot \cos\theta_4 + \\
& \cos\theta_2 \cdot \sin\theta_3 \cdot \sin\theta_4]^T \\
\mathbf{J}_{s,4} = & [((d_6 + a_5) \cdot \cos\theta_5 \cdot \cos\theta_1 \cdot \sin\theta_4 \cdot \sin\theta_3 + (-a_5 - d_6) \cdot \cos\theta_5 \cdot \cos\theta_4 \cdot \cos\theta_3 \cdot \cos\theta_1) \cdot \sin\theta_2 + (- \\
& a_5 - d_6) \cdot \cos\theta_5 \cdot \cos\theta_4 \cdot \cos\theta_2 \cdot \cos\theta_1 \cdot \sin\theta_3 + (-a_5 - d_6) \cdot \cos\theta_5 \cdot \cos\theta_3 \cdot \cos\theta_2 \cdot \cos\theta_1 \cdot \sin\theta_4, \\
& (((d_6 + a_5) \cdot \cos\theta_5 \cdot \sin\theta_4 \cdot \sin\theta_3 + (-a_5 - d_6) \cdot \cos\theta_5 \cdot \cos\theta_4 \cdot \cos\theta_3) \cdot \sin\theta_2 + (-a_5 - \\
& d_6) \cdot \cos\theta_5 \cdot \cos\theta_4 \cdot \cos\theta_2 \cdot \sin\theta_3 + (-a_5 - d_6) \cdot \cos\theta_5 \cdot \cos\theta_3 \cdot \cos\theta_2 \cdot \sin\theta_4) \cdot \sin\theta_1, ((-a_5 - \\
& d_6) \cdot \cos\theta_5 \cdot \cos\theta_4 \cdot \sin\theta_3 + (-a_5 - d_6) \cdot \cos\theta_5 \cdot \cos\theta_3 \cdot \sin\theta_4) \cdot \sin\theta_2 + (-a_5 - \\
& d_6) \cdot \cos\theta_5 \cdot \cos\theta_2 \cdot \sin\theta_4 \cdot \sin\theta_3 + (d_6 + a_5) \cdot \cos\theta_5 \cdot \cos\theta_4 \cdot \cos\theta_3 \cdot \cos\theta_2]^T \\
\mathbf{J}_{r,4} = & [(d_6 + a_5) \cdot \cos\theta_5 \cdot \sin\theta_1 + ((d_6 + a_5) \cdot \cos\theta_4 \cdot \cos\theta_1 \cdot \sin\theta_5 \cdot \sin\theta_3 + (d_6 + \\
& a_5) \cdot \cos\theta_3 \cdot \cos\theta_1 \cdot \sin\theta_5 \cdot \sin\theta_4) \cdot \sin\theta_2 + (d_6 + a_5) \cdot \cos\theta_2 \cdot \cos\theta_1 \cdot \sin\theta_5 \cdot \sin\theta_4 \cdot \sin\theta_3 + (-a_5 - \\
& d_6) \cdot \cos\theta_4 \cdot \cos\theta_3 \cdot \cos\theta_2 \cdot \cos\theta_1 \cdot \sin\theta_5, (((d_6 + a_5) \cdot \cos\theta_4 \cdot \sin\theta_5 \cdot \sin\theta_3 + (d_6 + \\
& a_5) \cdot \cos\theta_3 \cdot \sin\theta_5 \cdot \sin\theta_4) \cdot \sin\theta_2 + (d_6 + a_5) \cdot \cos\theta_2 \cdot \sin\theta_5 \cdot \sin\theta_4 \cdot \sin\theta_3 + (-a_5 - \\
& d_6) \cdot \cos\theta_4 \cdot \cos\theta_3 \cdot \cos\theta_2 \cdot \sin\theta_5) \cdot \sin\theta_1 + (-a_5 - d_6) \cdot \cos\theta_5 \cdot \cos\theta_1, ((d_6 +
\end{aligned}$$

$$\begin{aligned}
& a_5) \cdot \sin\theta_5 \cdot \sin\theta_4 \cdot \sin\theta_3 + (-a_5 - d_6) \cdot \cos\theta_4 \cdot \cos\theta_3 \cdot \sin\theta_5) \cdot \sin\theta_2 + (-a_5 - \\
& d_6) \cdot \cos\theta_4 \cdot \cos\theta_2 \cdot \sin\theta_5 \cdot \sin\theta_3 + (-a_5 - d_6) \cdot \cos\theta_3 \cdot \cos\theta_2 \cdot \sin\theta_5 \cdot \sin\theta_4]^T \\
\mathbf{J}_{p,4} = & [((-a_5 - d_6) \cdot \cos\theta_1 \cdot \sin\theta_5 \cdot \sin\theta_4 \cdot \sin\theta_3 + (d_6 + a_5) \cdot \cos\theta_4 \cdot \cos\theta_3 \cdot \cos\theta_1 \cdot \sin\theta_5) \cdot \sin\theta_2 + (d_6 \\
& + a_5) \cdot \cos\theta_4 \cdot \cos\theta_2 \cdot \cos\theta_1 \cdot \sin\theta_5 \cdot \sin\theta_3 + (d_6 + a_5) \cdot \cos\theta_3 \cdot \cos\theta_2 \cdot \cos\theta_1 \cdot \sin\theta_5 \cdot \sin\theta_4, (((-a_5 \\
& - d_6) \cdot \sin\theta_5 \cdot \sin\theta_4 \cdot \sin\theta_3 + (d_6 + a_5) \cdot \cos\theta_4 \cdot \cos\theta_3 \cdot \sin\theta_5) \cdot \sin\theta_2 + (d_6 + \\
& a_5) \cdot \cos\theta_4 \cdot \cos\theta_2 \cdot \sin\theta_5 \cdot \sin\theta_3 + (d_6 + a_5) \cdot \cos\theta_3 \cdot \cos\theta_2 \cdot \sin\theta_5 \cdot \sin\theta_4) \cdot \sin\theta_1, ((d_6 + \\
& a_5) \cdot \cos\theta_4 \cdot \sin\theta_5 \cdot \sin\theta_3 + (d_6 + a_5) \cdot \cos\theta_3 \cdot \sin\theta_5 \cdot \sin\theta_4) \cdot \sin\theta_2 + (d_6 + \\
& a_5) \cdot \cos\theta_2 \cdot \sin\theta_5 \cdot \sin\theta_4 \cdot \sin\theta_3 + (-a_5 - d_6) \cdot \cos\theta_4 \cdot \cos\theta_3 \cdot \cos\theta_2 \cdot \sin\theta_5)]^T \\
\mathbf{J}_{x,5} = & [\sin\theta_1 \cdot \cos\theta_5 + (\cos\theta_1 \cdot \cos\theta_3 \cdot \sin\theta_4 \cdot \sin\theta_5 + \cos\theta_1 \cdot \sin\theta_3 \cdot \cos\theta_4 \cdot \sin\theta_5) \cdot \sin\theta_2 - \\
& \cos\theta_1 \cdot \cos\theta_2 \cdot \cos\theta_3 \cdot \cos\theta_4 \cdot \sin\theta_5 + \cos\theta_1 \cdot \cos\theta_2 \cdot \sin\theta_3 \cdot \sin\theta_4 \cdot \sin\theta_5, ((\cos\theta_3 \cdot \sin\theta_4 \cdot \sin\theta_5 + \\
& \sin\theta_3 \cdot \cos\theta_4 \cdot \sin\theta_5) \cdot \sin\theta_2 + \cos\theta_2 \cdot \sin\theta_3 \cdot \sin\theta_4 \cdot \sin\theta_5 - \cos\theta_2 \cdot \cos\theta_3 \cdot \cos\theta_4 \cdot \sin\theta_5) \cdot \sin\theta_1 - \\
& \cos\theta_1 \cdot \cos\theta_5, (\sin\theta_3 \cdot \sin\theta_4 \cdot \sin\theta_5 - \cos\theta_3 \cdot \cos\theta_4 \cdot \sin\theta_5) \cdot \sin\theta_2 - \cos\theta_2 \cdot \cos\theta_3 \cdot \sin\theta_4 \cdot \sin\theta_5 \\
& - \cos\theta_2 \cdot \sin\theta_3 \cdot \cos\theta_4 \cdot \sin\theta_5]^T \\
\mathbf{J}_{y,5} = & [(-\cos\theta_1 \cdot \sin\theta_3 \cdot \sin\theta_4 + \cos\theta_1 \cdot \cos\theta_3 \cdot \cos\theta_4) \cdot \sin\theta_2 + \cos\theta_1 \cdot \cos\theta_2 \cdot \cos\theta_3 \cdot \sin\theta_4 + \\
& \cos\theta_1 \cdot \cos\theta_2 \cdot \sin\theta_3 \cdot \cos\theta_4, ((\cos\theta_4 \cdot \cos\theta_3 - \sin\theta_4 \cdot \sin\theta_3) \cdot \sin\theta_2 + \cos\theta_4 \cdot \cos\theta_2 \cdot \sin\theta_3 + \\
& \sin\theta_4 \cdot \cos\theta_2 \cdot \cos\theta_3) \cdot \sin\theta_1, (\cos\theta_3 \cdot \sin\theta_4 + \sin\theta_3 \cdot \cos\theta_4) \cdot \sin\theta_2 - \cos\theta_2 \cdot \cos\theta_3 \cdot \cos\theta_4 + \\
& \cos\theta_2 \cdot \sin\theta_3 \cdot \sin\theta_4]^T \\
\mathbf{J}_{z,5} = & [\sin\theta_1 \cdot \sin\theta_5 + (-\cos\theta_1 \cdot \sin\theta_3 \cdot \cos\theta_4 \cdot \cos\theta_5 - \cos\theta_1 \cdot \cos\theta_3 \cdot \sin\theta_4 \cdot \cos\theta_5) \cdot \sin\theta_2 + \\
& \cos\theta_5 \cdot \cos\theta_4 \cdot \cos\theta_1 \cdot \cos\theta_2 \cdot \cos\theta_3 - \cos\theta_5 \cdot \sin\theta_4 \cdot \cos\theta_1 \cdot \cos\theta_2 \cdot \sin\theta_3, ((- \\
& \cos\theta_5 \cdot \cos\theta_4 \cdot \sin\theta_3 - \cos\theta_5 \cdot \sin\theta_4 \cdot \cos\theta_3) \cdot \sin\theta_2 - \cos\theta_5 \cdot \sin\theta_4 \cdot \cos\theta_2 \cdot \sin\theta_3 + \\
& \cos\theta_5 \cdot \cos\theta_4 \cdot \cos\theta_2 \cdot \cos\theta_3) \cdot \sin\theta_1 - \cos\theta_1 \cdot \sin\theta_5, (-\sin\theta_3 \cdot \sin\theta_4 \cdot \cos\theta_5 + \\
& \cos\theta_3 \cdot \cos\theta_4 \cdot \cos\theta_5) \cdot \sin\theta_2 + \cos\theta_2 \cdot \cos\theta_3 \cdot \sin\theta_4 \cdot \cos\theta_5 + \cos\theta_2 \cdot \sin\theta_3 \cdot \cos\theta_4 \cdot \cos\theta_5]^T
\end{aligned}$$

$$\begin{aligned} \mathbf{J}_{s,5} = & [\sin\theta_1 \cdot \cos\theta_5 \cdot d_6 + (\cos\theta_1 \cdot \sin\theta_3 \cdot \cos\theta_4 \cdot \sin\theta_5 \cdot d_6 + \cos\theta_1 \cdot \cos\theta_3 \cdot \sin\theta_4 \cdot \sin\theta_5 \cdot d_6) \cdot \sin\theta_2 - \\ & \cos\theta_1 \cdot \cos\theta_2 \cdot \cos\theta_3 \cdot \cos\theta_4 \cdot \sin\theta_5 \cdot d_6 + \cos\theta_1 \cdot \cos\theta_2 \cdot \sin\theta_3 \cdot \sin\theta_4 \cdot \sin\theta_5 \cdot d_6, \\ & ((\cos\theta_3 \cdot \sin\theta_4 \cdot \sin\theta_5 \cdot d_6 + \sin\theta_3 \cdot \cos\theta_4 \cdot \sin\theta_5 \cdot d_6) \cdot \sin\theta_2 - \cos\theta_2 \cdot \cos\theta_3 \cdot \cos\theta_4 \cdot \sin\theta_5 \cdot d_6 + \\ & \cos\theta_2 \cdot \sin\theta_3 \cdot \sin\theta_4 \cdot \sin\theta_5 \cdot d_6) \cdot \sin\theta_1 - \cos\theta_1 \cdot \cos\theta_5 \cdot d_6, (\sin\theta_3 \cdot \sin\theta_4 \cdot \sin\theta_5 \cdot d_6 - \\ & \cos\theta_3 \cdot \cos\theta_4 \cdot \sin\theta_5 \cdot d_6) \cdot \sin\theta_2 - \cos\theta_2 \cdot \cos\theta_3 \cdot \sin\theta_4 \cdot \sin\theta_5 \cdot d_6 - \\ & \cos\theta_2 \cdot \sin\theta_3 \cdot \cos\theta_4 \cdot \sin\theta_5 \cdot d_6]^T \end{aligned}$$

$$\mathbf{J}_{r,5} = [0, 0, 0]^T$$

$$\begin{aligned} \mathbf{J}_{p,5} = & [(\cos\theta_1 \cdot \sin\theta_3 \cdot \sin\theta_4 \cdot d_6 - \cos\theta_1 \cdot \cos\theta_3 \cdot \cos\theta_4 \cdot d_6) \cdot \sin\theta_2 - \cos\theta_1 \cdot \cos\theta_2 \cdot \cos\theta_3 \cdot \sin\theta_4 \cdot d_6 - \\ & \cos\theta_1 \cdot \cos\theta_2 \cdot \sin\theta_3 \cdot \cos\theta_4 \cdot d_6, ((-\cos\theta_3 \cdot \cos\theta_4 \cdot d_6 + \sin\theta_3 \cdot \sin\theta_4 \cdot d_6) \cdot \sin\theta_2 - \\ & \cos\theta_2 \cdot \sin\theta_3 \cdot \cos\theta_4 \cdot d_6 - \cos\theta_2 \cdot \cos\theta_3 \cdot \sin\theta_4 \cdot d_6) \cdot \sin\theta_1, (-\sin\theta_3 \cdot \cos\theta_4 \cdot d_6 - \\ & \cos\theta_3 \cdot \sin\theta_4 \cdot d_6) \cdot \sin\theta_2 + \cos\theta_2 \cdot \cos\theta_3 \cdot \cos\theta_4 \cdot d_6 - \cos\theta_2 \cdot \sin\theta_3 \cdot \sin\theta_4 \cdot d_6]^T \end{aligned}$$

$$\begin{aligned} \mathbf{J}_{x,6} = & [\cos\theta_6 \cdot \sin\theta_1 \cdot \cos\theta_5 + ((\cos\theta_1 \cdot \cos\theta_6 \cdot \sin\theta_5 \cdot \cos\theta_4 - \cos\theta_1 \cdot \sin\theta_6 \cdot \sin\theta_4) \cdot \sin\theta_3 + \\ & \cos\theta_1 \cdot \cos\theta_3 \cdot \cos\theta_4 \cdot \sin\theta_6 + \cos\theta_1 \cdot \cos\theta_3 \cdot \sin\theta_4 \cdot \sin\theta_5 \cdot \cos\theta_6) \cdot \sin\theta_2 + \\ & (\cos\theta_6 \cdot \sin\theta_5 \cdot \sin\theta_4 \cdot \cos\theta_1 \cdot \cos\theta_2 + \sin\theta_6 \cdot \cos\theta_4 \cdot \cos\theta_1 \cdot \cos\theta_2) \cdot \sin\theta_3 - \\ & \cos\theta_6 \cdot \sin\theta_5 \cdot \cos\theta_4 \cdot \cos\theta_1 \cdot \cos\theta_2 \cdot \cos\theta_3 + \sin\theta_6 \cdot \sin\theta_4 \cdot \cos\theta_1 \cdot \cos\theta_2 \cdot \cos\theta_3, \\ & (((\cos\theta_6 \cdot \sin\theta_5 \cdot \cos\theta_4 - \sin\theta_6 \cdot \sin\theta_4) \cdot \sin\theta_3 + \cos\theta_6 \cdot \sin\theta_5 \cdot \sin\theta_4 \cdot \cos\theta_3 + \\ & \sin\theta_6 \cdot \cos\theta_4 \cdot \cos\theta_3) \cdot \sin\theta_2 + (\cos\theta_6 \cdot \sin\theta_5 \cdot \sin\theta_4 \cdot \cos\theta_2 + \sin\theta_6 \cdot \cos\theta_4 \cdot \cos\theta_2) \cdot \sin\theta_3 - \\ & \cos\theta_6 \cdot \sin\theta_5 \cdot \cos\theta_4 \cdot \cos\theta_2 \cdot \cos\theta_3 + \sin\theta_6 \cdot \sin\theta_4 \cdot \cos\theta_2 \cdot \cos\theta_3) \cdot \sin\theta_1 - \cos\theta_6 \cdot \cos\theta_1 \cdot \cos\theta_5, \\ & ((\sin\theta_4 \cdot \sin\theta_5 \cdot \cos\theta_6 + \cos\theta_4 \cdot \sin\theta_6) \cdot \sin\theta_3 - \sin\theta_5 \cdot \cos\theta_6 \cdot \cos\theta_4 \cdot \cos\theta_3 + \\ & \sin\theta_6 \cdot \sin\theta_4 \cdot \cos\theta_3) \cdot \sin\theta_2 + (-\sin\theta_5 \cdot \cos\theta_6 \cdot \cos\theta_4 \cdot \cos\theta_2 + \sin\theta_6 \cdot \sin\theta_4 \cdot \cos\theta_2) \cdot \sin\theta_3 - \\ & \sin\theta_5 \cdot \cos\theta_6 \cdot \sin\theta_4 \cdot \cos\theta_2 \cdot \cos\theta_3 - \sin\theta_6 \cdot \cos\theta_4 \cdot \cos\theta_2 \cdot \cos\theta_3]^T \end{aligned}$$

$$\begin{aligned}
\mathbf{J}_{y,6} = & [-\sin\theta_6 \cdot \sin\theta_1 \cdot \cos\theta_5 + ((-\cos\theta_1 \cdot \sin\theta_5 \cdot \sin\theta_6 \cdot \cos\theta_4 - \cos\theta_1 \cdot \sin\theta_4 \cdot \cos\theta_6) \cdot \sin\theta_3 + \\
& \cos\theta_1 \cdot \cos\theta_3 \cdot \cos\theta_4 \cdot \cos\theta_6 - \cos\theta_1 \cdot \cos\theta_3 \cdot \sin\theta_4 \cdot \sin\theta_5 \cdot \sin\theta_6) \cdot \sin\theta_2 + (- \\
& \sin\theta_6 \cdot \sin\theta_5 \cdot \sin\theta_4 \cdot \cos\theta_1 \cdot \cos\theta_2 + \cos\theta_6 \cdot \cos\theta_4 \cdot \cos\theta_1 \cdot \cos\theta_2) \cdot \sin\theta_3 + \\
& \sin\theta_6 \cdot \sin\theta_5 \cdot \cos\theta_4 \cdot \cos\theta_1 \cdot \cos\theta_2 \cdot \cos\theta_3 + \cos\theta_6 \cdot \sin\theta_4 \cdot \cos\theta_1 \cdot \cos\theta_2 \cdot \cos\theta_3, (((- \\
& \sin\theta_5 \cdot \sin\theta_6 \cdot \cos\theta_4 - \sin\theta_4 \cdot \cos\theta_6) \cdot \sin\theta_3 - \sin\theta_6 \cdot \sin\theta_5 \cdot \sin\theta_4 \cdot \cos\theta_3 + \\
& \cos\theta_6 \cdot \cos\theta_4 \cdot \cos\theta_3) \cdot \sin\theta_2 + (-\sin\theta_6 \cdot \sin\theta_5 \cdot \sin\theta_4 \cdot \cos\theta_2 + \cos\theta_6 \cdot \cos\theta_4 \cdot \cos\theta_2) \cdot \sin\theta_3 + \\
& \cos\theta_6 \cdot \sin\theta_4 \cdot \cos\theta_2 \cdot \cos\theta_3 + \sin\theta_6 \cdot \sin\theta_5 \cdot \cos\theta_4 \cdot \cos\theta_2 \cdot \cos\theta_3) \cdot \sin\theta_1 + \sin\theta_6 \cdot \cos\theta_1 \cdot \cos\theta_5, \\
& ((-\sin\theta_4 \cdot \sin\theta_5 \cdot \sin\theta_6 + \cos\theta_4 \cdot \cos\theta_6) \cdot \sin\theta_3 + \sin\theta_5 \cdot \sin\theta_6 \cdot \cos\theta_4 \cdot \cos\theta_3 + \\
& \cos\theta_6 \cdot \sin\theta_4 \cdot \cos\theta_3) \cdot \sin\theta_2 + (\sin\theta_5 \cdot \sin\theta_6 \cdot \cos\theta_4 \cdot \cos\theta_2 + \cos\theta_6 \cdot \sin\theta_4 \cdot \cos\theta_2) \cdot \sin\theta_3 + \\
& \sin\theta_5 \cdot \sin\theta_6 \cdot \sin\theta_4 \cdot \cos\theta_2 \cdot \cos\theta_3 - \cos\theta_6 \cdot \cos\theta_4 \cdot \cos\theta_2 \cdot \cos\theta_3]^T
\end{aligned}$$

$$\begin{aligned}
\mathbf{J}_{z,6} = & [\sin\theta_1 \cdot \sin\theta_5 + (-\cos\theta_1 \cdot \sin\theta_3 \cdot \cos\theta_4 \cdot \cos\theta_5 - \cos\theta_1 \cdot \cos\theta_3 \cdot \sin\theta_4 \cdot \cos\theta_5) \cdot \sin\theta_2 + \\
& \cos\theta_5 \cdot \cos\theta_4 \cdot \cos\theta_1 \cdot \cos\theta_2 \cdot \cos\theta_3 - \cos\theta_5 \cdot \sin\theta_4 \cdot \cos\theta_1 \cdot \cos\theta_2 \cdot \sin\theta_3, ((- \\
& \cos\theta_5 \cdot \cos\theta_4 \cdot \sin\theta_3 - \cos\theta_5 \cdot \sin\theta_4 \cdot \cos\theta_3) \cdot \sin\theta_2 - \cos\theta_5 \cdot \sin\theta_4 \cdot \cos\theta_2 \cdot \sin\theta_3 + \\
& \cos\theta_5 \cdot \cos\theta_4 \cdot \cos\theta_2 \cdot \cos\theta_3) \cdot \sin\theta_1 - \cos\theta_1 \cdot \sin\theta_5, (-\sin\theta_3 \cdot \sin\theta_4 \cdot \cos\theta_5 + \\
& \cos\theta_3 \cdot \cos\theta_4 \cdot \cos\theta_5) \cdot \sin\theta_2 + \cos\theta_2 \cdot \cos\theta_3 \cdot \sin\theta_4 \cdot \cos\theta_5 + \cos\theta_2 \cdot \sin\theta_3 \cdot \cos\theta_4 \cdot \cos\theta_5]^T
\end{aligned}$$

$$\mathbf{J}_{s,6} = [0, 0, 0]^T$$

$$\mathbf{J}_{r,6} = [0, 0, 0]^T$$

$$\mathbf{J}_{p,6} = [0, 0, 0]^T$$